universität wien

MASTERARBEIT / MASTER'S THESIS

Titel der Masterarbeit / Title of the Master's Thesis

The IL-34-PTN-PTPRZ1 axis in melanoma

verfasst von / submitted by

Mathias Mayerhofer BSc

angestrebter akademischer Grad / in partial fulfilment of the requirements for the degree of

Master of Science (MSc)

Wien, 2022 / Vienna 2022

Studienkennzahl lt. Studienblatt / degree programme code as it appears on the student record sheet:	UA 066 834
Studienrichtung lt. Studienblatt / degree programme as it appears on the student record sheet:	Masterstudium Molekulare Biologie
Betreut von / Supervisor:	Ao. Univ.-Prof. Dr. Dietmar Abraham

Acknowledgments

A special acknowledgment goes to Ao. Univ.-Prof. Dr. Dietmar Abraham (Medical University of Vienna, Center for Anatomy and Cell Biology, Vienna, AT) for the idea and guidance of this project. I am grateful to Ass.-Prof. Dr. Karin Zins (Medical University of Vienna, Center for Anatomy and Cell Biology, Vienna, AT) for her assistance and guidance in the lab as well as for proposed study designs. I am thankful to Sandra Trojanek (Medical University of Vienna, Center for Anatomy and Cell Biology, Vienna, AT) for sharing her scientific wisdom. Furthermore, the author acknowledges the Central European Institute of Technology (CEITEC, Bruno University of Technology, CZ) for performing the Liquid chromatography–mass spectrometry (LC-MS) analyses. Further acknowledgments go to Dr. Ana Maria Ramos Gonzalez (University CEU San Pablo, Department of Chemistry and Biochemistry in Madrid, ES) for providing the PTPRζ1 small-molecule inhibitor compounds 10a (MY10) and 12b (MY33-3).

Abstract

Melanoma is the most malignant type of human skin cancers and incidences have increased over the last several decades. Melanoma interacts with the tumor microenvironment, thus the mediated crosstalk between cancer, stromal cells, and immune cells within the surrounding microenvironment via cytokines, growth factors, and their receptors are important for cell motility, invasion, metastasis and proliferation. The cytokines, Interleukin-34 (IL-34) and pleiotrophin (PTN) are ligands for the receptors of PTPRζ1 and syndecan-1. In addition, IL-34 also shares with Colony stimulating factor-1 (CSF-1) another receptor, the CSF-1R. Thereby increasing the complexity of biological activities. IL-34 is involved in the innate immunity, inflammation, and cancer. However, while the roles of IL-34/- and CSF-1/CSF-1R axes have been extensively studied in myeloid cells and in several cancers, the implications of PTN, IL-34 and CSF-1 in signaling transduction via PTPRζ1 respectively CSF-1R and their effects on cellular behavior are still poorly understood in melanoma skin cancer. Using real-time qRT-PCR revealed that IL-34, CSF-1 and PTN do not significantly regulate gene expressions of *PTPRZ1*, *CSF-1R*, *SDC-1*, *IL-34*, *CSF-1* or *PTN* of melanoma SK-MEL-28- and WM-115 cell lines. *In vitro* experiments showed that PTN differentially affects FAK phosphorylation and migration of both melanoma cell lines. Moreover, IL-34 induces FAK phosphorylation of WM-115 cells and potentially of SK-MEL-28 cells. Furthermore, IL-34 might play a role in cell migration of both melanoma cell lines. In contrast, CSF-1 does not induce FAK phosphorylation and migration of both melanoma cell lines. Additionally, IL-34, CSF-1 and PTN do not increase the AKT- and ERK pathway above baseline activation levels. *In vitro* experiments of the PTPRζ1 inhibitor showed that 10 µM compound 12b induces the AKT pathway of SK-MEL-28 cells, as well as proliferation and potentially migration of both melanoma cell lines.

In conclusion, our study suggests differential regulation of PTPRζ1 and CSF-1R signaling in melanoma cells.

Zusammenfassung

Das Melanom ist der gefährlichste Typ von malignem Hautkrebs und sein Auftreten ist über die Jahrzehnte hinweg gestiegen. Das Melanom interagiert mit seinem Tumormikromilieu durch Zytokine, Wachstumsfaktoren, und deren Rezeptoren an Krebs-, Stroma- und Immunzellen und spielt dadurch eine wichtige Rolle in der Zellbewegung, Invasion, Metastasierung und Proliferation. Durch verschiedene Bindungsmöglichkeiten von Zytokinen an Rezeptoren erhöht sich die Komplexität der biologischen Aktivitäten. Interleukin-34 (IL-34) und Pleiotrophin (PTN) sind Zytokine sowie Liganden für die Rezeptoren PTPRζ1 und Syndecan-1. IL-34 sowie ein weiteres Zytokin, namens Colony stimulating factor-1 (CSF-1), können weiters an den Rezeptor CSF-1R binden. IL-34 spielt nicht nur eine entscheidende Rolle in der Tumorgenese, sondern auch im Hinblick auf die angeborene Immunität sowie hinsichtlich Inflammation. Obwohl die Rolle der IL-34/ CSF-1R sowie CSF-1/CSF-1R Signaltransduktions-Achsen in Myeloid Zellen und weiteren etlichen Krebsarten bis dato sehr intensiv erforscht wurden, sind die Einflüsse von PTN, IL-34 und CSF-1 an der Signaltransduktion von den Rezeptoren PTPRζ1 sowie CSF-1R und deren zellulärem Verhalten noch weitaus unerforscht und unschlüssig im Bereich von Hautkrebs. Die qRT-PCR Analyse zeigte, dass IL-34, CSF-1 und PTN die Genexpression von *PTPRZ1*, *CSF-1R*, *SDC-1*, *IL-34*, *CSF-1* und *PTN* in den Zelllinien SK-MEL-28 und WM-115 nicht signifikant regulieren. *In vitro* Experimente zeigten die unterschiedliche Wirkung von PTN auf die Phosphorylierung von FAK sowie auf die Zellmigration in beiden Melanom Zelllinien. Des Weiteren induziert IL-34 die Phosphorylierung von FAK in WM-115 Zellen, und hätte vermutlich den selben Einfluss in SK-MEL-28 Zellen. Weiters könnte IL-34 eine Rolle in der Zellmigration beider Zelllinien spielen. Im Gegensatz dazu induziert CSF-1 weder eine FAK Phosphorylierung noch Zellmigration in beiden Zelllinien. Zudem erhöhen die Zytokine, IL-34, CSF-1 und PTN nicht die AKT- und ERK Signalwege über das Level der Basisaktivität. Jedoch zeigten die *in vitro* Experimente des PTPRζ1 Inhibitors, compound 12b, in einer Verdünnung von 10 µM eine Induktion des AKT Signalweges in SK-MEL-28 Zellen sowie eine Zellproliferation in beiden Zelllinien. Weiters könnte compound 12b eine Rolle in der Zellmigration in beiden Zelllinien spielen.

Zusammenfassend zeigt unsere Studie, dass PTPRζ1 und CSF-1R Signaltransduktionskaskaden in Hautkrebszelllinien unterschiedlich reguliert werden.

Table of contents

A. Introduction

1. Melanocytes & Melanoma

Melanoma is a skin cancer disease caused by neoplasm malignancy of melanocytes. Melanocytes can be found in the basal layer of the skin's epidermis. They produce the pigment melanin (melanogenesis) as pigment granules also known as an organelle called melanosomes [1, 2, 3]. There are two types of melanin, the skin's sun-protective black to brown eumelanin and the reddish to brown pheomelanin which is not sun-protective [4, 5]. The ratio of eumelanin to pheomelanin defines the color of the hair, skin and eyes [6]. Furthermore, the epidermis is also comprised of 90% keratinocytes synthesizing keratin which is a major structural protein, and of a varied group of cytoskeletal scaffolding proteins forming the intermediate filament network offering structural support for keratinocytes to maintain skin's integrity [7]. In addition, there are other cell types in the epidermis such as Langerhans cells and Merkel cells [2]. Langerhans cells are dendritic cells which are essential in the immune response as antigen-presenting cells (APC) against pathogens [8]. Merkel cells play an important role in mechanoreceptor, neuro-endocrine, and nociceptive responses [9]. In general, the skin is the largest organ of the human body and functions as a physical barrier from the environment protecting from external factors such as pathogens, toxic chemical agents, ultraviolet (UV) radiation and mechanical stressors [2, 10].

Skin cancers can be divided into two main groups, (i) nonmelanoma skin cancers (NMSC) (~95%) including basal cell carcinoma (BCC) and squamous cell carcinoma (SCC); and (ii) melanoma skin cancer (~5%). Almost all NMSCs are comprised of BCC (71.6%) and SCC (26.1%) whereas the other NMSCs (2.3%) consist of Merkel cell carcinoma, sebaceous carcinoma, apocrine adenocarcinoma and other rare tumors [11, 12, 13]. Melanoma is the most malignant type of human skin cancers although early-stage of melanoma can be successfully treated with surgery whereas at later stages of metastasis, melanoma is resistant to conventional therapies [14, 15]. Thus, early diagnosis of melanoma is beneficial which is done by direct visual inspection of the skin, however, histopathology detection (biopsy) still remains the gold standard to evaluate the disease. Other detections methods are anatomical imaging approaches like in vivo noninvasive confocal microscopy, optical coherence tomography, ultrasound, terahertz pulsed imaging and magnetic resonance imaging, which all vary in resolution, penetration, spectra, the usage of a contrast agent and diagnosis accuracy [12].

The two main risk factors for the development of skin cancer are environmental and genetic risk factors [2, 16]. The most frequent environmental risk factor for almost all skin cancer forms is ultraviolet (UV) radiation from the sun which is damaging the DNA of skin cells including keratinocytes and melanocytes resulting in tanned and sunburned skin [16, 17]. There are three subtypes of UV rays varying in skin's penetration capability due to their wavelength, UVA with

the longest wavelength (315-400 nm) penetrating deep into the upper dermis causing collagen and elastic tissue damage, UVB (280-315 nm) absorbed by the epidermis, and UVC (100-280 nm) totally absorbed by the ozone layer [2, 17]. UVB rays can cause oxidative stress resulting in reactive oxygen species (ROS) production damaging directly DNA causing genetic alterations in melanocytes [18, 19]. The cancerogenic result of UVB rays is the formation of cyclobutane pyrimidine dimers (CPD) and 6-pyrimidine 4-pyrimidone photoproducts as well as UVB-induced lesions generating genetic mutations of cytosine (C) to thymine (T) and CC to TT transitions [18, 20]. There is an increased melanoma risk on the head and neck by outdoor workers in UV-intense areas whereas recreational sun exposure was a melanoma risk factor on the trunk and limbs and less on head and neck [21].

Melanoma incidences have increased over the last several decades, especially in many fair-skinned populations in regions such as North America, Northern Europe (Norway, Denmark, Netherlands, Sweden Germany, Switzerland, Belgium), Australia and New Zealand, the annual incidence raised by 4-6% [22, 23]. The International Classification of Diseases (ICD) is a system for describing and coding mortality and morbidity incidents, which is administered by most WHO member states [24]. Melanoma skin cancer is coded as C43 by ICD 11th Revision (ICD-11) whereas NMSCs are coded as C44 in which diagnosis data of BCCs and SCCs aren't separated, additionally NMSCs are often not routinely reported to cancer registries thus making accurate estimates of incidence difficult [11, 25, 26]. According to the Global Cancer Observatory (GCO) including the global cancer statistics of the GLOBOCAN 2020 database for 185 countries and 36 cancers, new melanoma cases are comprised of 324,635 (1.7% relative to the other cancer sites) and 57,043 of new deaths (0.6% relative to the other cancer sites) whereas 1,198,073 (6.2%) of new NMSCs (excluding BCC) cases and 63,731 (0.6%) new deaths (including all NMSC) [27]. Thus, new cases of melanoma cancer ranks 19th place in GLOBOCAN 2020 whereas in GLOBOCAN 2018, it ranked 21st with 287,723 (1.6%) new cases and 60,712 (0.6%) of deaths. In GLOBOCAN 2020, NMSC cases ranks fourth after female breast cancer (11.7%), lung cancer (11.4%), prostate cancer (7.3%) and NMSC surpassed colon cancer compared with GLOBOCAN 2018 [27, 28]. In 2020 in the United States (US), 60,190 (7% relative to 10 cancer sites in total) new melanoma cases are estimated in males and 40,160 (4% relative to 10 cancer sites in total) in females, ranking melanoma new cases in males the 5th and 6th in females (Fig. 1A). Furthermore, the estimated deaths in males are 4,610 and 2,240 in females. There is a continue increase of melanoma incidence in the US during the time span of 1975 to 2016 (Fig. 1B). Moreover, Melanoma shows a 5-year relative survival rate of 92% for all combined stages and all races (white and black), whereas at localized stage 99%, in regional stage 65% and only 25% in distant stage (Fig. 2D).

A

Estimated New Cases

Males			Females		
Prostate	191,930	21%	Breast	276,480	30%
Lung & bronchus	116,300	13%	Lung & bronchus	112,520	12%
Colon & rectum	78,300	9%	Colon & rectum	69,650	8%
Urinary bladder	62,100	7%	Uterine corpus	65,620	7%
Melanoma of the skin	60,190	7%	Thyroid	40,170	4%
Kidney & renal pelvis	45,520	5%	Melanoma of the skin	40,160	4%
Non-Hodgkin lymphoma	42,380	5%	Non-Hodgkin lymphoma	34,860	4%
Oral cavity & pharynx	38,380	4%	Kidney & renal pelvis	28,230	3%
Leukemia	35,470	4%	Pancreas	27,200	3%
Pancreas	30,400	3%	Leukemia	25,060	3%
All Sites	**893,660**	**100%**	**All Sites**	**912,930**	**100%**

Estimated Deaths

Males			Females		
Lung & bronchus	72,500	23%	Lung & bronchus	63,220	22%
Prostate	33,330	10%	Breast	42,170	15%
Colon & rectum	28,630	9%	Colon & rectum	24,570	9%
Pancreas	24,640	8%	Pancreas	22,410	8%
Liver & intrahepatic bile duct	20,020	6%	Ovary	13,940	5%
Leukemia	13,420	4%	Uterine corpus	12,590	4%
Esophagus	13,100	4%	Liver & intrahepatic bile duct	10,140	4%
Urinary bladder	13,050	4%	Leukemia	9,680	3%
Non-Hodgkin lymphoma	11,460	4%	Non-Hodgkin lymphoma	8,480	3%
Brain & other nervous system	10,190	3%	Brain & other nervous system	7,830	3%
All Sites	**321,160**	**100%**	**All Sites**	**285,360**	**100%**

B

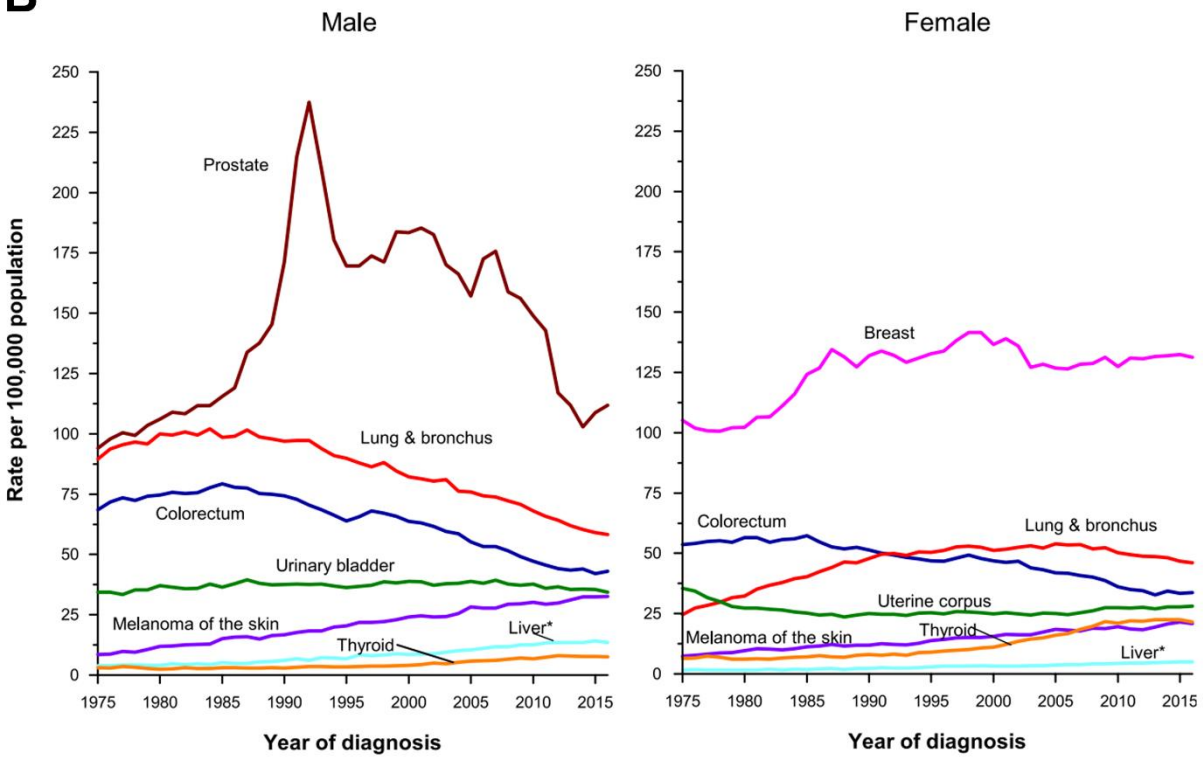

Figure 1. Melanoma and other cancer trends in the United States: A: In 2020, the 10 leading cancers for the estimated new cancer cases and deaths in males and females. Basal cell and squamous cell skin cancers and in situ carcinoma are excluded except urinary bladder.

Numbers are rounded to the nearest 10. **B:** The incidence trends for melanoma and other selected cancers in both genders during 1975 to 2016. Rates are age adjusted to the 2,000 US standard population. *Liver cancers in males and females include intrahepatic bile duct. **A-B:** The original and primary source for this information is “Cancer Statistics, 2020” [29].

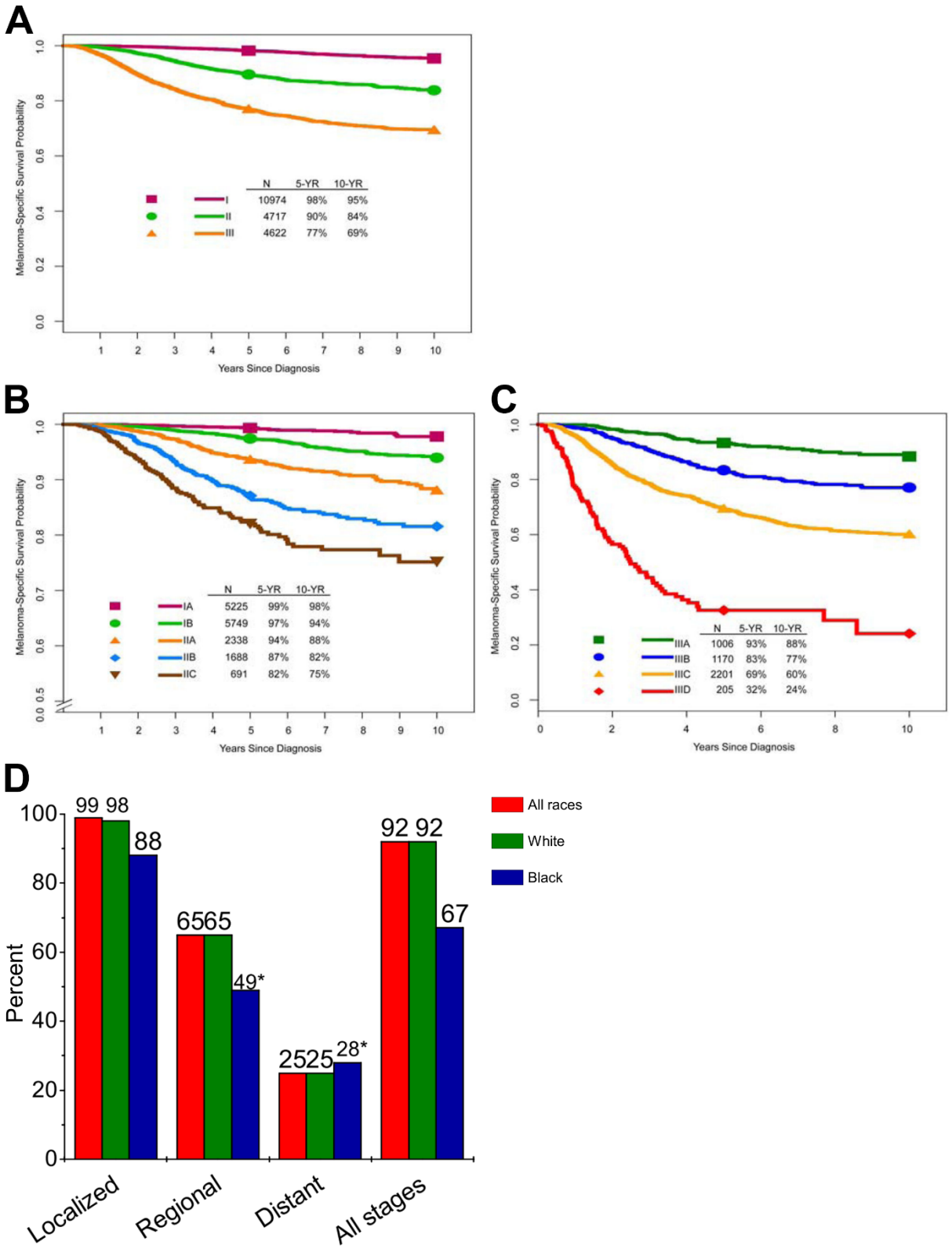

Figure 2. Melanoma-Specific Survival: A-C: Kaplan-Meier melanoma specific survival curves over a time span of 10 years. It also shows a detailed 5-year and 10-year survival

probability (%) and sample size (N) illustrating melanoma patients from the United States, Europe and Australia. The original and primary source for this information is the AJCC Cancer Staging Manual, eighth edition (2017) [30]. **A:** Kaplan-Meier melanoma-specific survival curves according to stage in patients with stage I, II, and III melanoma. **B:** Kaplan-Meier melanoma-specific survival curves according to stage I and II subgroups. Patients with N0 melanoma are filtered, thus patients with T2+ melanoma are included only if they had negative sentinel lymph nodes (SLN), whereas those with T1N0 melanoma are included regardless of whether they had SLN biopsy. **C:** Kaplan-Meier melanoma-specific survival curves according to stage III subgroups. **D:** In the US, 5-year relative survival rates in melanoma arranged by localization (localized, regional and distant) and all stages as well as by race (white population shown in green, and blacks depicted in blue whereas all races is represented in red) during 2009 to 2015. *The standard error of the survival rate is between 5 and 10 percentage points. The original and primary source for this information is Cancer Statistics, 2020 (2020) [29].

Furthermore, there is a large 5-year survival difference for all combined stages of 25% between the black and white population. The average annual percent change (AAPC) in melanoma mortality of both genders decreased significantly by 6.4% during 2013 to 2017 as well as by 2.9% between 2008 to 2017 whereas from 2008 to 2013 showed 0% [29]. The recent mortality decline in melanoma might demonstrate improved survival due to new treatments for metastatic melanoma such as ipilimumab, the first immune checkpoint inhibitor approved by the US Food and Drug Administration (FDA) in 2011, and vemurafenib, a BRAF inhibitor utilized for advanced melanoma treatment [29, 31, 32]. In the US, calculations from 2014 to 2016 show a probability of developing invasive cancer from birth to death is in males 3.6% (1 in 28) and 2.5% (1 in 41) in females. Additionally, the cohorts of birth to the age of 49, 50 to 59 as well as 60 to 69 are all under 1% of the invasive cancer developing probability in both genders and starting to increase at the age of 70 and above, 2.6% (1 in 38) in males and 1.2% (1 in 86) in females [29].

2. Classification of melanoma & progression

Melanoma can be subdivided into four main subtypes comprising (i) superficial spreading melanoma (SSM), (ii) nodular melanoma (NM), (iii) lentigo maligna melanoma (LMM) and (iv) acral lentiginous melanoma (ALM). About ~66.4% of melanoma are accounted by SSM and ~13.7% by the NM whereas ~12.3% are LMM, ~1.5% ALM, ~0.9 acral melanoma (AM), and ~5.1% other subtypes [1, 33, 34]. Based on the latest information from genetic and molecular studies, the World Health Organization (WHO) classified skin tumors in their 11th volume in the 4th edition of the WHO series on the Classification of Tumours, “WHO Classification of Skin Tumours” published in 2018 [35]. Nine distinct melanoma types are distinguished in causal related to sun exposure and those that are not as well as nodular melanoma, which are all additionally characterized by their epidemiology, clinical and histologic morphology, and genomic characteristics. The melanoma types of causal related to sun exposure are further subcategorized by the histopathologic degree of cumulative solar damage (CSD) of the

surrounding skin, into low and high CSD based on the degree of solar elastosis. Therefore, melanomas are divided in the first category of (i) melanomas typically associated with CSD comprising (Pathway I) superficial spreading melanoma/low-CSD melanoma, (Pathway II) lentigo maligna melanoma/high-CSD melanoma, and (Pathway III) desmoplastic melanoma. The second melanoma category is (ii) melanomas not consistently associated with cumulative solar (no CSD) which contains (Pathway IV) spitz melanomas, (Pathway V) acral melanoma, (Pathway VI) mucosal melanoma, (Pathway VII) melanomas arising in congenital nevi, (Pathway VIII) Melanomas arising in blue nevi, and (Pathway IX) uveal melanoma (Table 1).

Table 1. Classification of Melanoma (Modified from 2018 WHO Classification)[a]

A. Melanomas typically associated with CSD
Pathway I. Superficial spreading melanoma/low-CSD melanoma
Pathway II. Lentigo maligna melanoma/high-CSD melanoma
Pathway III. Desmoplastic melanoma
B. Melanomas not consistently associated with cumulative solar damage (no CSD)
Pathway IV. Spitz melanomas
Pathway V. Acral melanoma
Pathway VI. Mucosal melanomas
Pathway VII. Melanomas arising in congenital nevi
Pathway VIII. Melanomas arising in blue nevi
Pathway IX. Uveal melanoma
C. Nodular melanoma (may occur in any or most of the pathways)

Abbreviation: CSD, cumulative solar damage

[a] Primary source for this information is "The 2018 World Health Organization Classification of Cutaneous, Mucosal, and Uveal Melanoma - Detailed Analysis of 9 Distinct Subtypes Defined by Their Evolutionary Pathway" [36]

Nodular melanoma may occur in several of these pathways. Every single melanoma subtype has its own evolutionary lineage also known as pathway starting from a distinct precursor lesion followed by a different progression risk through melanoma stages to develop in an invasive tumorigenic melanoma resulting in a variable threat to metastasize [36]. In general, most of melanomas evolve through two steps of progression, the first is characterized by early lesions recognized as a pigmented patch expanding along the radii of an imperfect circle horizontally within in the skin which is known as radial growth phase (RGP) (Fig. 3). In the second step of progression, a tumor is developed which may infiltrate into the dermis or elevate the epidermis forming a nodule resulting in an vertical growth above and/ or below the skin, known as vertical growth phase (VGP) [36, 37]. Furthermore, melanoma in the absence of VGP lesions have excellent prognosis with very low risk of metastasis [38, 39].

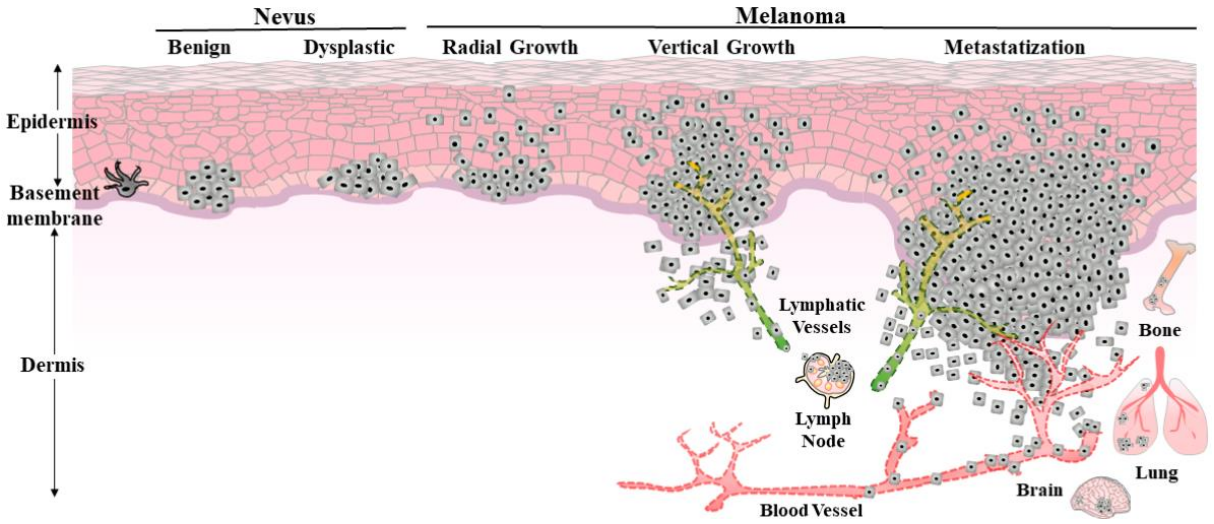

Figure 3. Schematic representation of melanoma progression: Proliferation and aggregation of melanocytes at the basement membrane in the epidermis leads to the initial step of nevus formation, benign nevus followed by altered growth pattern into dysplastic nevus. Continuous and unchecked melanocyte proliferation allows penetration of the epidermal/dermal junction by a radial growth phase. During vertical growth phase, cells grow into the dermis leading to interaction with other cell types and gain physical access to lymphatics and blood vessels resulting in brain, lung and bone metastasis. Primary source "Biomarkers for Diagnosis, Prognosis and Response to Immunotherapy in Melanoma" [40].

Based on the growing and developing RGP stage of melanoma, early melanoma can be described in the ABCDE mnemonic. The "A" stands for asymmetry, "B" for border irregularity, "C" for color variegation, "D" diameter larger than 6 mm, and "E" for evolution/elevation or timing of lesion's growth [22].

The SSM/low CSD melanoma is enlarging radially on sun exposed areas of the human body and is spreading upward also known as pagetoid epidermal invasion. Further characteristics are lesions which are flat, slow-growing, irregularly bordered lesions with variegated pigment [41, 42]. The most common driver mutation in SSM is the *BRAF* gain of function mutation which in its most common mutation results in a substitution from a valine (V) to a glutamic acid (E) at position 600 also known as $BRAF^{V600E}$ [43, 44, 45]. Additional to BRAF or NRAS mutations is a telomerase (*TERT*) promoter mutation in most intermediate lesions and melanoma in situ whereas the biallelic *CDKN2A* inactivation is associated during the transition to invasive melanoma. *PTEN* and *TP53* mutations were only present in advanced primary melanomas [36, 46, 47].

Nodular melanoma is a rapidly growing lesion lacking RGP, characterized by VGP and forms a tumor very early with the potential for metastasis [37, 48]. The tumors are mostly ulcerated, and NM are further characterized by elevation above the epidermis forming a commonly amelanotic, distinguished by a pink papulonodular lesion, and additionally may infiltrate the dermis. NM can occur in any of the classified pathways and share genetic alteration of other

melanomas [36, 48]. A high frequency of *BRAF* and *NRAS* mutations was found in nodular melanoma [49, 50]. NM have a worse prognosis on average compared to other melanomas [48].

Lentigo maligna melanoma is also known as melanoma arising in a Hutchinson melanotic freckle [51]. LMM is associated with severe cumulative solar damage causing solar elastosis, lentiginous growth pattern in the epidermis defined by melanocytic proliferation as single cells along the dermal-epidermal junction [36, 52]. It has a RGP of which lesions evolve from patch to plaque stages followed by a slower tumorigenic VGP compared to SSM as well as a poorly circumscribed border, and less pigmentation than SSM whereas some LMM lesions are almost entirely amelanotic [36, 44, 53]. Driver mutations in LMM include *NF1*, $BRAF^{V600K}$, or other non-V600E mutations, *NRAS*, and occasionally *KIT* [36, 44, 54].

Changes in various signaling pathways by impairment or hyper-activation in the cell cycle and thereby controlling the proliferation of cells as well as the capability of evading cell death may lead to malignant transformation and human cutaneous melanoma development. Major signaling pathways in melanoma for the regulation of cell cycle progression and apoptosis include cyclin/CDK, Ras/Raf/MEK/MAPK, JNK/c-Jun/AP-1, PI3K/Akt/PTEN/mTOR, IKK/I-κB/NF-κB, Wnt/ β-catenin, Notch, Jak/STAT and MITF [2, 55].

The cell cycle leads to cellular division and duplication of cells. Normal somatic cells are dependent upon mitogenic signals such as growth factors and cytokines to proliferate [56]. The cell cycle contains a G1 phase comprising the preparation of DNA synthesis, a DNA synthesis phase (S), a G2 phase including the preparation for mitosis and a mitosis phase (M). The transitions from G1 to S phase as well as G2 to M phase are controlled by checkpoint proteins. The progression through all the stages is controlled by a complex mechanism regulated by cyclin-dependent kinases (CDKs) and their cyclin partners. The cell cycle regulation is impaired in cancer cells leading to uncontrolled proliferation [56, 57]. The transcription factor E2F regulates the G1/S phase transition leading to the expression of targets genes involving DNA synthesis. E2F activity is inhibited by binding of the tumor suppressor retinoblastoma (pRb), its phosphorylation by CDK4/6-cyclin D1 and CDK2-cyclin E1 complexes leads to dissociation of the pRb/E2F complex liberating E2F [57, 58]. Cyclin/CDK activity is regulated by CDK inhibitors such as $p21^{CIP1}$, $p27^{KIP1}$ and $p57^{KIP2}$ which are encoded by the *CDKN1* gene family (*CDKN1A*, *CDKN1B* and respectively *CDKN1C*). There are also other CDK inhibitors such as $p16^{INK4a}$, $p15^{INK4b}$, $p18^{INK4c}$ and $p19^{INK4d}$ which are encoded by the *CDKN2* family including genes *CDKN2A*, *CDKN2B*, *CDKN2C* and respectively *CDKN2D*. They are specifically inhibiting CDK4 and CDK6 [59]. In 40% of familial melanoma, *CDKN2A* is mutated and inactivated which usually encodes two tumor suppressor proteins $p16^{INK4a}$ and $p14^{ARF}$. In about 50% of melanomas, $p16^{INK4a}$ shows deletions, 9% point mutations and 20-75% promoter and hypermethylation [60, 61]. Mutations of the other tumor suppressor protein $p14^{ARF}$ allow degradation of p53 by releasing its binding partner, a nuclear-localized E3 ubiquitin ligase, the

murine double minute 2 (MDM2) resulting in reduction of cell cycle arrest and apoptosis [4, 62]. However, mutations of *TP53* gene encoding p53 are rare in melanoma [61, 63]. In some rare cases in familial melanoma, CDK4 is amplificated or mutated resulting in incapable binding and inhibitory function of $p16^{INK4a}$ [64, 65]. The disruption of the G1/S checkpoint in melanoma plays a pivotal role at the transition to invasive melanoma [46].

Another important altered pathway in melanoma is the Ras/Raf/MEK/MAPK pathway which is a central regulator of cell proliferation and survival. Rat sarcoma (Ras) is a small GTPase situated at the plasma membrane activating downstream the Raf/MEK/MAPK as well as the PI3K/Akt pathway. The two most frequent mutations in the Ras/Raf/MEK/MAPK pathway are $BRAF^{V600E}$ and $NRAS^{Q61(K/L/R)}$ [46, 55]. The N-Ras mutant is unable to hydrolyze GTP resulting in constitutive downstream signaling. 15-30% of melanoma cases are associated with a *NRAS* mutation whereas mutations of other RAS isoforms are rare [55, 66]. Neurofibromin 1 (NF1) is a tumor suppressor and its inactivation in melanoma leads to longer RAS activation, sustained MAPK pathway and driving proliferation [67]. The mutation of serine/threonine protein kinase BRAF generating a constitutive active conformation by alteration of the glycine-rich loop in the catalytic domain resulting in a constitutive activation of MEK which further activates the growth-promoting extracellular signal-regulated kinase (ERK) pathway [3, 68]. MAPK signaling can lead to increased cyclin D1 expression leading to interaction with CDK4/6 resulting in phosphorylation and inhibition of retinoblastoma [55, 69].

The phosphatidylinositol-3-kinase (PI3K)/Akt pathway regulates cell growth and proliferation. Furthermore, growth factor stimulated receptor tyrosine kinase (RTK) can activate PI3K or directly by RAS [62, 70,71]. PI3K activates downstream AKT which leads to cell growth and survival by multiple effectors such as mTOR, Bad and Mdm2 [72, 73, 74]. In melanoma, the tumor suppressor PTEN of the PI3K/Akt pathway can be mutated and inactive contributing to melanoma development [75, 76]. Upstream of MAPK and PI3K pathways resides a RTK called C-KIT which is rarely mutated, however, *c-KIT* mutations in melanoma are important in the pathogenesis of melanoma, especially in acral and mucosal melanoma [62, 77, 78].

In 1-2% of familial melanoma, Microphthalmia transcription factor (*MITF*) is mutated which regulates the development, differentiation and function of melanocytes [79, 80, 81]. Low *MITF* expression results in increased invasiveness of melanoma cells whereas high expression is associated with decreased invasiveness [62, 82].

The upregulation of the NF-κB levels may play a role in progression of melanoma by a number of constitutively high expression of NF-κB-regulated chemokines as well as in metastasis [83, 84, 85, 86]. NF-κB might also induce the overexpression of matrix metalloproteinases 9 (MMP-9) and MMP-2 inducing degradation of the extracellular matrix (ECM) by the activation of osteopontin (OPN) [87, 88].

3. Staging of melanoma

Staging of melanoma includes four main systems (i) the Clark scale, (ii) the Breslow scale, (iii) TNM staging and (iv) Number stages. Five anatomical levels of invasion or depth of the lesion through the layers of the dermis is described by the Clark scale whereas the thickness of melanoma in the skin is defined by the Breslow scale classified by stages regarding tumor measurements in millimeters. The number staging system is comprised of Stage 0 to Stage 4 combining information on lesion's depth and the TNM staging [1, 37, 89]. The TNM (Tumor, Node, Metastasis) staging system implemented by the American Joint Committee on Cancer (AJCC) is most widely accepted for staging and classification at initial diagnosis in melanoma. In 2018, the eighth edition AJCC melanoma staging system was implemented in the United States. Since 1998, the AJCC uses a large internationally database (ten institutions in the United States, Europe and Australia) consisting of more than 46,000 patients with diagnosed melanoma stages I, II, and III as well as stage IV which includes 10,000 patients during a time span of eight years. The melanoma specific survival (MSS) of all patients of the AJCC database regarding melanoma stages I, II, and III is shown in Fig. 2A. The stage I patients had a 5-year and 10-year MSS rates of 98% and 95%, stage II patients of respectively 90% and 84% (Fig. 2B) whereas stage III patients of respectively 77% and 69% (Fig. 2C) [90, 30]. Furthermore, most of melanoma patients in early-stage (stage I and II) have an overall well prognosis whereas prognosis differs in stage III. Stage IV melanoma patients had a poor prognosis with a median survival of 6-7.5 months after initial Stage IV diagnosis and a 5-year survival of less than 10% [90, 91, 92]. The TNM classification includes three categories, Breslow tumor thickness measurements and ulceration (T-category), the distant metastases to lymph nodes and various tissues, and serum lactate dehydrogenase (LDH) level (M-category) as well as the N-category. The N-category is defined by the number of tumor-involved regional lymph nodes and the extent of nodal metastases which are referred as regional lymph nodes metastases. Furthermore, "clinically occult" regional nodal metastasis is defined in a patient with no clinical or radiographic evidence of regional lymph node metastasis, however, microscopically identification of tumor-involved regional nodal metastasis are detected by sentinel lymph node (SLN) biopsy which used to be referred as microscopic nodal metastasis. In contrast, "clinically detectable" nodal metastases are identified by clinical, radiographic or ultrasound examination which are used to be referred as macroscopic nodal metastasis [90, 30]. The majority of diagnosed melanoma patients with regional metastasis is comprised of clinically occult nodal metastasis which have a better survival rate than patients with clinically evident disease [93]. The second criteria of the N-category is the presence of in-transit, satellite and/ or microsatellite metastases which were grouped together as one N-category criterion which is recently referred as non-nodal locoregional metastases. The satellite metastases used to be characterized as any foci of clinically evident cutaneous and/or subcutaneous

metastases occurring within 2 cm of the primary tumor. The microsatellites are defined as microscopic cutaneous and/or subcutaneous metastases adjacent or deep to, and completely discontinuous from the primary melanoma with stroma between them and no minimum distance from the primary tumor. In-transit metastases were used to be considered as cutaneous and/or subcutaneous metastases including a distances of more than 2 cm from the primary tumor. Recently satellite and in-transit metastases were merged together and are associated as intralymphatic regional metastases. Thus, the N-category can be categorized by N1, N2 and N3. The subcategory N1 is defined by one tumor-involved node or any number of in-transit, satellite, and/or microsatellite metastases with no tumor-involved nodes. N2 category is characterized by two or three tumor-involved nodes or any number of in-transit, satellite, and/or microsatellite metastases with one tumor-involved node. N3 category is classified by four or more tumor-involved nodes or any number of in-transit, satellite, and/or microsatellite metastases with two or more tumor-involved nodes. An additional subcategory of “a” is characterized as clinically occult and “b” for clinically detectable. The subcategory “c” varies depending on the subcategory of N1 to N3. N1c comprises no regional lymph node disease, N2c has one clinically occult or is clinically detectable whereas N3c has two or more clinically occult or is clinically detectable.

The T-category is defined into eight T subcategories (T1a-T4b), the melanoma thickness thresholds are classified of 1.0, 2.0 and 4.0 mm and should be rounded to the nearest 0.1mm. Thus, T2 subcategory includes tumor thickness from 1.05 to 2.04 mm. The subcategory T1a is defined as nonulcerated melanomas with primary tumor thickness less than 0.8 mm whereas T1b subcategory has a thickness from 0.8 to 1.0 mm. The T3 subcategory has a primary tumor thickness bigger than 2.0 mm and up to 4.0 mm whereas thickness bigger than 4.0 mm is considered as T4 category. Moreover, subcategory “a” describes without ulceration whereas “b” is associated with ulceration. The definition of ulceration is the full thickness absence of an intact epidermis above of the primary tumor in combination with a host reaction such as fibrinous and acute inflammatory exudate above the primary tumor.

The M category is subcategorized from M1a(0) to M1d(1) depending on the anatomic site(s) of metastasis and status of the LDH level. M1a is including non-visceral distant metastasis such as distant cutaneous, subcutaneous tissue, muscle and distant (nonregional) lymph nodes. M1b is defined by lung metastasis including with or without M1a definition. Melanoma metastases to any other visceral site excluding the CNS are categorized by M1c whereas M1d includes metastasis of the CNS involving the brain, spinal cord and other components of the CNS. Elevated LDH level is designated as “1” and “0” for not elevated [90, 30]. The summary of the staging system by AJCC including all three categories (T, N, M) in combination with their subcategories regarding their specific prognostic stage groups is shown in Table 2.

Table 2. Summary of AJCC Pathological (pTNM) prognostic Stage Groups[a]

WHEN T IS…	AND N IS…	AND M IS…	THEN THE PATHOLOGICAL STAGE GROUP IS…
Tis	N0[b]	M0	0
T1a	N0	M0	IA
T1b	N0	M0	IA
T2a	N0	M0	IB
T2b	N0	M0	IIA
T3a	N0	M0	IIA
T3b	N0	M0	IIB
T4a	N0	M0	IIB
T4b	N0	M0	IIC
T0	N1b, N1c	M0	IIIB
T0	N2b, N2c, N3b or N3c	M0	IIIC
T1a/b–T2a	N1a or N2a	M0	IIIA
T1a/b–T2a	N1b/c or N2b	M0	IIIB
T2b/T3a	N1a–N2b	M0	IIIB
T1a–T3a	N2c or N3a/b/c	M0	IIIC
T3b/T4a	Any N ≥N1	M0	IIIC
T4b	N1a–N2c	M0	IIIC
T4b	N3a/b/c	M0	IIID
Any T, Tis	Any N	M1	IV

[a] The original and primary source for this information is the AJCC Cancer Staging Manual, eighth edition (2017) published by Springer International Publishing (Gershenwald JE, Scolyer RA, Hess KR, et al. Melanoma of the skin [30].

[b] Pathological stage 0 (melanoma in situ) and T1 don't require pathological evaluation of lymph nodes to complete pathological staging. Usage of clinical N category information to assign their pathological stage.

4. Tumor microenvironment of melanoma

Melanoma cells interact with the tumor microenvironment (TME), thus the mediated crosstalk between cancer, stromal cells, and immune cells within the surrounding microenvironment via cytokines, growth factors, and their receptors are important for cell motility, invasion and metastasis [94, 95]. Therefore, tumor cells reciprocally interact with the adjacent stroma and don't act in isolation leading to co-evolution of the primary tumor as well as of stromal cells [96, 97]. The TME is composed of the tumor stroma including fibroblasts, keratinocytes, endothelial cells, immune cells, soluble molecules and the extracellular matrix (ECM) (Fig. 4) [98, 99].

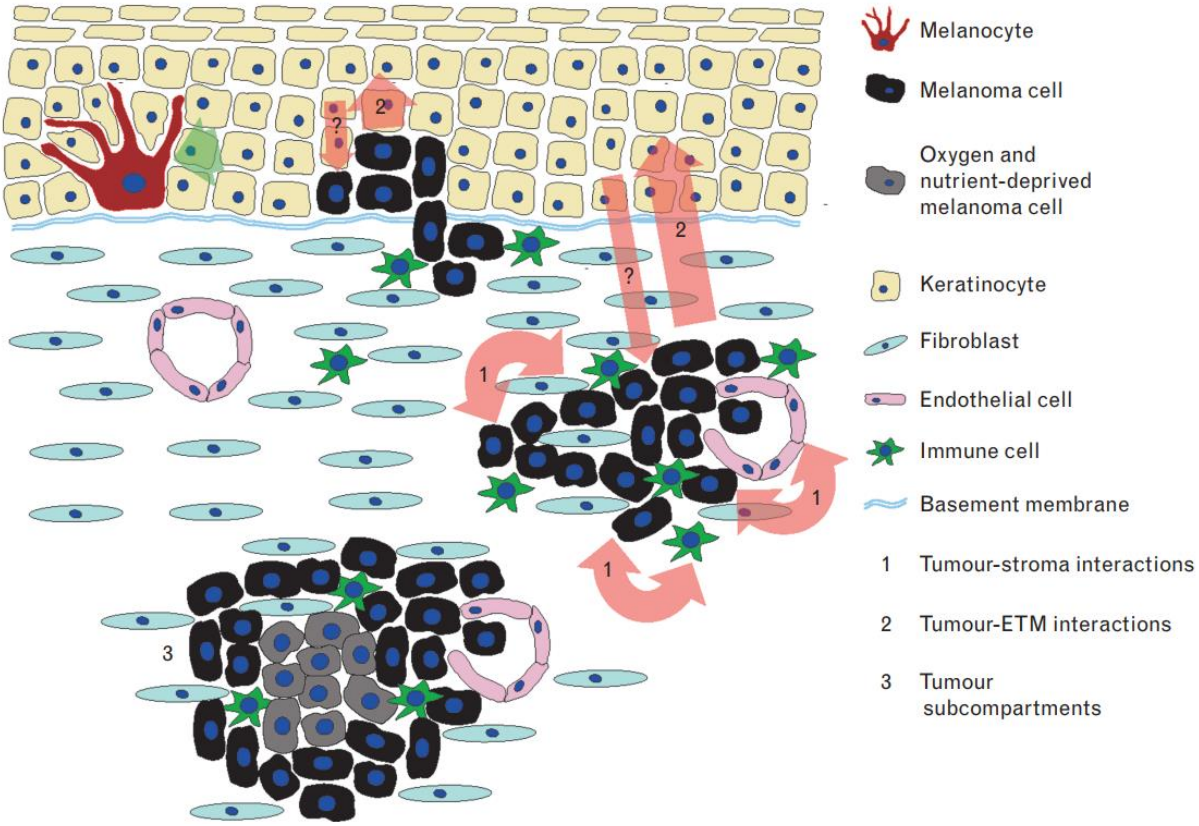

Figure 4. Schematic representation of melanoma tumor microenvironment: The bilateral paracrine communication between melanoma cells and the stroma, which includes fibroblasts, endothelial cells, immune cells, soluble molecules, and the extracellular matrix (1 - red two-way arrows) The melanoma cells dissemination taking control over the epidermal tumor microenvironment (ETM) (2 - red one-way arrows). Primary source is "Melanoma's connections to the tumour microenvironment" [98].

4.1. Cancer-associated fibroblasts (CAFs) in melanoma

In the TME, fibroblast are activated by transformed cells due to paracrine stimulation resulting in cancer-associated fibroblast (CAFs) which have pleiotropic pro-tumorigenic functions in melanoma such as in proliferation and the remodeling of the ECM for tumor invasion [95, 100]. CAFs have heterogenous subtypes and properties with various functions depending on the organ origin [101]. However, commonly used biomarkers for CAFs are α-smooth muscle actin (α-

SMA), fibroblast activation protein (FAP), S100A4, platelet-derived growth factor receptors (PDGFRα/β) or vimentin [102]. Melanoma-associated fibroblasts overexpress various pro-mitogenic and pro-angiogenic factors such as basic-fibroblast growth factor (b-FGF), hepatocyte growth factor (HGF), stromal-derived factor (SCF), and vascular endothelial growth factor (VEGF) confirming the pro-mitogenic attitude of melanoma-associated fibroblasts [103]. Additionally, melanoma CAFs express α-smooth muscle actin (α-SMA) which is a cytoskeletal protein associated with transforming growth factor ß TGF-β production contributing to tumor progression and ECM remodeling [102, 103]. Furthermore, CAFs can influence cancer cells via autocrine and paracrine signaling by secreting additional growth factors such as TGF-β, fibroblast growth factor 5 (FGF5), stromal-derived factor (LIF), growth arrest-specific protein 6 (GAS6), platelet derived growth factor (PDGF) and osteopontin (OPN) [101]. The immune-regulatory ability of melanoma CAFs is demonstrated by the production variety of cytokines and chemokines such as interleukin-1 α (IL-1α), IL-1β, IL-6, IL-8, and C-X-C motif chemokine ligand 10 (CXCL10). Additionally, inflammatory cytokines IL-6, IL-8 are linked with melanoma invasiveness [103, 104]. The melanoma CAFs overexpress programmed death ligand-1 and -2 (PD-L1 and PD-L2) which are immune checkpoint molecules expressed on the cell surface inducing T cell deactivation [103, 99]. Furthermore, higher motility is associated with melanoma cells cultured with CAF supernatants compared with normal fibroblasts and demonstrate longer persistence of phosphorylated FAK which is linked to higher metastatic and aggressive potential of melanoma [103, 105]. Melanoma-associated fibroblast show an upregulation of matrix metalloprotease such as MMP1 which indirectly plays a role in tumor invasion by matrix degradation [95, 103].

4.2. Tumor-associated macrophages (TAMs) in melanoma

In the TME, tumor cells co-exist with immune cells such as macrophages, dendritic cells (DCs), mast cells, natural killer (NK) cells, as well as T and B lymphocytes [106]. The tumor-associated macrophages (TAMs) content of the primary melanoma tumor ranges from 9% to 30%, a similar pattern can be seen in breast cancer [107]. Furthermore, extensive TAM infiltration often correlates with poor prognosis in several cancers such as in breast-, cervix- and bladder cancer as well as in melanoma [108, 109]. Moreover, TAMs are found in melanoma and play a role in stimulating angiogenesis and vascularization, stroma formation and dissolution, promoting tumor growth as well as enhancing migration and invasion [110, 111]. TAMs are formed from blood circulating monocytes and recruited by cancer cells derived chemoattractants like cytokines and chemokines such as colony stimulating factor-1 (CSF-1), CCL-2, interleukin-34 (IL-34), vascular endothelial growth factor A (VEGFA) or CXCL12 [110, 112]. TAMs are involved in melanomagenesis and regarding cancer initiation, they create an inflammatory microenvironment followed by suppressing the anticancer activity of the immune system [110].

Therefore, in the TME, macrophages have initially an anti-tumor activity which is associated with classically activated polarized M1 macrophages. During tumor progression, a gradual switching of TAMs polarization from M1 to M2-like macrophages occurs leading to pro-tumor activity [113]. Melanoma cells produce autocrine factors modulating the activity of the immune response cells as well as the TME, which include Granulocyte-macrophage colony-stimulating factor (GM-CSF), CCL2, IL-8/CXCL-8, TGF-β, IL-1, IL-6 and IL-10. The GM-CSF and CCL2 have the highest influence on melanoma macrophages [110, 114]. GM-CSF secretion results in inhibition of the cytotoxic effect of macrophages. High concentration of CCL2 leads to M1 macrophage infiltration aiming to destroy the tumor whereas the decreased concentration of CCL2 resulting in M2 macrophage accumulation leading to tumor growth [114, 115]. Additionally, CCL2 and GM-CSF facilitates angiogenesis by stimulating the expression of hypoxia-inducible factor-1 α (HIF-1α) and hypoxia response element (HRE) resulting in increased VEGF-A expression [110, 116]. The production of IL-6 by melanoma leads to TAMs growth followed by IL-10 expression which drive immunosuppression [110, 114].

4.3. Cytokines & receptors in melanoma

4.3.1. IL-34/CSF-1R & IL-34/PTPRζ1

In 2008, the human IL-34 was identified as a selective protein promoting monocyte viability. The human *IL-34* gene shares an amino acid sequence identity of 99,6% with the chimpanzee, 72% with rats, and 71% with mice [117]. IL-34 demonstrates no sequence similarity with any other growth factor, including macrophage colony-stimulating factor (M-CSF-1, also known as CSF-1) [118, 119]. However, IL-34 and CSF-1 bind to the same receptor M-CSF-1 receptor (M-CSF1-R; also known as CSF1-R, CD115, FMS) and they can activate different signaling pathways and mediate distinct biological functions due to different cytokine interactions with CSF-1R (Fig. 5) [118, 120].

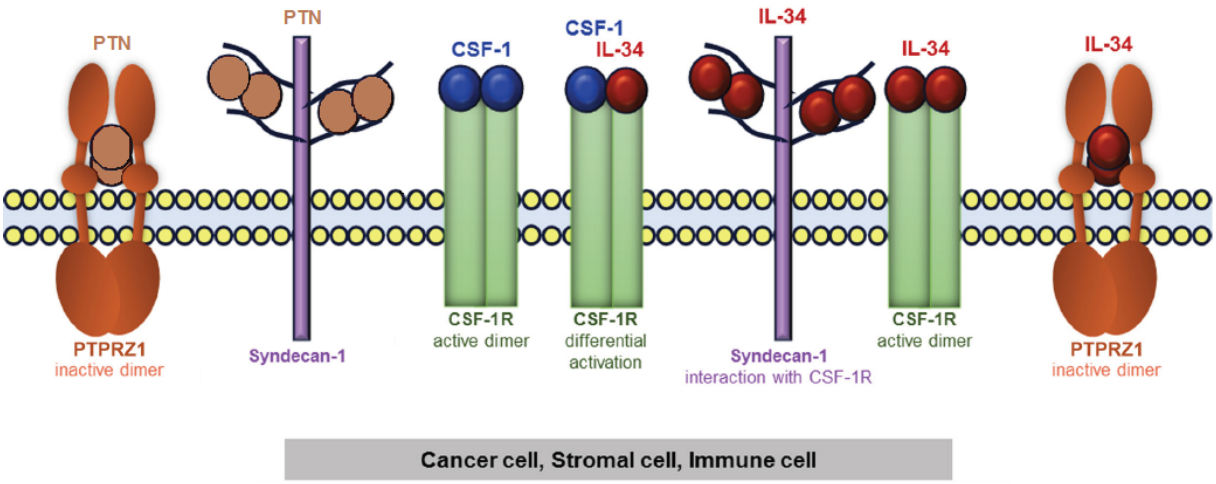

Figure 5. Schematic representation of IL-34, CSF-1 and PTN receptors in tumor tissue

consisting of cancer cells, stromal cells, and immune cells: IL-34 and CSF-1 bind to CSF-1R. Heteromeric CSF-1/IL-34 can also form, which may differentially regulate activation/localization of CSF-1R. Additionally, IL-34 can bind to syndecan-1, which then regulates CSF-1R activity. IL-34 and PTN bind to PTPRZ1. Finally, PTN also binds to syndecan-1. Edited image from primary source "Impact of IL-34 mRNA expression breast cancer" [121].

IL-34 and CSF-1 have similar helical bundle folds and both of these cytokines are head-to-head dimers of which IL-34 is non-covalently associated whereas CSF-1 is linked through interchain disulfide bonds. Additionally, N-linked oligosaccharides are crucial for IL-34 stability but not for CSF-1 [122]. Moreover, CSF-1 has hydrophilic hydrogen-bond interactions with the CSF-1R whereas IL-34 appears to have hydrophobic interactions with this receptor resulting in a prolonged and strong transmembrane signaling [117, 118, 119, 120]. Additionally, IL-34 and CSF-1 have different binding anchorage points with CSF-1R which could result in distinct signaling pathways [118, 123]. Moreover, the binding affinity of IL-34 to CSF-1R is higher than of CSF-1 [124]. Further differences in the complexes of IL-34:CSF-1R and CSF-1:CSF-1R are a 27° change of the receptor domain D3 orientation relative to D1-D2. Thus, IL-34 binding causes a rotation between D2 and D3 resulting in an elongated/linear pose which is differently compared to the kinked configuration of CSF-1 bound form [119]. Furthermore, the apparent rigidity of the IL-34 structure is different from the more plastic CSF-1 structure which undergoes local rearrangements to accommodate receptor binding [119, 125]. Moreover, CSF-1 is clamped deeper by the CSF-1R D2-D3 junction compared to IL-34, thus overlapping but different sets of CSF-1R segments are used in binding each of these ligands. In order to compensate for the loss of some D2 interactions, IL-34 adopts amino-terminal and carboxy-terminal extensions to contact D3 [126].

IL-34 and CSF-1 are both homodimeric cytokines competing to bind to CSF-1R, however, an in vitro study demonstrated that these cytokines could even form heterodimers which may play a role in the tissue homeostasis and development (Fig. 5) [127]. IL-34 and CSF-1 also have similarities in supporting cell growth and survival of monocytes as well as their differentiation into immunosuppressive M2 macrophages which can be prevented by IFNγ and GM-CSF [128, 129]. Additionally, IL-34 and CSF-1 allows for complementary activation of the CSF-1R [124]. Differences between these cytokines were found in chemokine production in which IL-34 stimulated macrophages inducing eotaxin-1 (CCL11) whereas CSF-1 mediated signaling led to increased concentrations of monocyte chemotactic protein 1 (MCP-1, also known as CCL2) [120]. In addition, IL-34 can lead to elevated secretion of IL-10 and CCL17 in macrophages compared with CSF-1 exposed macrophages [130]. Biological functions of IL-34/CSF-1R various depending on cell types, however, may include differentiation, proliferation, adhesion and migration of cells as well as angiogenesis and inflammation [131]. The cancer cell production of IL-34 binds via autocrine signaling with CSF-1R on their tumor cell surface, thereby activating

pathways to stimulate cancer cell growth and diffusion as well as their resistance to chemotherapeutic drugs [118, 132]. In addition, paracrine signaling also plays an important role by secretion of IL-34 by cancer cells or/ and immune cells triggering CSF-1R on TAMs leading to angiogenesis as well as extravasation of immune-inflammatory cells [118, 133, 134] The binding of IL-34 to CSF-1R can trigger various signaling pathways such as NF-κB, phosphoinositide 3-kinase (PI3K)/AKT, p38 mitogen-activated protein kinase (MAPK), extracellular signal-regulated protein kinases 1 and 2 (ERK1/2), c-Jun N-terminal kinase (JNK), Janus kinase (JAK), signal transducer, and activator of transcription (STAT)3 (Fig. 6) [118].

Syndecan-1 (also known as CD138) was discovered as an additional functional IL-34 receptor which also regulates the IL-34 activation levels of the CSF-1R. Moreover, IL-34 induced myeloid cell migration [135].

Recently, it was shown that IL-34 additionally binds to another receptor, the receptor-type protein–tyrosine phosphatase zeta (PTP-ζ1, also known as RPTPβ/ζ, PTPRζ1 and PTPRZ1) a cell surface chondroitin sulfate proteoglycan that is primarily expressed on neuronal progenitors and glial cells (Fig. 5, 6) [136]. Additionally, PTPRζ1 is expressed in human cutaneous melanoma [137, 138]. Based on TCGA data, *PTPRZ1* gene expression is up-regulated in cervical squamous cell carcinoma and endocervical adenocarcinoma (CESC), glioblastoma multiforme (GBM), LGG, lung squamous cell carcinoma (LUSC), and down-regulated in breast invasive carcinoma (BRCA), colon adenocarcinoma (COAD), prostate adenocarcinoma (PRAD), rectum adenocarcinoma (READ), and stomach adenocarcinoma (STAD) [139]. Additionally, *PTPRZ1* is expressed in melanocytes, keratinocytes and fibroblasts [140]. Ligand binding to PTPRζ1 leads to oligomerization of the receptor resulting in inactivation of phosphatase activity and thereby increased tyrosine phosphorylation of substrates [141]. In glioblastoma cells, the binding of IL-34 and PTPRζ1 triggered a series of intracellular events that inhibited motility, clonogenicity, and proliferation via increased tyrosine phosphorylation of paxillin and focal adhesion kinase (FAK) [118, 136].

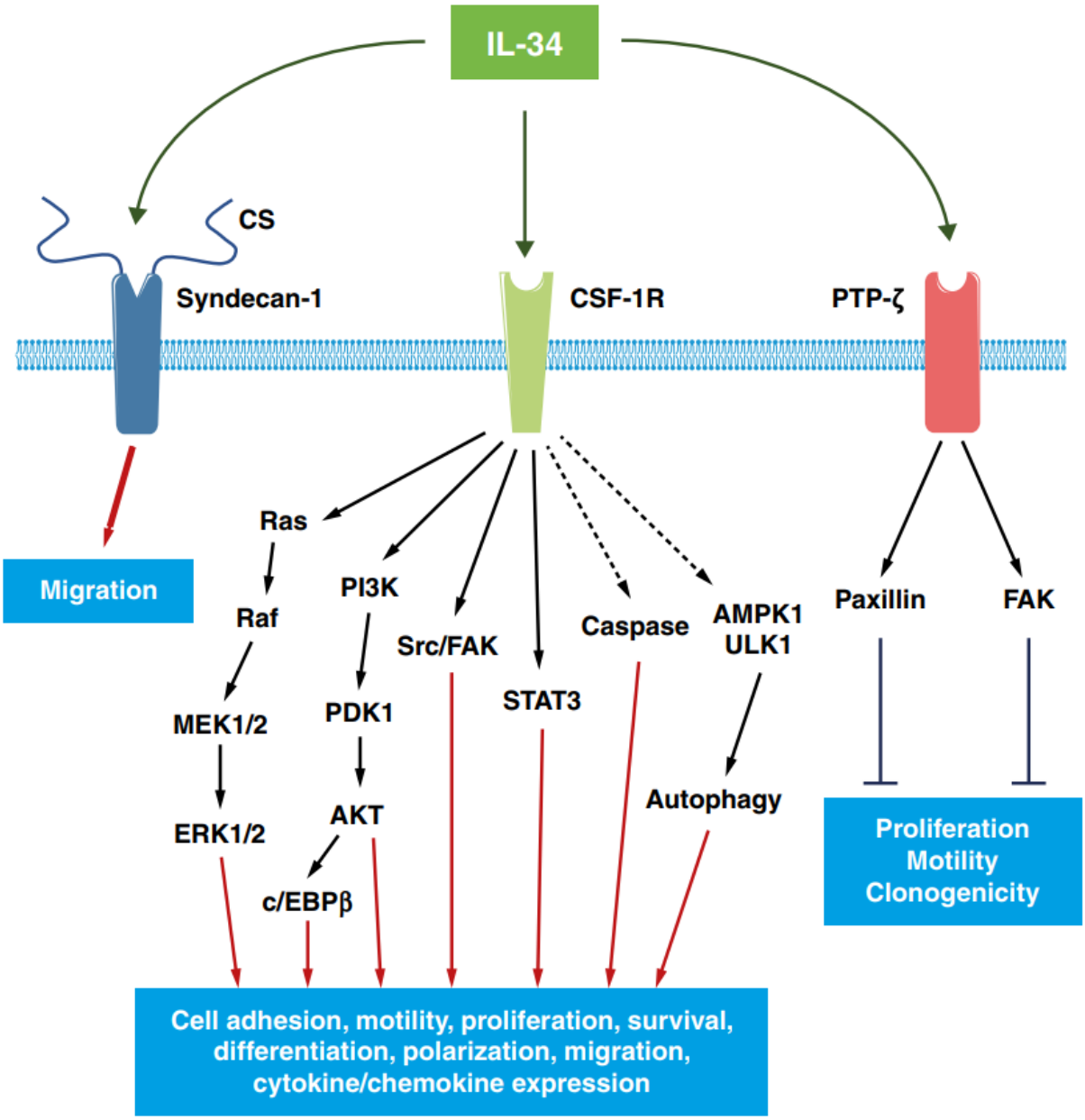

Figure 6. Schematic representation of IL-34 binding to PTPRζ1, CSF-1R & Syndecan-1: IL-34 binds to the extracellular domains of CSF-1R and PTP-ζ in addition to the chondroitin sulfate (CS) chains of syndecan-1, leading to activation of several signaling pathways such as extracellular signal-regulated kinase 1/2 (ERK1/2), AKT, focal adhesion kinase (FAK), and signal transducer and activator of transcription 3 (STAT3) and Paxillin. These pathways are regulating major cellular functions such as cell differentiation, proliferation, survival, polarization, metabolism, cytokine/ chemokine expression in addition to cellular adhesion and migration. Edited from primary source "Interleukin-34, a comprehensive review" [142].

IL-34 is produced by various cell populations such as endothelial cells, adipocytes, neurons, macrophages, fibroblasts, and epithelial cells. In addition this cytokine is constitutively expressed in several human tissues such as brain, thymus, heart, liver, spleen, testis, prostate, ovary, small intestine and colon [118]. In the skin, epidermal keratinocytes express IL-34 which is critical for the development and maintenance of Langerhans cells [143,] Furthermore, IL-34 synthesis is increased by pro-inflammatory cytokines such as TNF-α and IL-1β in several cell

types such as fibroblasts and epithelial cells through NF-κB- and MAP kinase-dependent pathways [118, 144, 145, 146]. IL-34 is expressed in various cancers types such as brain-, breast-, colorectal-, lung-, neck-, biliary-, ovarian- and skin cancer of which lung- and colorectal cancer were associated with unfavorable prognosis and poor survival thus IL-34 might be involved in tumorigenesis [118, 147, 148, 149]. In a metastatic refractory melanoma patient, increased IL-34 expression was detected in the melanoma tissue which acquired resistance to anti-PD-1 immunotherapy (Nivolumab) [150].

Collectively, IL-34 binding to M-CSF1-R, PTPRζ1 as well as to Sydecan-1 can activate several signaling pathways that regulate major cellular functions, including differentiation, polarization, survival, proliferation cytokine/chemokine expression, motility, and migration (Fig. 6, 9) [118]. However, whether binding of IL-34 to its mentioned receptors play a role in melanoma as well its downstream signaling are not well understood.

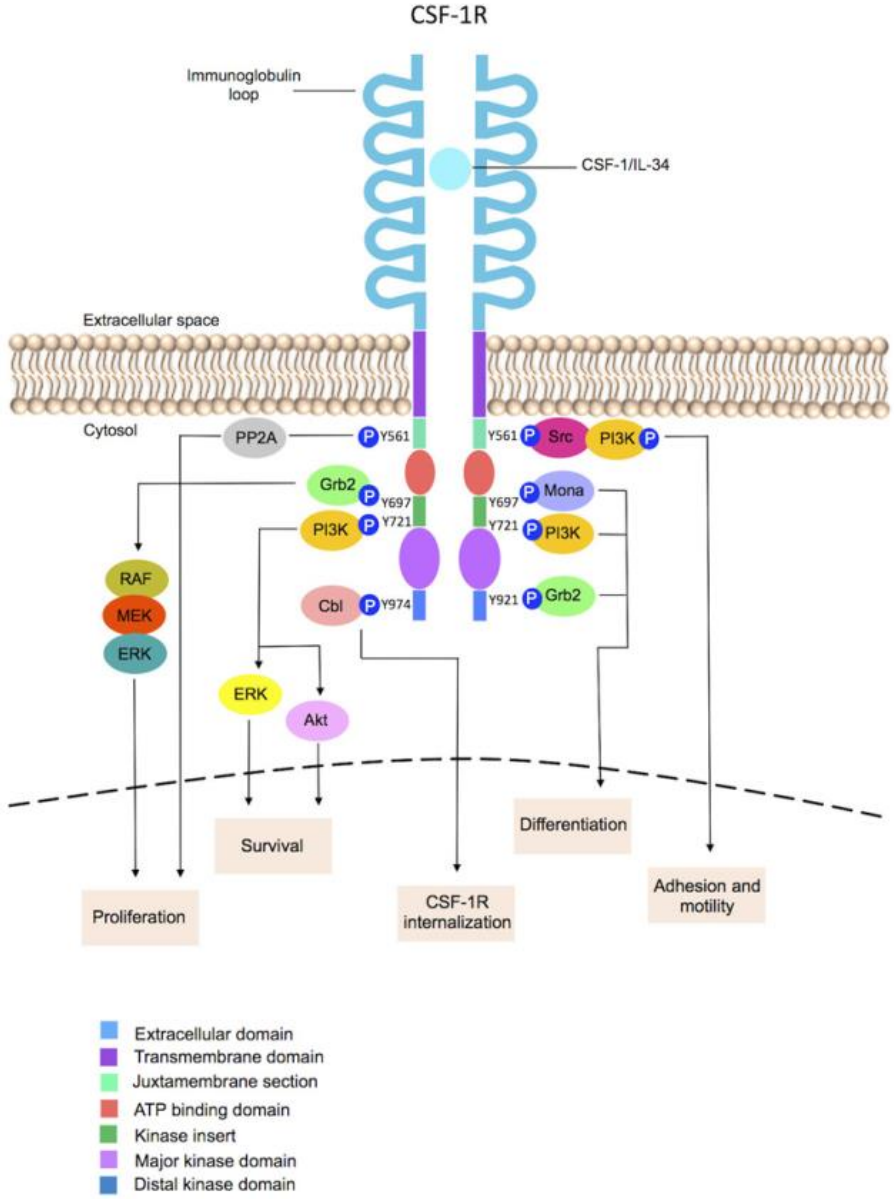

Figure 9. Schematic representation of CSF-1 binding to CSF-1R: The binding of CSF-1 or

IL-34 induces CSF-1R dimerization, resulting in auto-phosphorylation and the association of signaling molecules with CSF-1R via their phosphotyrosine-binding domain. The downstream pathways leading to gene expression promoting such as proliferation, differentiation, survival as well as adhesion and motility of the cell. Abbreviations: Cbl, Casitas B lineage; MEK, mitogen-activated protein kinase kinase; Mona, monocyte adaptor. Primary source is “Role of the colony-stimulating factor (CSF)/CSF-1 receptor axis in cancer” [151].

4.3.2. PTN/PTPRζ1

Pleiotrophin (PTN) is a secreted polypeptide and it’s part of the heparin-binding growth factors family together with Midkine (MK). PTN used to be known as p18, heparin-binding growth factor-8, heparin-binding growth-associated molecule, osteoblast-specific factor 1, heparin-binding neurotrophic factor and heparin affin regulatory peptide. PTN protein is highly conserved among species including human, rat, mouse, chicken and bovine. It is homologous to MK sharing about 50% sequence identity [152, 153, 154]. Originally, PTN was described as a neurite outgrowth promoting molecule in brain neurons suggesting to play a role in the growth and maturation of the brain [155]. Moreover, during embryonic development and neonatal life, PTN shows enhanced expression whereas low levels in adults [152, 153]. PTN is mostly expressed in the central nervous system (CNS) with functions as a neuromodulatory molecule. Furthermore, *PTN* is expressed in melanocytes and fibroblasts [140]. Additionally, significant expression was described in the placenta, the seminal tissue and the testis, the eye, the bladder, brain, prostate, and the stomach as well as by fibroblasts induced pluripotent stem cells (PSC) and embryonic stem cells (ESC) [152, 156, 157]. In addition, PTN plays a role in angiogenesis, tissue regeneration, cell growth, proliferation and differentiation as well as cell adhesion [158, 156]. PTN binds to various receptors of which binding to Syndecan-3 (Fig. 7) was discovered first, however, it also binds to syndecan-1 and 4, mainly via their chondroitin sulfate (CS) chains [152, 159]. Additional receptors of PTN are anaplastic lymphoma kinase (ALK), αvβ3 integrins, nucleolin (NCL), neuropilin-1 and PTPRζ1 which results in various activation of pathways related to angiogenesis and several other pro-tumorigenic signaling cascades (Fig. 7) [139, 152, 160, 161, 162, 163]. PTN binding to PTPRζ1 induces ligand-dependent homodimerization resulting in functionally auto-inhibition of the catalytic phosphatase activity of PTPRζ1 and thereby increasing tyrosine phosphorylation levels [157, 164]. Furthermore, binding of PTN to PTPRζ1 can lead to phosphorylation and activation of several downstream substrates such as c-Src, ALK, β-catenin, FAK, PI3K, ERK1/2, Fyn as well as beta-adducin through protein kinase C (PKC) alpha or beta (Fig. 7, 8) [152, 154, 161, 165, 164, 166, 167, 168, 169]. Moreover, these phosphoprotein substrates play a role in PTN/PTPRζ1 signaling in various cellular compartments with different functions such as regulation of cytoskeleton, regulation of chromatin structure, cell migration, tumor cell invasion, tumor growth and metastasis [139, 165]. PTN binding to PTPRζ1 is achieved by high and low-affinity sites of proteoglycan together with chondroitin sulfate structures, especially the CS-A is essential for stable interaction which is commonly found on PTPRζ1 [170,

[158]. However, the distinct region(s) of the PTN binding to PTPRζ1 have not been identified. Furthermore, it was shown that PTN failed to compete binding to PTPRζ1 against IL-34/PTPRζ1 indicating that binding of IL-34 involves a different CS polysaccharide glycosaminoglycan (GAG) moiety on PTPRζ1 or that PTN binds CS with a lesser affinity than IL-34 [136, 152, 171].

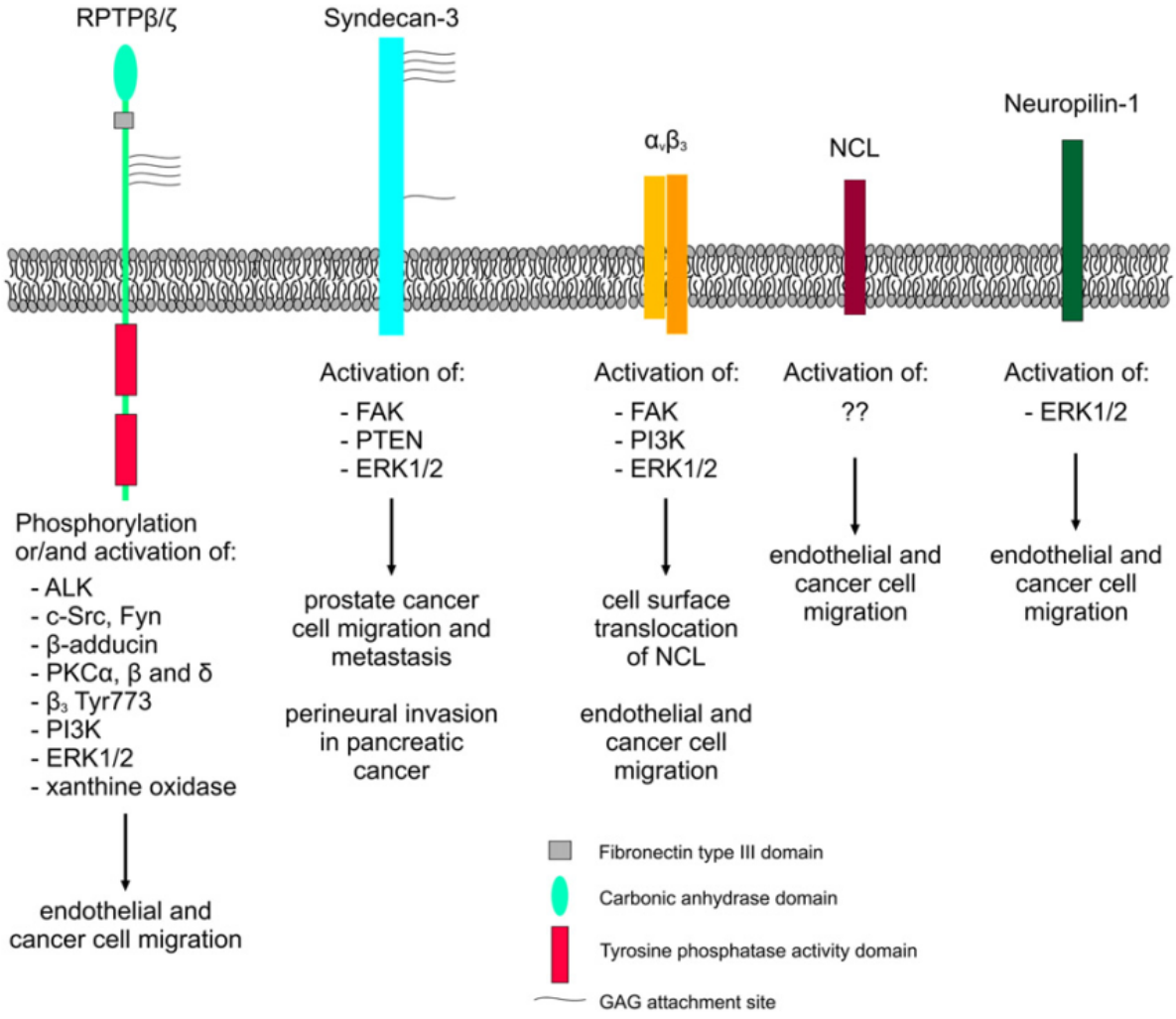

Figure 7. Schematic representation of PTN binding to PTPRζ1, Syndecan-3, αvβ3 integrins, NCL and neuropilin-1: The most important downstream pathways and functions by PTN receptors that are related to angiogenesis and cancer. Primary source "Pleiotrophin and its receptor protein tyrosine phosphatase beta/zeta as regulators of angiogenesis and cancer" [152].

PTN may play a role in tumorigenesis in several cancer such as breast cancer, testicular cancer, glioblastoma, neuroblastoma, lung cancer and melanoma [152, 172, 173, 174, 175, 176, 177]. Furthermore, gene profiling data demonstrated PTN overexpression in melanomas compared with nevi, additionally, lesional PTN expression was associated with metastasis [152, 178, 179]. Moreover, PTN might play a role in regulating angiogenesis and metastasis of melanomas [177]. Recently, it was shown that PTN and PTPRζ1 expression were suppressed by menin which

resulted in inhibiting melanoma proliferation and migration [167]. Another study in melanoma demonstrated the PTN down-regulation resulted in down-regulation of the cell cycle regulator cyclin E and upregulation of the cell cycle inhibitor $p21^{WAF1/Cip1}$ [180].

However, further investigation is needed of PTN binding to PTPRζ1 in melanoma as well as its downstream signaling.

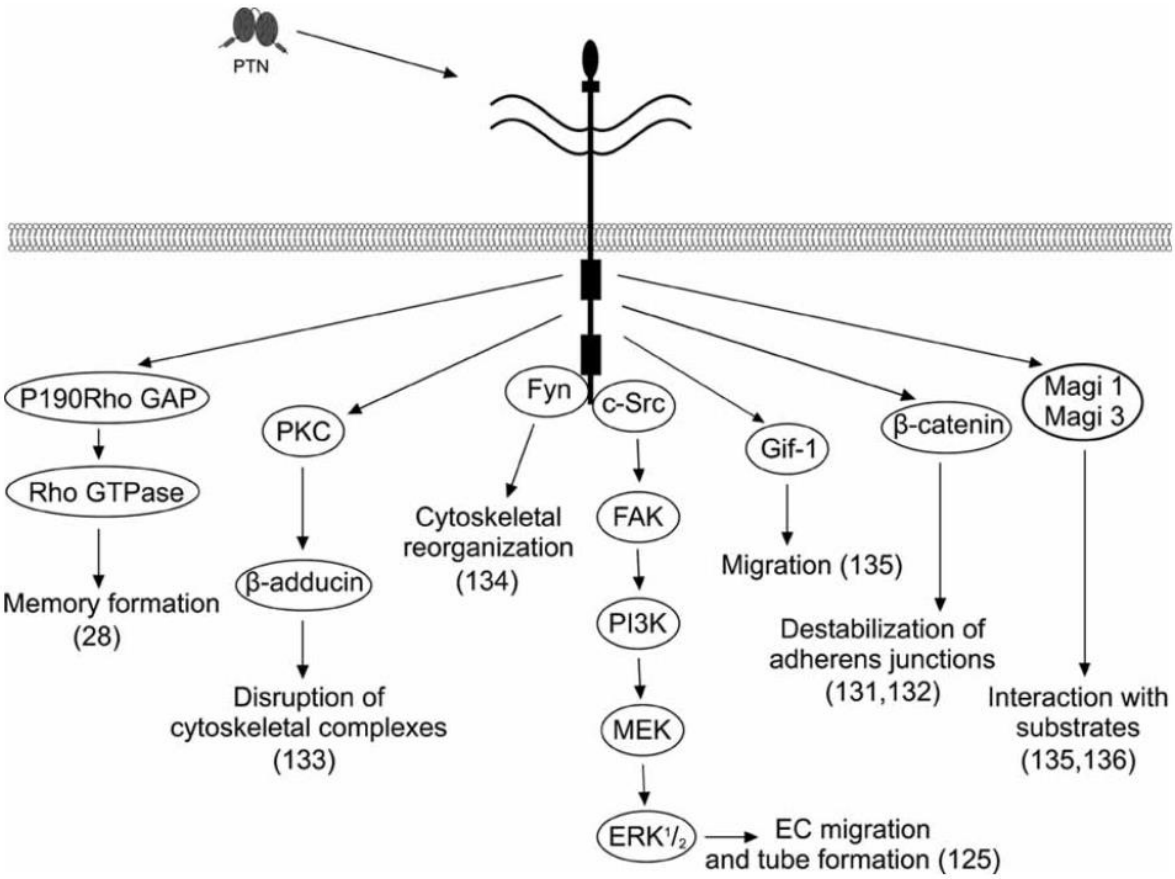

Figure 8. Schematic representation of PTN binding to PTPRζ1: The most important downstream pathways leading to biological activities. Primary source "Pleiotrophin as a Possible New Target for Angiogenesis-Related Diseases and Cancer" [153].

4.3.3. CSF1/CSF1R

The colony-stimulating factor-1 receptor (CSF-1R) is a transmembrane glycoprotein binding colony-stimulating factor-1 (CSF-1) and IL-34. Upon binding of either these ligands, the CSF-1R dimerizes and transphosphorylates resulting in signal transduction activation [117, 119, 151, 181]. The CSF-1/CSF-1R axis plays an important role in tumor survival, proliferation, motility as well as in modulation of the tumor microenvironment via macrophage recruitment subsequently TAM polarization which mediate immune suppression and promoting metastatic dissemination [113, 151]. The CSF-1R contains a highly glycosylated extracellular region comprised of five immunoglobulin domains (D1–D5) of which D2-D3 domains are essential for CSF-1 binding to CSF-1R [122]. The cytoplasmic kinase domain of CSF-1R contains several

tyrosine phosphorylation sites including within the juxtamembrane domain (JMD) (Tyrosine (Tyr)^{546} and Tyr^{561}), the kinase insert (Tyr^{699}, Tyr^{708} and Tyr^{723}) and the distal kinase domain (Tyr^{809}, Tyr^{923} and Tyr^{969}) [151, 182, 183, 184]. The JMD is crucial for the autoinhibitory function of CSF-1R which is achieved by its binding to a hydrophobic site adjacent to the ATP binding pocket results in inhibiting the activation loop from adopting an active conformation [182]. The non-covalent dimerization of CSF-1R chains upon ligand binding leads to the major phosphorylation of tyrosine 561 which is associated with full receptor activation enabling to be a binding site for c-Src kinases and could lead to disruption in cellular adhesion as well as motility [182, 184]. The CSF-1R has several phosphorylation sites which subsequently activate several adapter proteins such as several Src family kinases, the p85 subunit of PI3K, phospholipase C-γ2 (PLC-γ2), suppressor of cytokine signaling-1 (Socs1), growth factor receptor-bound protein 2 (Grb2) and c-Cbl. These activated proteins results in signaling of different downstream substrate proteins including ERK1/2, PI3K, FAK, Raf and MAP kinase and Akt which promote gene expressions involving proliferation, differentiation and survival of cells (Fig. 9) [151, 185, 186, 187, 188, 189, 190, 122].

CSF-1R is expressed in higher levels on monocytes and tissue macrophages, osteoclasts, myeloid dendritic cells and microglia controlling their development [122]. The homodimeric glycoprotein CSF-1 is produced by fibroblasts, endothelial cells, monocytes, macrophages, osteoblasts, microglia, keratinocytes, bone marrow stromal cells, natural killer cells, B-cells and T-cells and several tumor cells [151, 191]. Under physiological conditions, CSF-1 is essential as a haematopoietic growth factor regulating survival, proliferation, differentiation and motility of cells of the monocyte lineage as well as bone remodeling by osteoclasts [151, 190, 192]. CSF-1 and CSF-1R play a role in several cancers such as breast cancer, ovarian cancer, colorectal cancer, pancreatic cancer as well as Hodgkin's lymphoma [193, 194, 195, 196, 197]. Furthermore, CSF-1R can be activated in cancer cells by expression of CSF-1 or via paracrine signaling secretion by TAMs [99, 151, 190, 122]. CSF-1 is also expressed in melanoma and in addition, patients with metastatic melanoma have elevated CSF-1 levels in the blood [198].

However, whether binding of CSF-1 to CSF-1R plays a role in melanoma as well as its downstream signaling is unclear.

B. Aims of the study

Melanoma cell lines differ due to somatic mutations but they recapitulate the mutational and transcriptional profiles of patient tumors making melanoma cell lines suitable for tumor models. Furthermore, it is crucial to understand similarities and differences between melanoma cell lines to answer specific research questions [199]. SK-MEL-28 cells and WM-115 cells share similarities of harboring *BRAF* (p.V600E in SK-MEL-28, homozygous, likely oncogenic mutation; and p.V600D in WM-115) missense mutation, *NRAS* wildtype (wt),and *PTEN* (p.T167A) missense mutation in SK-MEL-28 whereas *PTEN* loss of heterozygosity in WM-115 [200, 201, 202, 203, 204, 205]. Loss of functional PTEN results in constitutively active phospho-Akt status in SK-MEL-28 cells by activated PI3K/Akt pathway as well as in WM-115 cells [76, 206, 204]. *BRAF* mutations generates an active conformation resulting in an increased BRAF kinase activity leading activation of the MAPK pathway [45]. Differences in SK-MEL-28 cells are additionally containing an *EGFR* (p.P753S, homozygous, tentative oncogenic variant) missense mutation, *TP53* (p.L145R, homozygous, likely oncogenic mutation) mutation, *CDK4* (p.R24C) mutation; CDKN2A wt and TERT (c.161A>C) promoter mutation [201, 202, 207, 208, 209, 210, 211]. In comparison, WM-115 cells have a *CDKN2A* copy number alteration (homozygous deletion) [199, 212]. In a ranking of 42 melanoma cell lines based on average Pearson's correlation of their expression profiles, it was suggested that SK-MEL-28 cell line is more similar to patient tumors with a correlation coefficient of 0.519 compared to the WM-115 cell line with a correlation coefficient of only 0.449 [199]. Collectively, WM-115 demonstrates a primary melanoma cell line in vertical growth phase whereas SK-MEL-28 represents a more malignant melanoma cell line, thus these cell lines are beneficial to utilize and for describing various melanoma tumor phenomena [213].

Interleukin-34 (IL-34) is a newly discovered member of the interleukin family which together with Colony stimulating factor-1 (CSF-1) share the same Colony stimulating factor-1 receptor (CSF-1R, CD115), a receptor tyrosine kinase [117]. In addition, IL-34 also binds protein tyrosine phosphatase β/ζ (PTPRζ1, PTPRZ1), a member of the receptor tyrosine phosphatase family, and syndecan-1 (SDC1, CD138) [136, 135]. Moreover, pleiotrophin (PTN) is an additional ligand of PTPRζ1 and syndecan-1 [170, 159], thereby increasing the complexity of biological activities.

Melanoma cells interact with the tumor microenvironment (TME), thus the mediated crosstalk between cancer, stromal cells, and immune cells within the surrounding microenvironment via cytokines, growth factors, and their receptors are important for cell motility, invasion and metastasis [94, 95]. CSF-1 and IL-34 promote the differentiation and survival of monocytes and macrophages as well as polarization into immunosuppressive M2 macrophages via CSF-1R [130]. In addition, IL-34 plays a role in innate immunity, inflammation and cancer as well as in promoting recruitment of M2-polarized tumor-associated macrophages (TAMs) [133, 214]. In

melanoma, CSF-1R and IL-34 are autocrinally regulated in BRAF V600E resistance [215]. Furthermore, TAMs secrete PTN to promote PTPRζ1 paracrine signaling in glioblastoma stem cells (GSC) for tumor growth, thus there is a molecular crosstalk between TAMs and GSCs [216]. In the skin epidermis, keratinocytes produce IL-34 for the development of Langerhans cells [217]. Moreover, melanoma expresses PTPRζ1, CSF-1R and SDC1 [138, 137, 215, 218].

However, while the role of IL-34/- and CSF-1/CSF-1R axes have been extensively studied in myeloid cells and in several cancers, the implications of PTN, IL-34 and CSF-1 in signaling transduction via PTPRζ1 respectively CSF-1R and their effects on cellular behavior are still poorly understood in melanoma skin cancer cells.

Therefore, the aim of my study was to characterize and address the potential roles of IL-34, CSF-1 and PTN in inducing signaling transduction and in cellular behavior of melanoma cell lines.

The roles of these cytokines in inducing signaling transduction in melanoma cell lines were addressed by using recombinant human (rh)IL-34, rhCSF-1, rhPTN and PTPRζ1 inhibitor compound 12b (MY33-3) on melanoma cell lines and were determined by Western blotting and gene expression analysis. The cellular behavior was defined by proliferation and by migration assays.

In conclusion, our study indicates that PTPRζ1 and CSF-1R signaling are differentially regulated in melanoma cell lines.

C. Material and Methods

1. Cell culture

1.1. Cell lines

The cell lines used in this study were human adherent melanoma cells. WM-115 cells (CRL-1675™, ATCC®, US) is a human melanoma cell line originally isolated from a 58-year-old female adult. SK-MEL-28 cells (HTB-72™, ATCC®, US) is a human malignant melanoma cell line that originates from an axillary lymph node of a 51 year-old male adult.

1.1.1. Maintenance

SK-MEL-28 cells (HTB-72™, ATCC®, US) and WM-115 cells (CRL-1675™, ATCC®, US) are melanoma cell lines which were cultured in 100 mm sterile cell culture dishes (Falcon® #353003, Corning, US) containing the cell culture medium Minimum essential Medium – (MEM) Eagle EBSS with L-glutamine (EMEM) (#BE12-611F, Lonza, CH) which was supplemented with 10% heat inactivated fetal bovine serum (FBS) (#10270-106, Gibco™, US) and 100 U/mL penicillin/streptomycin (p/s) (#P4333, Sigma-Aldrich, US). The SK-MEL-28 cells were incubated at 37°C and 5% CO_2 whereas WM-115 cells were incubated at 35°C in CO_2 incubators (#CB150, Binder, DE).

1.1.2. Subculturing process

Melanoma cells were split at 80% cell monolayer confluency in the cell culture petri dish. The cell culture medium EMEM and Dulbecco's Phosphate Buffered Saline (DPBS) without Calcium and Magnesium (#BE17-512F, Lonza, CH) were pre-warmed at room temperature (RT). Afterwards, the media in the cell culture dishes were removed which was followed by washing twice with DPBS and subsequently 1x Trypsin-EDTA (10x Trypsin-EDTA, #L11-003, PAA Laboratories, AT) in DPBS was added and incubated for 5 minutes at 37°C in CO_2 incubators. The trypsinization was stopped by adding fresh cell culture medium EMEM. Then, the cells were transferred from the cell culture dishes into a tube (Greiner Bio-One™, AT) containing cell culture medium EMEM followed by centrifugation at 1500 rpm for 3 minutes at 20°C. The supernatant was removed and the cell pellet was resuspended in fresh cell culture medium EMEM for a split in subcultivation ratios of 1:4 to 1:8 for SK-MEL-28 cells and of 1:2 to 1:4 for WM-115 cells. Cell culture medium renewal was carried out twice to three times per week.

1.2. Cryopreservation

For cryopreserving these cultured melanoma cells were isolated in log-phase of growth. The procedure was identical to the subculturing process, however, after centrifugation, the cell pellet was resuspended with freezing medium which was afterwards transferred into cryovials (2mL Cryo.s™ #122263, Greiner Bio-One, AT). The freezing medium contained cell culture medium EMEM and the cryoprotective agent of 5% dimethyl sulfoxide (DMSO) (#D8418, Sigma-Aldrich, US). The cryovials were put into a styrofoam container for freezing the cells at a slow rate in an ultra-low temperature freezer at -80°C (#VWR24086V, VWR, US). For long-term storage of cells, cryovials were transferred to a liquid nitrogen storage vessel.

1.3. Cell counting

The melanoma cells were counted for seeding prior starting experiments by Neubauer counting chamber (Laboroptik, UK) or by LUNA-FL™ Automated Cell Counter (#L20001, Logos Biosystems, KR).

1.3.1. Neubauer cell chamber (haemocytometer)

After trypsinization and centrifugation of the melanoma cells, as in the procedure of subculturing process, 1 mL cell culture medium EMEM was added to the cell pellet, resuspended and 10 µL of this cell suspension was diluted in 990 µL DPBS in an Eppendorf tube resulting in a dilution factor of 1:100. Then, the counting chamber and the glass coverslip were cleaned with 70% ethanol. A random sample of this cell suspension was pipetted at the border of the glass coverslip which was placed onto the Neubauer counting chamber (Laboroptik, UK) resulting in filling up the space between them by capillary force. The chamber contained two identical squares of which each of them had an surface area of 9 mm^2. These squares were divided into nine primary squares with an surface area of 1 mm^2 of which only the four corner squares were relevant for counting cells by using 100x magnification of the light microscope (Nikon Eclipse TE2000-U, JP). Cells were counted in all eight corner squares, however, cells located on the grid border line would be counted if they were positioned on the bottom- and left grid border line. The counted cell number was divided by eight, resulting in the mean which was multiplied by 10^4 and by the dilution factor of 100 leading to the number of cells per milliliter. The multiplication of 10^4 was due to the volume of one corner square which was the result of its surface area of 1 mm x 1 mm and multiplied by the distance between the Neubauer cell chamber and coverslip of 0,1 mm leading to 0,1 mm^3 which equals 0,0001 mL. Therefore, to determine the cell number per milliliter, the mean of the counted cell figure had to be multiplied by 10^4. After finishing counting, the Neubauer cell chamber and the glass coverslip was rinsed with water and cleaned with 70% ethanol.

1.3.2. LUNA-FL™ Automated Cell Counter

After trypsinization and centrifugation of the melanoma cells, as in the procedure of subculturing process, 1 mL cell culture medium EMEM was added to the cell pellet followed by resuspension. A random sample of this cell suspension was pipetted to 0,4% Trypan Blue Stain (T13001, Logos Biosystems, KR) in an Eppendorf tube in a ratio 1:1. This sample was loaded on a LUNA™ Cell Counting Slides (L12001, Logos Biosystems, KR) which was inserted into the LUNA-FL™ Automated Cell Counter (#L20001, Logos Biosystems, KR) for bright field optics cell counting. To achieve a more accurate result of the cell number per milliliter, the sample was counted twice and the mean was used for further experiments.

2. Reagents

2.1. PTPRζ1 inhibitors

The protein tyrosine phosphatase, receptor-type, Z polypeptide 1 (PTPRZ1) small-molecule inhibitor compounds MY10 (compound 10a, (Trifluoromethyl)(4-((4-((trifluoromethyl)thio)benzyl)oxy) phenyl)sulfane) and MY33-3 (compound 12b, Bis(4-((trifluoromethyl)thio)benzyl)amine hydrochloride) were a gift from Dr. Ana Maria Ramos Gonzalez, University CEU San Pablo, Department of Chemistry and Biochemistry in Madrid, Spain [219]. A 20 mM stock solution in 100% DMSO was prepared for the experiments which was stored at -20°C. The dissolved powder was sonicated at 220 volt, 0.5 ampere, 50 hertz, 150 watt.

2.2. Recombinant cytokines

The used cytokines for experiments were recombinant human colony stimulating factor 1 (rhCSF-1) (Chiron, US), recombinant human interleukin 34 (rhIL-34) (#5265-IL, R&D systems, US) and recombinant human pleiotrophin (rhPTN) (#252-PL, R&D systems, US). All recombinant cytokines were stored at -20°C.

3. Biological assays

3.1. Viability assay following compound 10a and 12b treatment

Cell viability analysis was done by using Acridine Orange/Propidium Iodide (AO/PI) double staining method or by the Trypan Blue Stain method. $2x10^5$ WM-115 melanoma cells were seeded per well in 12-well plates (#10062-894, VWR, US) in a total volume of 100 µL. Melanoma cells were treated for 24 hours with 4% DMSO, compound 10a with concentrations of 20-, 50- and 100 µM, and with compound 12b with concentration levels of 1-, 2-, 5-, 10-, 20-, 50-, 100 µM.

3.1.1. Trypan Blue Staining

A random sample of the trypsinized, centrifugated, cell pellet resuspended in culture medium EMEM WM-115 melanoma cells was pipetted to 0,4% Trypan Blue Stain (T13001, Logos Biosystems, KR) in an Eppendorf tube in a ratio 1:1. This sample was loaded on a LUNA™ Cell Counting Slides (L12001, Logos Biosystems, KR) which was inserted into the LUNA-FL™ Automated Cell Counter (#L20001, Logos Biosystems, KR) for bright field optics cell counting. Viable cells have intact cell membranes and are not stained by the vital dye Trypan Blue Stain, thereby they are remaining colorless whereas nonviable cells are stained blue. The percentage of the cells viability was calculated by the number of viable cells multiplied by 100 and divided by the total number of cells. The quantification calculations were done in Microsoft Excel (365, Microsoft, US).

3.1.2. Acridine Orange/Propidium Iodide staining (AO/PI)

A random sample of the harvested WM-115 melanoma cells was pipetted to Acridine Orange/Propidium Iodide Stain (F23001, Logos Biosystems, KR) in a ratio of 18:2. The resuspended mix was pipetted into a LUNA™ Cell Counting Slides (L12001, Logos Biosystems, KR) and the cells were counted by dual fluorescence cell counting LUNA-FL™ Automated Cell Counter (#L20001, Logos Biosystems, KR). The cell viability dye caused viable nucleated cells to fluoresce green and nonviable nucleated cells to fluoresce red. Acridine orange permeated viable cells binding nucleic acids whereas its binding to dsDNA caused green fluorescence and binding to ssDNA or RNA causing red fluorescence. Propidium iodide was also able to bind nucleic acids, however, it was not capable permeating intact cell membranes, thus taken up only in nonviable cells and cells with compromised membranes. Propidium iodide binding to nucleic acids resulted in red fluorescence and its fluorescence increased by 20-30 percent. The PI signal absorbs the AO signal in nonviable cells, thereby preventing double positive results which was due to the Förster resonance energy transfer

(FRET). The excitation wavelengths of AO was 500 nm and of PI was 533 nm and the emission wavelengths of AO was 526 nm and of PI was 617 nm. Therefore, AO stained all cells whereas PI stained only dead cells. If Acridine orange and Propidium iodide existed together, the Acridine orange fluorescence was mostly quenched by PI. Consequently, Acridine orange green fluorescence was found only in live cells whereas PI red fluorescence was found only in dead cells. The percentage of viable cells was calculated by the number of viable cells multiplied by 100 and divided by the total number of cells. The quantification calculations were done in Microsoft Excel (365, Microsoft, US).

3.2. Cell proliferation assay

To determine cell proliferation of melanoma cells, cell proliferation reagent WST-1 (#11644807001, Roche Diagnostics, US) was used. Viable cells cleaved tetrazolium salts (WST-1, slightly red) to formazan (dark red) by cellular enzymes. An increase in the number of viable cells resulted in an increase in the overall mitochondrial dehydrogenases activity of the mitochondrial succinate-tetrazolium-reductase system upon reduction by NADH to NAD+ resulting in an increased amount of formed formazan dye. The quantification of the formazan dye produced by metabolically active cells was measured by using spectrophometer plate reader (Multiscan FC, Thermo Fisher Scientific, US).

3.2.1. Melanoma cell proliferation in response to compound 10a and 12b

SK-MEL-28 cells and WM-115 cells were seeded at a density of 5000 cells per well in a 96-well plate (#655180, Cellstar Greiner Bio-One, AT) in a total volume of 100 µL of EMEM supplemented with 2% FBS and 100 U/mL p/s (2% EMEM). SK-MEL-28 cells were treated for 24 and 48 hours whereas WM-115 cells treatment duration was 48 hours with 4% DMSO, compound 10a and compound 12b with concentration levels of 1-, 2-, 5-, 10-, 20-, 50-, 100 µM. Afterwards, cell proliferation reagent WST-1 (#11644807001, Roche Diagnostics, US) was added in a dilution 1:10 and incubated. The absorbance was measured after 30, 60 and 120 minutes in SK-MEL-28 cells and after 15, 30, 60 and 180 minutes in in WM-115 cells by a plate reader (Multiscan FC, Thermo Fisher Scientific, US). The last measurements were used for quantification by subtracting the absorbance value at 620 nm from the absorbance value at 450 nm with the provided software (SkanIt 3.0, Thermo Fisher Scientific, US). The quantification calculations were done in Microsoft Excel (365, Microsoft, US).

3.2.2. Melanoma cell proliferation in response to rhIL-34 and rhCSF-1 with and without compound 12b

SK-MEL-28 cells and WM-115 cells were seeded at a density of 5000 cells per well in a 96-well plate (#655180, Cellstar Greiner Bio-One, AT) in a total volume of 100 µL of EMEM supplemented with 2% FBS and 100 U/mL p/s (2% EMEM). The melanoma cells were treated for 48 hours with 1% DMSO and 10 µM of compound 12b in combination and without 200 ng/mL cytokines rhIL-34 (#5265-IL, R&D systems, US) and rhCSF-1 (Chiron, US). The compound 12b was added 15 minutes prior adding cytokines. Afterwards, cell proliferation reagent WST-1 (#11644807001, Roche Diagnostics, US) was added in a dilution 1:10 and incubated. The absorbance was measured after 15, 30, 60 and 120 minutes in melanoma cells by a plate reader (Multiscan FC, Thermo Fisher Scientific, US). The last measurements were used for quantification by subtracting the absorbance value at 620 nm from the absorbance value at 450 nm with the provided software (SkanIt 3.0, Thermo Fisher Scientific, US). The quantification calculations were done in Microsoft Excel (365, Microsoft, US).

3.3. Migration assay

3.3.1. Melanoma cell migration in response to compound 10a and 12b

WM-115 cells were seeded at a density of $1x10^5$ onto the top of each Boyden migration chamber, ThinCerts™ – TC Inserts, 12-well, 8.0-µm pore size (#665638, Greiner Bio-One, AT) in a 12-well plate (#734-2324, VWR, US) in a total volume of 100 µL of EMEM supplemented with 2% FBS and 100 U/mL p/s. Additionally, compound 12b in concentration levels of 1-, 2-, 5-, 10-, 20-, 50-, 100 µM and of compound 10a in dosages of 20- and 50 µM as well as 200 ng/mL of rhIL-34 (#5265-IL, R&D systems, US) were added into the Boyden migration chamber. The bottom chamber was filled with one mL of EMEM supplemented with 10% FBS and 100 U/mL p/s. The WM-115 cells migrated for 48 hours, afterwards, the medium was discarded and the membranes were washed twice with PBS. Cells from the upper side of the membrane were removed with cotton swabs. The membranes were excised using a scalpel, inverted and transferred to a PBS filled tissue culture well. Next, membranes were fixed in methanol for 20min at -20°C. After washing in PBS again, membranes were stained with 1 µg/ml 4'-6-Diamidino-2-phenylindole (DAPI, Invitrogen, US) in PBS (1:5000) for 10 minutes at room temperature and washed again in PBS. Subsequently, membranes were embedded in Citifluor AF1 antifadent mountant solutions (#AGR1320, Agar Scientific, UK) on a microscope slides and held together by a cover slip. Images of the membranes containing migrated cells were acquired digitally by a fluorescence microscope (Nikon Eclipse 80i, JP) equipped with DAPI filters at 40X magnification and single images of the membrane were stitched together

by the microscope software (NIS-Elements BR 4.13.05). The fluorescent cells were counted by ImageJ (v.1.53j, National Institutes of Health, US). The quantification calculations were done in Microsoft Excel (365, Microsoft, US). Additional images were taken from representative sections on the membranes.

3.3.2. Melanoma cell migration in response to rhIL-34, rhCSF-1 and rhPTN with and without compound 12b

SK-MEL-28- and WM-115 cells were seeded at a density of $5x10^4$ onto the top of each Boyden migration chamber, ThinCerts™ – TC Inserts, 12-well, 8.0-µm pore size (#665638, Greiner Bio-One, AT) in a 12-well plate (#734-2324, VWR, US) in a total volume of 100 µL of EMEM supplemented with 2% FBS and 100 U/mL p/s. Additionally, 200 ng/mL rhIL-34 (#5265-IL, R&D systems, US) rhCSF-1 (Chiron, US) and rhPTN (#252-PL, R&D systems, US) were added with and without 10 µM of compound 12b into the Boyden migration chamber. The compound 12b was added 15 minutes prior adding cytokines. The bottom chamber was filled with one mL of EMEM supplemented with 10% FBS and 100 U/mL p/s. The melanoma cells migrated for 48 hours. The procedure is identical to the described above (3.3.1.) but in addition the fluorescent cells were counted by Fusion software EVOLUTION-CAPT (v17.01, Vilber Lourmat, DE). The quantification calculations were done in Microsoft Excel (365, Microsoft, US).

4. RNA expression

4.1. Total RNA isolation

SK-MEL-28 cells and WM-115 cells were seeded at a density of $2x10^5$ cells per well in a 6-well plate (#130184, Thermo Fisher Scientific, US) in a total volume of 2 mL of EMEM supplemented with 10% FBS and 100 U/mL p/s (10% EMEM). The melanoma cells were starved overnight and treated for 48 hours with 125 ng/mL cytokines rhIL-34 (#5265-IL, R&D systems, US), rhCSF-1 (Chiron, US) and rhPTN (#252-PL, R&D systems, US). The total RNA was isolated from lysed cells by adding 1 mL of TRIzol® reagent (#15596026, Thermo Fisher Scientific, US) directly into each well and passing the cell lysate several times through a pipette. The homogenized cell lysate was transferred into an Eppendorf tube and incubated at room temperature (RT) for 5 minutes to permit the complete dissociation of nucleoprotein complexes. Then, 200 µL chloroform per 1 mL TRIzol® reagent was added, vortexed for 20 seconds and incubated for three minutes at RT. The samples were centrifuged at 12000 x g at 4°C for 15 minutes by a refrigerated centrifuge (4k15, #10740, Sigma Laborzentrifugen, DE) allowing the mixture to separate into a lower red phase containing proteins, an interphase

(phenol-chloroform phase) including DNA, and a colorless upper aqueous phase comprising RNA. The aqueous phase was transferred into a fresh Eppendorf tube. In order to precipitate the RNA, 500 µL ice cold isopropanol per 1 mL of TRIzol® reagent was added, vortexed and incubated at -20°C for 30 minutes overnight for a higher RNA yield. Afterwards, the Eppendorf tubes were centrifuged at 12000 x g at 4°C for 30 minutes resulting in a gel-like pellet containing the RNA precipitate. The supernatant was removed and the RNA pellet was washed once with 1 mL 80% ice cold ethanol per 1 mL of TRIzol® reagent followed by centrifugation of the samples at 4°C for 8 minutes. Then, the supernatant was removed and the RNA pellet dried for at least 15 minutes at RT. At the end, the RNA was dissolved in 20 µL Diethylpyrocarbonate (DEPC)-treated water, incubated at 65°C for 10 minutes on a heating block. The concentration and purity were measured by using an UV-Vis spectrophotometer (NanoDrop 2000c, #F665, Thermo Fisher Scientific, US).

4.2. Complementary DNA (cDNA) synthesis

In order to synthesize the first strand complementary DNA (cDNA), the Thermo Scientific RevertAid RT Reverse Transcription Kit (#K1691, Thermo Fisher Scientific, US) was used. For first Strand cDNA synthesis, 5 µg of total RNA and 0.5 µg oligo dT-primer (100 pMol) (#SO131) were added to DEPC-treated water (#R0601) resulting in a final volume of 12.5 µL. The mixture was vortexed, spun down and incubated at 65°C for 5 minutes on a heating block followed by a brief centrifugation and cooling for 5 minutes on ice. After another brief centrifugation, the following components were added in the chronological order of 4 µL of Reaction Buffer, 0.5 µL (20 U) Thermo Scientific™ RiboLock RNase Inhibitor (#EO0831), 2 µL dNTP Mix (10 mM each (#R0191)) and 1 µL (200 U) RevertAid Reverse Transcriptase resulting in a total volume of 20 µL. Afterwards, the mixture was mixed gently, centrifuged and incubated at 42°C for 60 minutes. The reaction was terminated by heating at 70°C for 10 minutes. The resulting cDNA was stored at -20°C.

4.3. Quantitative real-time polymerase chain reaction (qRT-PCR)

The quantitative real-time polymerase chain reaction (qRT–PCR) analysis was performed by using the FastStart DNA Master SYBR® Green mix (Roche Diagnostics, US). It was a ready-to-use PCR reaction mix for the amplification of cDNA and the detection by the LightCycler® (LC) Carousel-Based System (LC#1401186, Roche Diagnostics, US). At the beginning of PCR amplification, the reaction mixture contained denatured DNA, the primers and SYBR Green I dye. The unbound SYBR Green I dye exhibited very low fluorescence, however, its fluorescence increased upon binding to double stranded (ds)DNA starting with the annealing of the primers and enhanced even more during elongation by binding to the newly synthesized

DNA. The increase of fluorescence was monitored in real time. During denaturation of the DNA for the next heating cycle, the SYBR Green I dye molecules were released and the fluorescence decreased. The generated amount of dsDNA was directly proportional to the fluorescence of SYBR Green I dye.

The cDNA was diluted 1:10 by adding DEPC water. 1 µL of the diluted cDNA was mixed in case of one sample with 0.5 µL forward primer (10 pMol), 0.5 µL reverse primer (10 pMol), 1.5 µL LightCycler FastStart DNA Master SYBR® Green I mix (containing FastStart Taq DNA Polymerase, reaction buffer, dNTP mix (with dUTP instead of dTTP), SYBR Green I dye, and 10 mM MgCl2), 1.3 µL $MgCl_2$ and 10.2 µL DEPC water. Depending on the sample size, a master mix was prepared with these components and multiplied by the number of the sample size in case of a total volume of 15 µL. In case of qRT-PCR for CSF-1 and CSF-1R, a total volume of 20 µL was needed containing of 1 µL of the diluted cDNA mixed in case of one sample with 2 µL forward primer, 2 µL reverse primer, 2 µL LightCycler FastStart DNA Master SYBR® Green I mix, 2.4 µL $MgCl_2$ and 10.6 µL DEPC water. Depending on the sample size, a master mix was prepared with these components and multiplied by the number of the sample size. The specific primers of huPTPRZ1, huPTPRZ1, huCSF-1R huSDC1, huIL-34, huCSF-1, huPTN and huB2M were used (Table 3). The qRT-PCR had certain amplification parameters (Table 4). After PCR, a melting curve analysis was performed by slowly heating to 95°C causing melting of dsDNA and a corresponding decrease of SYBR Green I fluorescence. It confirmed that only the desired PCR product was amplified. The fluorescence decrease was displayed as melting peaks of which each represented the characteristic melting temperature (Tm) of a particular DNA product in which the DNA was 50% double-stranded and 50% single-stranded. In the present of primer-dimers or other nonspecific products, additional melting peaks would be shown. The relative quantification of the measurements was achieved by normalizing the interested gene to the specific measurement of the housekeeping gene β_2-microglobulin (B2M), a component of MHC class 1 molecule expressed ubiquitously in every cell. The PCR data were analyzed by using the LC Data Analysis software (v.3.5.3, Roche Diagnostics, US) and the quantification calculations were done in Microsoft Excel (365, Microsoft, US).

Table 3. Human specific primer sequences used in qRT-PCR

Gene	Forward Primer (5'-3')	Reverse Primer (5'-3')	Length (bp)	An-neal-ing T (°C)	Melt-ing T (°C)	Extens-ion duration (s)
huPTPRZ1	TCTACTGCTTTGATGCGGACC	ACGACTAACACTTTCGACTCC	152	62	80	20
huCSF-1R	CTGAGCAAGACCTGGACAAGG	TGCTGTTCACCAGGATGCCAG	378	62	86	20
huSDC1	GGGACTCAGCCTTCAGACAG	CTCGTCAATTTCCAGGAGGA	128	62	88	24
huIL-34	AATCCGTGTTGTCCCTGTTG	CAGTACAGCAGCTCCATGACC	103	64	86	24
huCSF-1	GCTGTTGTTGGTCTGTCTC	CATGCTCTTCATAATCCTTG	335	60	85	16
huPTN	CCATGAAGACCCAGAGATG	TTGGTCAGTTTGCCACAG	202	60	86	16
huB2M	GATGAGTATGCCTGCCGTGTG	CAATCCAAATGCGGCATCT	114	62	82	16

Table 4. qRT-PCR amplification parameters

Step	Temperature	Duration	Number of cycles
Initiation	95°C	10 minutes	
Denaturation	95°C	15 seconds	45 cycles
Annealing	See Table 3.	5 seconds	
Extension	72 ^{0}C	See Table 3.	
Melting curve analysis	Heated to 95°C in 0.1°C steps/second		

5. Protein expression

5.1. Western blotting

5.1.1. Protein extraction

5.1.1.1. Protein extraction in response to rhIL-34, rhCSF-1 and rhPTN with and without compound 12b

For protein extraction, the melanoma cells were seeded 5x10^5 cells per 100 mm sterile cell culture dishes (Falcon® #353003, Corning, US) and 2x10^5 cells per well in a 6-well plate (#130184, Thermo Fisher Scientific, US) in EMEM supplemented with 10% FBS and 100 U/mL p/s (10% EMEM). At 80% cell monolayer confluency, cells were starved for 24 hours in EMEM supplemented with 100 U/mL p/s without FBS. On the next day, the media was removed and EMEM supplemented with 2% FBS and 100 U/mL p/s was added to the melanoma cells in combination with 125 ng/mL rhIL-34 (#5265-IL, R&D systems, US), rhCSF-1 (Chiron, US) and

rhPTN (#252-PL, R&D systems, US) for stimulation in 100 mm sterile cell culture dishes for five minutes. The five-minute cytokine stimulation in combination with 10 µM of compound 12b were done in 6-well plate by adding compound 12b 15 minutes prior the addition of cytokines. The cytokine stimulation time series of 1-, 5-, 15-, 30-, 60 minutes were done in 100 mm sterile cell culture dishes by adding 100 ng/mL of cytokines for stimulation. After the certain stimulation duration, the mixture of culture medium, cytokines and compound 12b was removed, washed twice with cold PBS followed by adding RIPA buffer for an incubation of five minutes while keeping the plate on ice with occasionally swirling of the plate for uniform spreading. The melanoma cells were lysed in RIPA buffer (#89901, Thermo Fisher Scientific, US). The RIPA buffer contained of 25 mM Tris-HCl pH 7.6, 150 mM NaCl, 1% NP-40, 1% sodium deoxycholate, 0.1% SDS, and in addition 1mM serine protease inhibitor phenylmethylsulfonyl fluoride (PMSF) as well as 1X Halt™ Protease and Phosphatase Inhibitor Single-Use Cocktail 100X, EDTA-Free (#78443, Thermo Fisher Scientific, US) were added to the RIPA buffer. The Halt™ Protease and Phosphatase Inhibitor Single-Use Cocktail 100X was comprised of protease and phosphatase inhibitors aprotinin, bestatin, E-64, leupeptin, sodium fluoride, sodium orthovanadate, sodium pyrophosphate, β-glycerophosphate. The cell lysate was gathered to one side of the plate by using a cell scraper (#99003, TPP Techno Plastic Products, CH) and the harvested cell lysate was collected and transferred into an Eppendorf tube. The samples were centrifuged at 15000 x g for 15 minutes at 4°C by a refrigerated centrifuge (4k15, #10740, Sigma Laborzentrifugen, DE). The supernatant containing proteins was transferred to a new Eppendorf tube leaving the pellet containing cell debris behind.

5.1.1.2. Protein extraction for baseline protein expression

The procedure was identical to the described above (5.1.1.1.) but melanoma cells were seeded $5x10^5$ cells per 100 mm sterile cell culture dishes (Falcon® #353003, Corning, US) in EMEM supplemented with 10% FBS and 100 U/mL p/s (10% EMEM) and proteins were extracted at 80% cell monolayer confluency.

5.1.2. Protein quantification

Protein concentration was determined by using the colorimetric Bradford protein assay. The Bradford protein assay depended on the composition of the amino acids of the measured proteins. Coomassie Brilliant Blue G-250 bound primarily to basic (especially arginine) and aromatic amino-acid residues. The formation of a complex between the dye, Brilliant Blue G, and proteins resulted in a shift in the absorption maximum of the dye from 465 nm to 595 nm. In the first step, the Bio-Rad-Protein-Assay Dye Reagent Concentrate (#5000006, Bio-Rad Laboratories, DE) was diluted in a ratio 1:5 with double distilled (dd) water and 1 mL was added

into a glass cuvette in combination with 1, 2, 5, 10, 20 µg/µL BSA to produce a standard curve. Next, 1-5 µL of the protein isolated sample with unknown concentration was added to the diluted Bio-Rad-Protein-Assay Dye Reagent Concentrate and the absorbance of 595 nm was measured by NanoDrop Spectrophotometer 2000c (#F665, Thermo Fisher Scientific, US). The final protein concentration was calculated by dividing the measured concentration by the added volume for measuring of the protein sample lysate.

5.1.3. SDS-PAGE and Western blotting

The calculated protein sample of 10 µg in case of protein extraction in response to rhIL-34, rhCSF-1 and rhPTN with compound 12b whereas without compound 12b 25 µg was added in a ratio 1:$^{3}/_{5}$ to 5X FSB sample loading buffer and 1M dithiothreitol (DTT) (FSB:DTT = 2:1). The mixture was heated to 95°C for 5 minutes to denature proteins by disrupting hydrogen bonds and reduction of disulfide bridges. The protein sample mix was loaded onto a 8% polyacrylamide (PA) gel and proteins were separated by size during sodium dodecyl sulfate polyacrylamide gel electrophoresis (SDS-PAGE) in a Bio-Rad Mini-Protean® Tetra system (Bio-Rad Laboratories, DE) under the conditions of 100 V, 160 mA and 100 watt. For the use as size standards in SDS-PAGE and western blotting, the PageRuler™ Prestained Protein Ladder (#26616, Thermo Fisher Scientific, US) or Spectra™ Multicolor Broad Range Protein Ladder (#26624 Thermo Fisher Scientific, US) were used. The separated proteins in the PA gel were semi-dry transferred onto a 0.2 µm nitrocellulose (NC) blotting membrane (#10600015 Amersham™ Protran™, GE Healthcare, UK) by Trans-Blot® Turbo™ System (Bio-Rad Laboratories, DE) under the conditions of 25 V, 1 A for 30 minutes. To determine successful blotting from the gel to the membrane, reversible Ponceau S staining was used by two minutes of incubation and washed away by tris-buffered saline (TBS) and Polysorbate 20 (Tween 20) (TBST). The membrane was blocked in 5% bovine serum albumin (BSA) (#9048-46-8, VWR, AT) in TBST for one hour and incubated with the primary antibody which was diluted in 5% BSA in TBST (Table 5) overnight. The next day, unbound primary antibodies were washed away with TBST, three times for ten minutes, followed by a 2-hour incubation at room temperature with horseradish peroxidase (HRP)-conjugated secondary antibody diluted in TBST (Table 5). Afterwards, unbound secondary antibodies were washed away with TBST, three times for ten minutes. In case of loading control GAPDH, the TBST-washed membrane was incubated with Anti-GAPDH HRP-conjugated mAb (#60004, Proteintech, US) diluted in TBST in a ratio of 1:10000 for two hours at room temperature without the usage of a secondary antibody. After three time washing in TBST for ten minutes, the membrane was ready for detection. Proteins were visualized by WesternBright™ ECL western blotting detection kit (#K-12045-D50, Advansta, US). The ECL chemiluminescence was recorded using the FusionFX Imaging Systems (FusionFX, Vilber Lourmat, DE). The protein quantification analysis was

done by Fusion software EVOLUTION-CAPT (v17.01, Vilber Lourmat, DE) whereas the quantification calculations were done in Microsoft Excel (365, Microsoft, US).

5.1.4. Membrane stripping

The use of stripping was to remove primary and secondary antibodies from a Western blot membrane to investigate another protein of interest or loading control. The membrane was covered in stripping buffer for ten minutes at room temperature. This mild stripping buffer contained in one liter ddH_2O 15 g glycine, 1 g SDS, 10 mL Tween20 and the mixture was adjusted to pH 2.2 by 1M HCl. Afterwards, the stripping buffer was discarded and incubated again with fresh stripping buffer for ten minutes. Then washing twice with PBS each time for ten minutes, followed by washing twice with TBST each step for five minutes. Next, the membrane blocked in 5% BSA in TBST for one hour. The followed steps for primary antibody incubation to protein quantification was identical to the procedure described above (5.1.3).

Table 5. Summary of primary and secondary Antibodies

Primary Antibody	Dilution	Size [kDa]	Secondary Antibody	Dilution
Monoclonal anti-hPTPRZ1 rat IgG (#MAB2688, R&D systems, US)	1:500	250	Anti-rat IgG, HRP-linked Antibody (#7077, Cell Signaling, US)	1:10000
Anti-FAK (D2R2E) Rabbit mAb (#13009, Cell Signaling Technology, US)	1:1000	125	Anti-rabbit secondary Antibody Amersham ECL Rabbit IgG, HRP-linked whole Ab (from donkey), (#NA934-1ML, GE Healthcare Life Sciences, UK)	1:10000
Anti-phospho-FAK (Tyr397) (D20B1) Rabbit mAb (#8556, Cell Signaling Technology, US)	1:1000	125		
Anti-Akt (pan) (C67E7) Rabbit mAb (#4691, Cell Signaling Technology, US)	1:1000	60		
Anti-Phospho-Akt (Ser473) (D9E) XP® Rabbit mAb (#4060, Cell Signaling Technology, US)	1:2000	60	Anti-rabbit secondary Antibody Amersham ECL Rabbit IgG, HRP-linked whole Ab (from donkey), (#NA934-1ML, GE Healthcare Life Sciences, UK)	1:10000
Anti-p44/42 MAPK (Erk1/2) Rb Antibody (#9102, Cell Signaling Technology, US)	1:2000	44/42		
Anti-phospho-p44/42 MAPK (Erk1/2) (Thr202, Tyr204 /	1:2000	44/42		

Thr185, Tyr187) Rb Antibody (#9101, Cell Signaling Technology, US)				
Anti-KIAA1211 Rb polyclonal antibody (#PA5-60292, Invitrogen, US)	1:1000	120-130		
Anti-ANKRD28/PITK Rb polyclonal Ab, (#A300-974A-M, Bethyl-Laboratories, US)	1:1000	117		
Anti-Phospho-ANKRD28/PITK (Ser1040) Rabbit Polyclonal Antibody (#PA5-64647, Invitrogen, US)	1:1000	117		
Anti-PYGB Rb polyclonal antibody (#12075-1-AP, Proteintech, US)	1:1000	97		
Anti-NF-κB p65 (D14E12) Rb monoclonal Antibody (#8242, Cell Signaling Technology, US)	1:1000	65		
Anti-IκB epsilon (NFKBIE) (7A4) Rb monoclonal Antibody (#bsm-54094R, Bioss, US)	1:1000	40		
Anti-phospho-IκB epsilon (Ser22), Rb polyclonal Antibody (#bs-15582R, Bioss, US)	1:1000	40		
Anti-GAPDH HRP-conjugated mAb (#60004, Proteintech, US)	1:10000	36	No secondary antibody necessary	
Anti-α-Tubulin Mouse mAb (#T5168, Sigma-Aldrich, US)	1:2000	50	Goat Anti-Mouse IgG HRP-conjugated Antibody (#AP181P, Merck, DE)	1:10000

6. Fluorescence microscopy

6.1. F-actin visualization of the cytoskeleton in response to rhIL-34, rhCSF-1 or rhPTN with as well as in combination or without compound 12b

Human WM-115 and SK-MEL28 cells were starved for 24 hours by EMEM supplemented with 100 U/mL p/s without FBS in 100 mm sterile cell culture dishes. An 8 Chamber Polystyrene Vessel Tissue Culture Treated Glass Slide (#354108, BD Falcone™ CultureSlides, BD Biosciences, US) was coated with 0.2% gelatin in distilled water, incubated for one hour at 37°C, the remaining liquid was removed and air dried for another ten minutes. $1x10^4$ starved melanoma cells were added into Eppendorf tubes with EMEM supplemented with 2% FBS and 100 U/mL p/s. Afterwards 200 ng/mL rhIL-34 (#5265-IL, R&D systems, US), rhCSF-1 (Chiron, US) or rhPTN (#252-PL, R&D systems, US) was added to the Eppendorf tubes. 10 µM compound 12b was added 15 minutes prior the addition of cytokines. The whole content of Eppendorf tubes was transferred into wells of the chambered coverglass and incubated for 48 hours. Next the mixtures of cytokine as well as cytokine combined compound 12b were removed and the chambers were washed twice with pre-warmed PBS. The melanoma cells were fixed with 4% formaldehyde (pH 6.9) solution in PBS for ten minutes at room temperature (RT). The cell membranes were permeabilized with 0.1% Triton X-100 in PBS at RT for five minutes followed by washing twice with PBS. Afterwards, the F-actin cytoskeleton was stained with phalloidin and counterstained with DAPI binding DNA. The staining solution contained Phalloidin-Atto 488 Bio-Reagent (#49409, Sigma-Aldrich, US) in a ratio 1:200 to PBS and DAPI (Invitrogen, US) in a ratio of 1:2000 to PBS. The melanoma cells were incubated for 20 minutes at RT with the staining solution. After removing the chambers, the microscope slide was mounted in Citifluor AF1 antifadent mountant solutions (#AGR1320, Agar Scientific, UK) and covered by a coverslip. Fluorescence was observed with a fluorescence microscope (Nikon Eclipse 80i, JP) equipped with DAPI and fluorescein-isothiocyanate (FITC) filters at 40X, 200X and 600X magnification and images were digitally acquired.

7. Statistical analysis

Data were provided as mean±SD (standard deviation). All statistical analyses were performed using GraphPad Prism Version 6.01. Statistical analysis was done using one-way analysis of variance (ANOVA) by the usage of multiple comparison analysis Tukey test (later mentioned as one-way ANOVA). Additionally, the unpaired t-test with Welch's correction (later mentioned as Welch's t-test) was used when appropriate. A p-value lower than 0.05 was associated with significance (*$p<0.05$, **$p<0.01$, ***$p<0.001$, ****$p<0.0001$). The error bars indicate standard deviation (SD).

D. Results

1. Baseline signaling differ in human melanoma skin cancer cells

Melanoma cell lines differ due to somatic mutations but they recapitulate the mutational and transcriptional profiles of patient tumors making melanoma cell lines suitable for tumor models. Furthermore, it is crucial to understand similarities and differences between melanoma cell lines to answer specific research questions [199]. WM-115 demonstrates a primary melanoma cell line in vertical growth phase whereas SK-MEL-28 represents a more malignant melanoma cell line, thus these cell lines are beneficial to utilize and for describing various melanoma tumor phenomena [213]. It is known that FAK signaling is associated with an aggressive melanoma phenotype regulating invasion and migration, whereas the RAS-RAF-MEK-ERK MAPK pathway plays a role in proliferation [105, 220]. Additionally, PI3K/Akt/mTOR signaling has an important role in several cellular processes such as survival and cell proliferation [2, 220]. To assess whether protein phosphorylations of key signaling pathways differ at baseline expression level in these two melanoma skin cancer cell lines, we extracted proteins of untreated SK-MEL-28 and WM-115 melanoma cells. When analyzed by Western blotting (Fig. 10A), we found differences in protein phosphorylation between these melanoma cell lines. In WM-115 cells, the phosphorylation expression of protein kinase B (AKT) at Ser347 (Fig. 10D) was ~2.4-fold higher and of extracellular signal-regulated kinase 1/2 (ERK 1/2, later referred as ERK) at Thr202, Tyr204, Thr185 and Tyr187 (Fig. 10E) was ~2.3-fold higher than compared to SK-MEL-28 cells. However, in SK-MEL-28 cells, expression of phosphorylated focal adhesion kinase (FAK) at Tyr397 (Fig. 10C) was ~2.3-fold higher than compared to WM-115 cells. Furthermore, the protein expression of PTPRζ1 (Fig. 10B) was ~50% lower in SK-MEL-28 cells compared to WM-115 cells.

Collectively, our results demonstrate that phosphorylation of FAK, AKT and ERK differ at baseline expression level between these melanoma cell lines. AKT and ERK are more active in the primary WM-115 melanoma cell line, which also has higher PTPRζ1 expression whereas the FAK pathway is more active in the malignant SK-MEL-28 melanoma cell line.

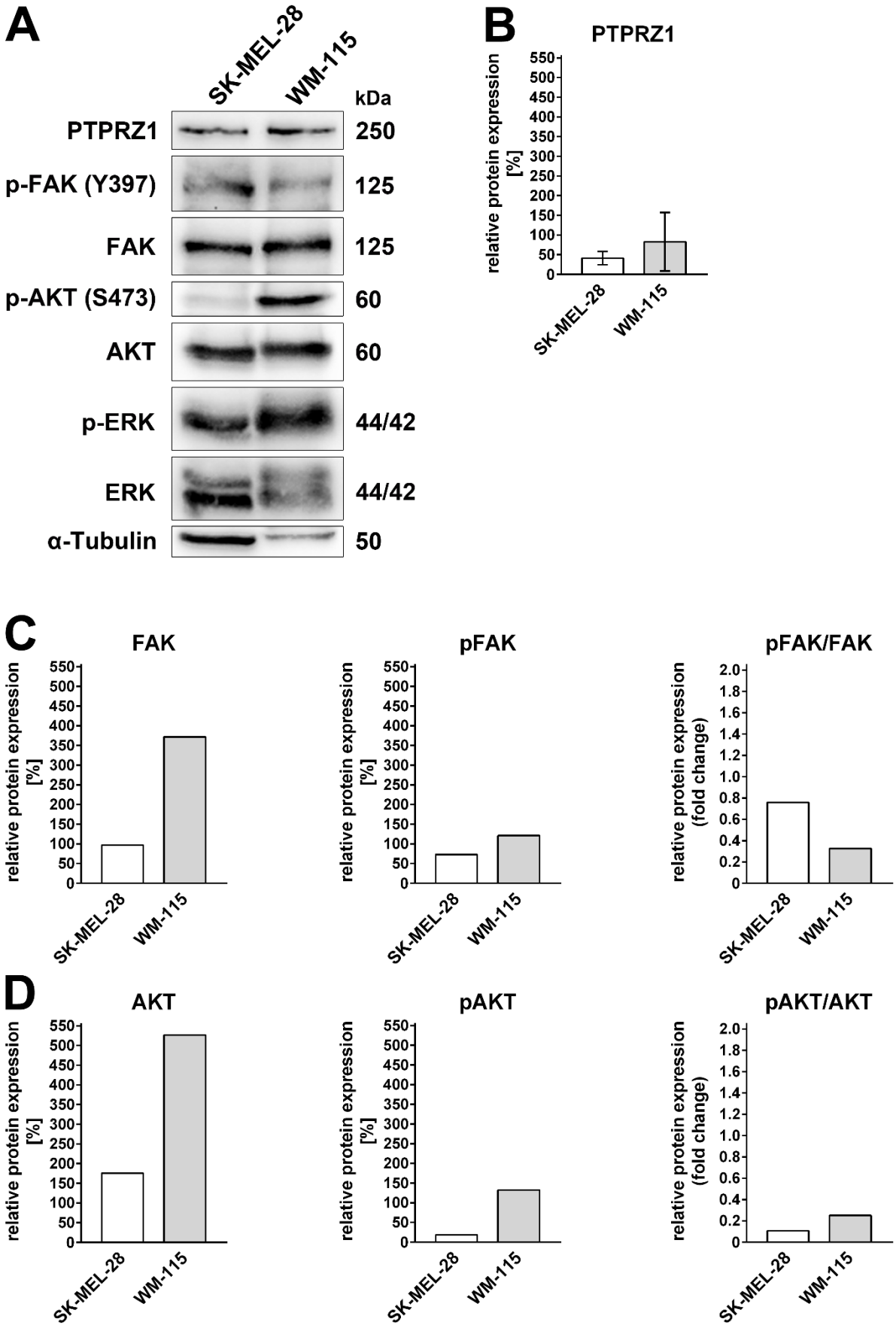

Figure 10. Baseline protein expression in melanoma skin cancer cell lines: A: Untreated SK-MEL-28 cells and WM-115 cells were cultured in medium EMEM supplemented with 10%

FBS and 100 U/mL p/s for protein expression at baseline. Western blot images of indicated proteins in melanoma cell lines are shown. p- indicates phosphorylated proteins. α-Tubulin was used as loading control. **B-E:** Quantification of protein expressions in melanoma cell lines relative to the protein expression of SK-MEL-28 cells. **B:** Quantification of protein expression levels of PTPRζ1. **C:** Quantification of protein expression levels of FAK and pFAK. **D:** Quantification of protein expression levels of AKT and pAKT.

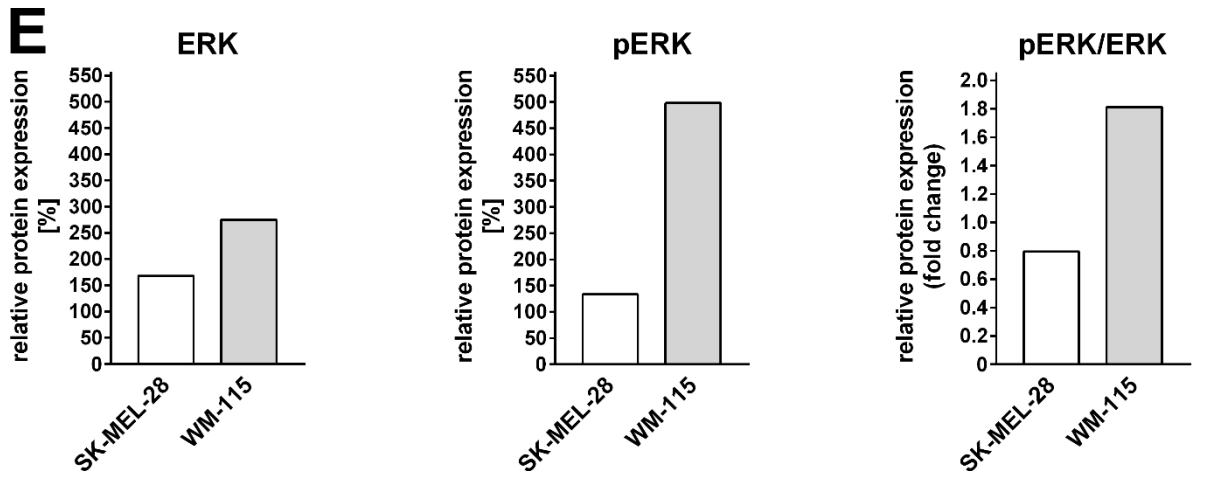

Figure 10. Baseline protein expression in melanoma skin cancer cell lines: E: Quantification of protein expression levels of ERK and pERK.

2. Comparison of gene expressions in melanoma skin cancer cell lines upon stimulation with rhIL-34, rhCSF-1 or rhPTN

It is known that IL-34 binds and signals via CSF-1R, Syndecan-1 and PTPRζ1, whereas PTN binds receptors of SDC-1 and PTPRζ1 and in case of CSF-1 binding with CSF-1R (Fig. 5) [118, 153, 151]. To experimentally evaluate whether expression of *PTPRZ1*, *CSF-1R*, *SDC-1*, *IL-34*, *CSF-1* and *PTN* is directly regulated in melanoma cell lines, we assessed the effect of recombinant human (rh)IL-34, rhCSF-1 and rhPTN on SK-MEL-28 cells and WM-115 cells. To do so, SK-MEL-28 and WM-115 cells were starved overnight and then treated with 125 ng/mL recombinant human IL-34, CSF-1 or PTN for 48 hours and RNA expression levels were measured by quantitative real-time (qRT)-PCR. In SK-MEL-28 cells, rhCSF-1 treatment led to an ~2.2-fold increase in *PTPRZ1* gene expression (Fig. 11A), ~3.4-fold increase in *CSF-1R* (Fig. 11B), ~2.5-fold increase in *IL-34* (Fig. 11D) and ~2.4-fold increase in *CSF-1* (Fig. 11E). Although these data did not meet statistical significance by one-way ANOVA by the usage of multiple comparison analysis Tukey test, the results indicate that CSF-1 but not IL-34 and PTN increase *CSF-1R*, *PTPRZ1*, *IL-34* and *CSF-1* gene expression. In contrast, in WM-115 cells rhCSF-1 treatment only resulted in ~4.5-fold increased *CSF-1R* (Fig. 11H) gene expression. In addition, rhIL-34 treatment also non-significantly increased *CSF-1R* (Fig. 11H) gene expression ~2.6-fold.

Collectively, our results indicate that rhCSF-1 and rhIL-34 treatment results in moderate differential changes in *CSF-1R* gene expression in WM-115 cells and SK-MEL-28 cells.

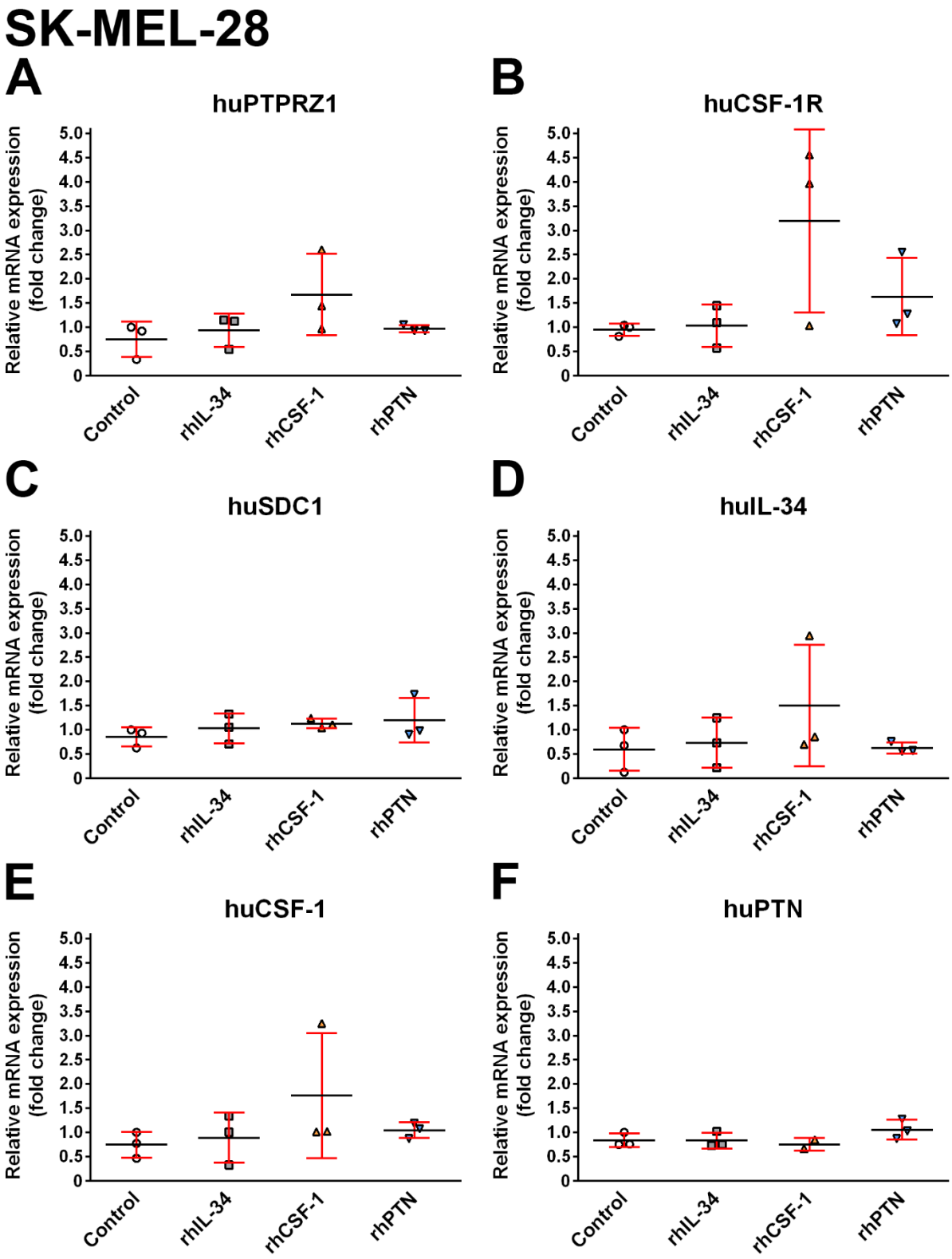

Figure 11. Comparison of gene expressions in melanoma cell lines upon stimulation with rhIL-34, rhCSF-1 or rhPTN: A-L: Melanoma cell lines were treated for 48 hours with 125 ng/mL recombinant human (rh)IL-34, rhCSF-1 or rhPTN. The mRNA levels were measured by qRT-PCR. Red error bars indicate standard deviation (SD) and the black lines show the mean. **A-F:** Quantifications of mRNA in SK-MEL-28 cells. **B:** mRNA expression levels of *huCSF-1R*. **C:** *huSDC1* expression levels. **D:** Expressions of *hu-IL-34*. **E:** mRNA expressions of *huCSF-1*. **F:** Relative *huPTN* mRNA expressions.

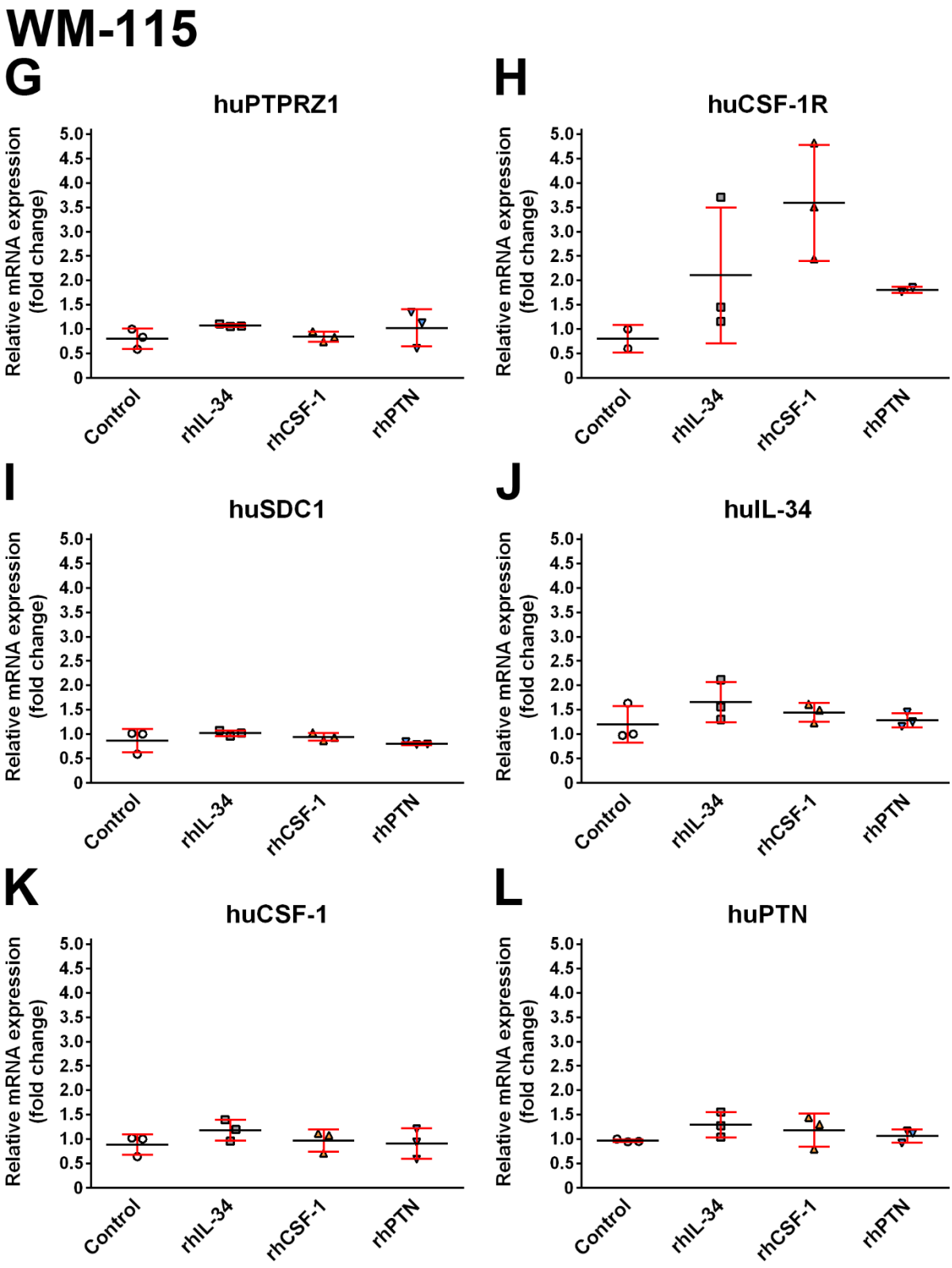

Figure 11. Comparison of gene expressions in melanoma cell lines upon stimulation with rhIL-34, rhCSF-1 or rhPTN: G-L: Quantifications of mRNA in WM-115 cells treated for 48 hours with 125 ng/mL recombinant human rhIL-34, rhCSF-1 or rhPTN. **G:** Relative *huPTPRZ1* mRNA expressions. **H:** mRNA expression levels of *huCSF-1R*. **I:** *huSDC1* expression levels. **J:** Expressions of *hu-IL-34*. **K:** mRNA expressions of *huCSF-1*. **L:** Relative *huPTN* mRNA expressions.

3. Signaling in melanoma skin cancer cell lines upon stimulation with rhIL-34, rhCSF-1 or rhPTN

To determine activated downstream signaling transduction of PTPRζ1 and CSF-1R in melanoma cell lines, we examined phosphorylation of various downstream substrates upon stimulation with rhIL-34, rhCSF-1 and rhPTN. To do so, we treated starved overnight SK-MEL-28 cells and WM-115 cells with 125 ng/mL rhIL-34, rhCSF-1 or rhPTN for five minutes and analyzed by Western blotting (Fig. 12A). In SK-MEL-28 cells, rhPTN treatment led to a statistical significant ~4.6-fold increase ($p=0.0005$) in FAK phosphorylation (Fig. 12B), and an ~1.9-fold increase (n.s.) in Signal transducer and activator of transcription 3 (STAT3) phosphorylation on tyrosine residue Tyr705 (Fig. 12B). In addition, rhCSF-1 treatment also increased STAT3 phosphorylation ~1.6-fold (Fig. 12B) as well as FAK phosphorylation 2.3-fold (Fig. 12B) whereas rhIL-34 treatment only increased FAK phosphorylation 1.9-fold (Fig. 12B) but did not increase STAT3 phosphorylation (Fig. 12B). Although most of these data did not meet statistical significance by one-way ANOVA, the results demonstrate PTN increases FAK phosphorylation and indicate that IL-34 and CSF-1 increase phosphorylation of FAK whereas CSF-1 and PTN but not IL-34 increase STAT3 phosphorylation. In contrast, in WM-115 cells rhIL-34, rhCSF-1 and rhPTN treatments showed no increase in FAK phosphorylation (Fig. 12C). However, in WM-115 cells rhPTN treatment led to a statistical significant ~2.3-fold increase ($p=0.0243$) in STAT3 phosphorylation (Fig. 12C). In addition, rhIL-34 and rhCSF-1 treatments also non-significantly increased STAT3 phosphorylation ~1.9-fold (n.s.) respectively ~1.8-fold (n.s.) (Fig. 12C). In SK-MEL-28 cells as well as in WM-115 cells treatments of rhIL-34, rhCSF-1 and rhPTN showed no significant increase of PTPRZ1 expression (Fig. 12B respectively 12C), AKT phosphorylation (Fig. 12B respectively 12C), and ERK phosphorylation (Fig. 12B respectively 12C).

Collectively, our results demonstrate rhPTN treatment increases FAK phosphorylation in SK-MEL28 cells and STAT3 phosphorylation in WM-115 cells. Furthermore, indicating that rhIL-34 and rhCSF-1 treatment results in moderate differential changes of FAK phosphorylation only in SK-MEL-28 cells but also moderate differential changes of STAT3 phosphorylation by rhIL-34, rhCSF-1 and rhPTN treatment in both cell lines except of rhIL-34 treatment in SK-MEL-28 cells.

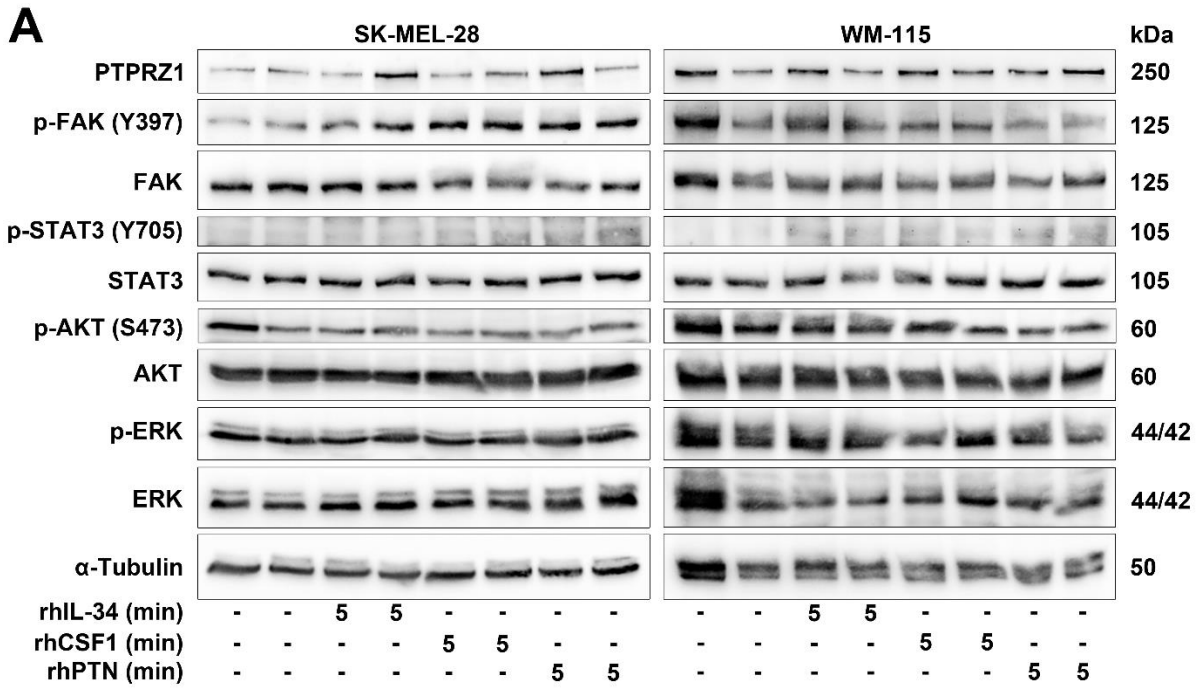

Figure 12. Cell signaling upon stimulation with rhIL-34, rhCSF-1 or rhPTN in SK-MEL-28 & WM-115 cells: A: Western blot images of indicated proteins in melanoma cell lines are shown. SK-MEL-28 and WM-115 were treated for 5 minutes with 125 ng/mL rhIL-34, rhCSF-1 or rhPTN. p- indicates phosphorylated proteins.

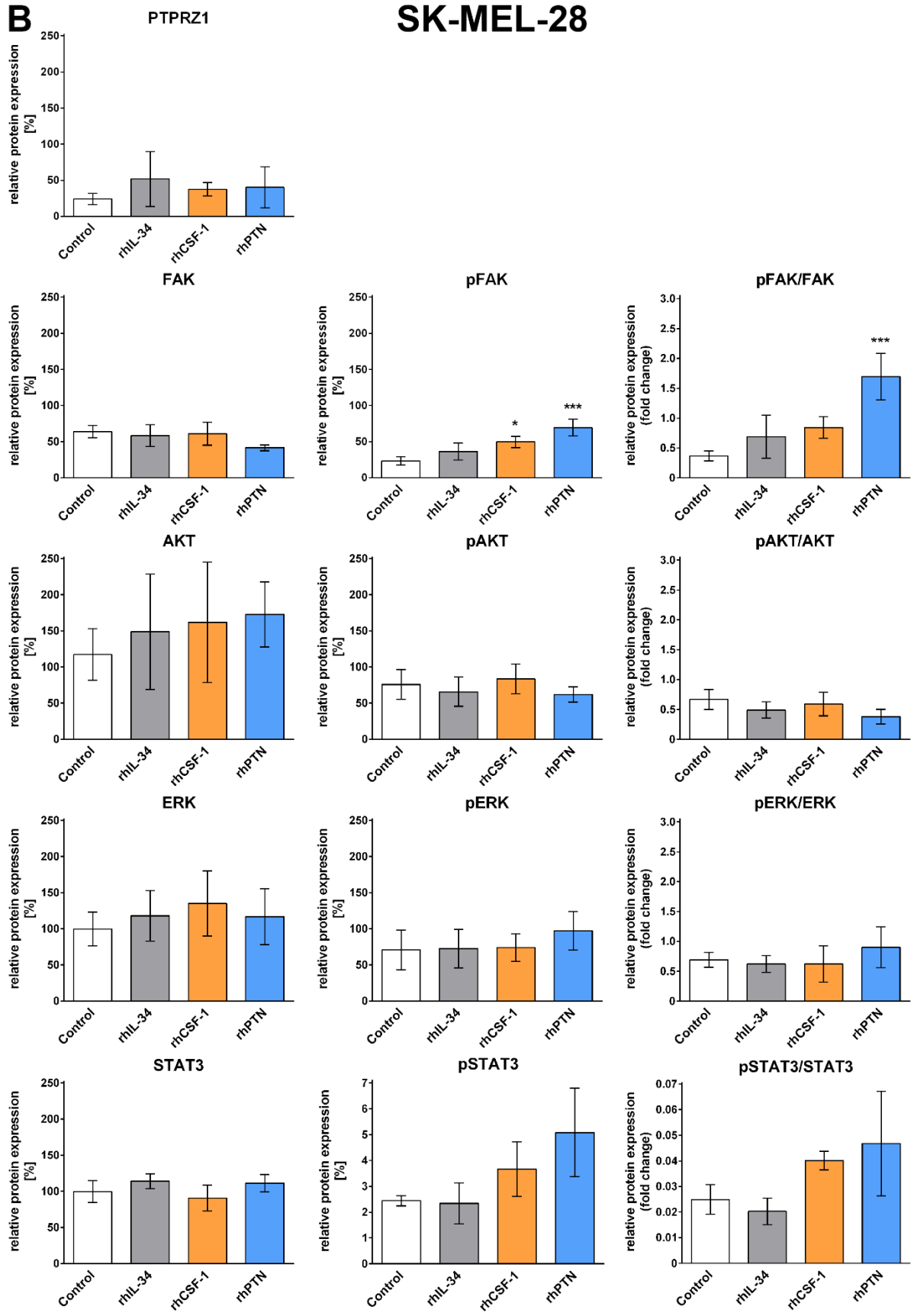

Figure 12. Cell signaling upon stimulation with rhIL-34, rhCSF-1 or rhPTN in SK-MEL-28 cells: B: Quantification of protein expressions in SK-MEL-28 cells.

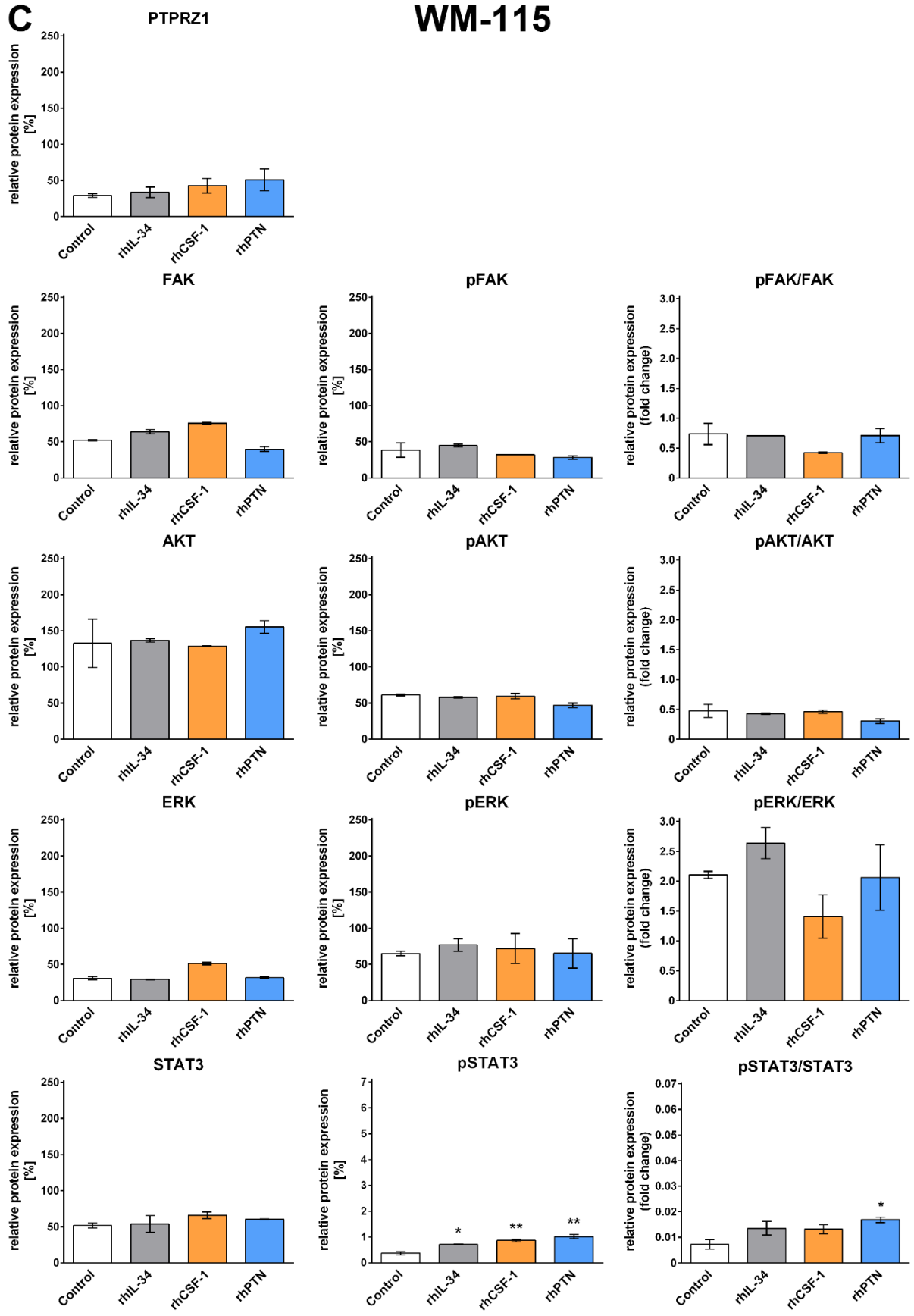

Figure 12. Cell signaling upon stimulation with rhIL-34, rhCSF-1 or rhPTN in WM-115 cells: C: Quantification of protein expressions in WM-115 cells.

3.1. Time series of FAK signaling transduction in melanoma WM-115 cells upon stimulation with rhIL-34, rhCSF-1 or rhPTN

In order to further investigate activated downstream signaling transduction of PTPRζ1 and CSF-1R in melanoma cell lines and to assess whether phosphorylation of downstream substrate activation varies in a cytokine time-dependent manner, we incubated WM-115 cells with rhIL-34, rhCSF-1 and rhPTN for various durations of time. To do so, we incubated starved overnight WM-115 cells with 100 ng/mL rh-IL-34 or rhCSF-1 for one, five, fifteen, thirty and sixty minutes whereas 100 ng/mL rhPTN treatment included incubation periods of 5, 15, 30 and 60 minutes. When analyzed by Western blotting, rhIL-34 treatment led to increased FAK phosphorylation on tyrosine residue Tyr397 (Fig. 13A) of one minute by ~1.82-fold, 5 minutes by ~2.89-fold ($p=0.0487$), 15 minutes by ~2.91-fold ($p=0.0463$), 30 minutes by ~1.70-fold and 60 minutes by ~1.65-fold (Fig. 13B). Furthermore, FAK phosphorylations reached their peaks at 5 and 15 minutes of rhIL-34 treatment which were statistical significant demonstrating rhIL-34 treatment increases FAK phosphorylation. Also, treatment with rhPTN (Fig. 13E) led to an elevated FAK phosphorylation at 5 minutes by ~1.78-fold ($p=0.0473$) and 15 minutes by ~1.24-fold, followed by decreased FAK phosphorylation at 30 minutes by ~0.54-fold and at 60 minutes by ~0.79-fold (Fig. 13F). Phosphorylation of FAK reached its highest peak at 5 minutes of rhPTN treatment which was statistical significant demonstrating rhPTN treatment increases FAK phosphorylation. In contrast, rhCSF-1 treatment only led to moderate increase of FAK phosphorylation (Fig. 13C) of one minute by ~1.51-fold, 5 minutes by ~1.30-fold, 15 minutes by ~1.38-fold, 30 minutes by ~1.34-fold and 60 minutes by ~1.13-fold (Fig. 13D). Phosphorylation of FAK reached its highest peak at one minute by rhCSF-1 treatment. However, these data did not meet statistical significance, indicating that rhCSF-1 treatment moderately increases FAK phosphorylation. The rhPTN treatment also showed moderate increase of ERK phosphorylation (Fig. 13G) with its peaks at 5 minutes by ~1.32-fold and 30 minutes by ~1.42-fold (Fig. 13I) demonstrating that rhPTN treatment only moderately differentially changes the ERK phosphorylation. The Western blot (Fig. 13G) also showed that rhPTN treatment increases STAT3 phosphorylation on tyrosine residue Tyr705 (Fig. 13H) reaching the highest peak by ~1.74-fold at 5 minutes followed by ~0.88-fold decrease at 15 minutes and increase by ~1.07-fold at 30 minutes and decreased at 60 minutes by~0.44-fold. The results indicate that rhPTN treatment increases STAT3 phosphorylation at 5 minutes incubation period.

Collectively, our results demonstrate that rhPTN and rhIL-34 treatment results in increased FAK phosphorylation in WM-115 cells whereas rhCSF-1 treatment resulting only in moderate differential changes of the FAK phosphorylation, and indicating that rhPTN treatment increases STAT3 phosphorylation in WM-115 cells.

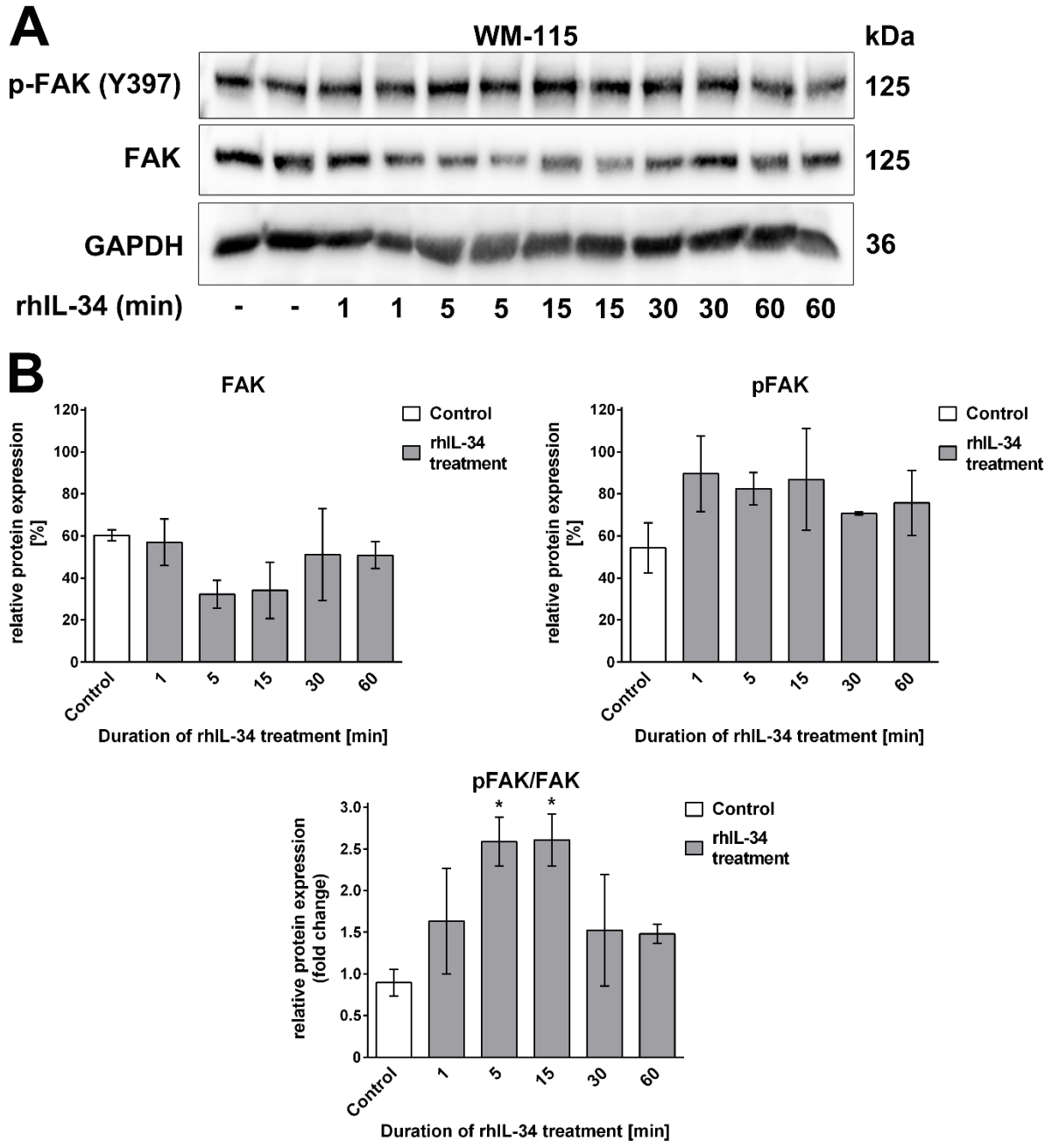

Figure 13. Time series of rhIL-34, rhCSF-1 or rhPTN stimulation in WM-115 cells: A-I: The melanoma WM-115 cells were treated with 100 ng/mL rhIL-34, rhCSF-1 or rhPTN in a time span of 60 minutes and measured during various time points. **A:** Shown are representative Western blots of WM-115 cells stimulated by 100 ng/mL recombinant human IL-34 with time measurements of 1, 5, 15, 30 and 60 minutes. **B:** Protein quantifications of rhIL-34 stimulation over a time span of 60 minutes.

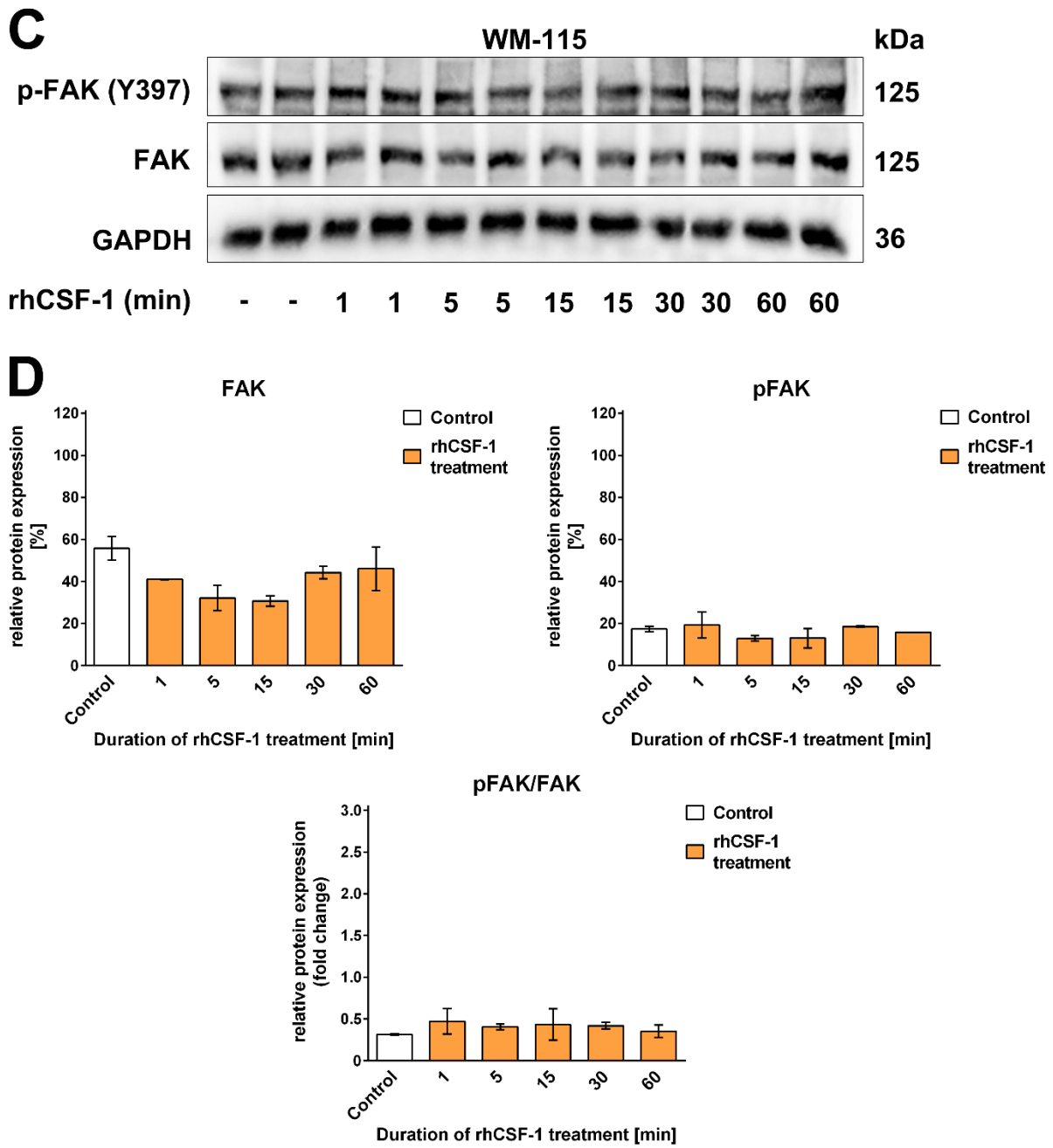

Figure 13. Time series of rhIL-34, rhCSF-1 or rhPTN stimulation in WM-115 cells: C: Shown are representative Western blots of WM-115 cells stimulated by 100 ng/mL recombinant human CSF-1 with time measurements of 1, 5, 15, 30 and 60 minutes. **D:** Protein quantifications of rhCSF-1 treatment of various time points.

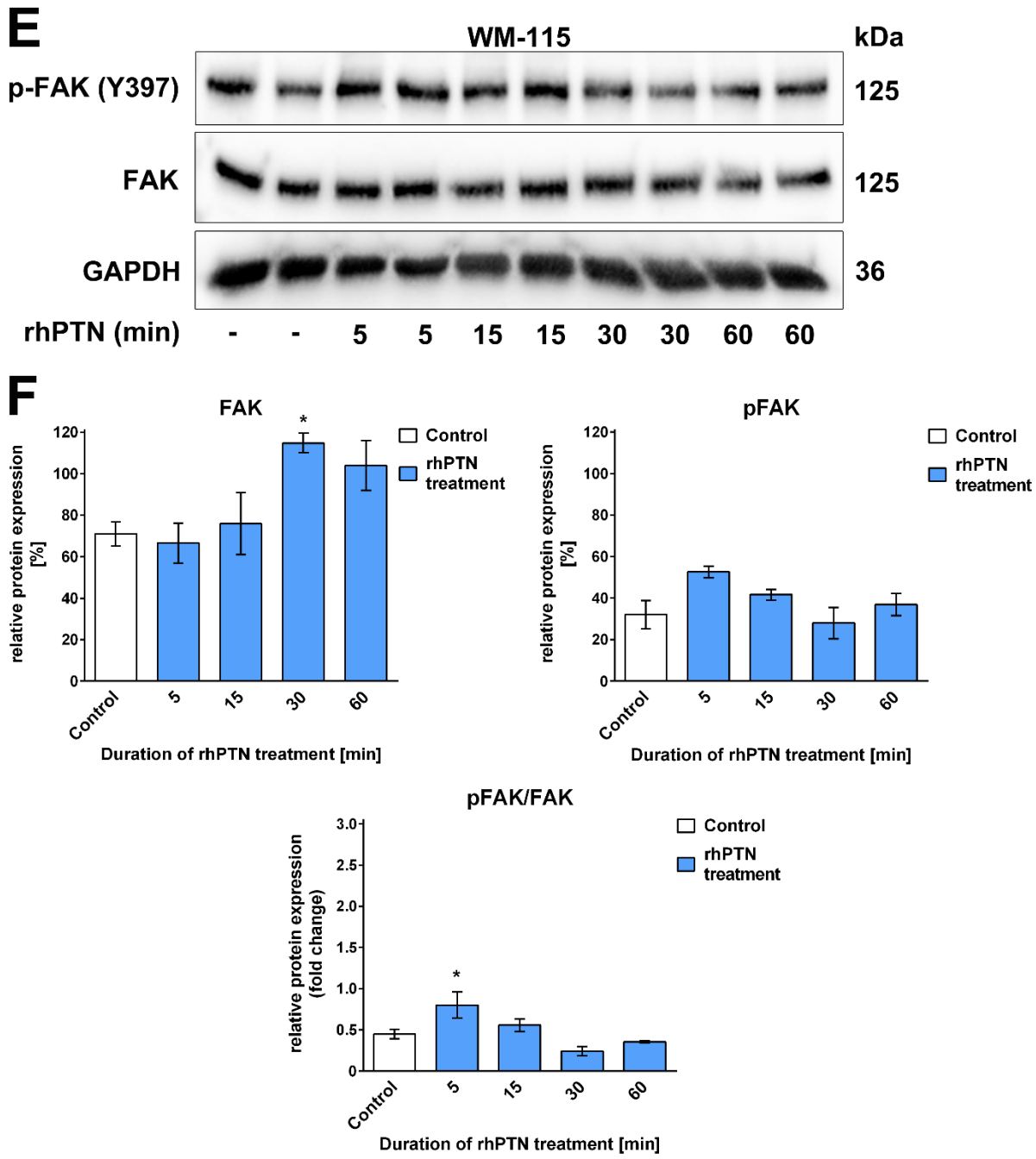

Figure 13. Time series of rhIL-34, rhCSF-1 or rhPTN stimulation in WM-115 cells: E: Shown are representative Western Blots in melanoma cells stimulated with 100 ng/mL rhPTN over a duration of 60 minutes with time measurements of 5, 15 ,30 , 60 minutes. **F:** Protein quantifications of rhPTN stimulation over a time span of 60 minutes.

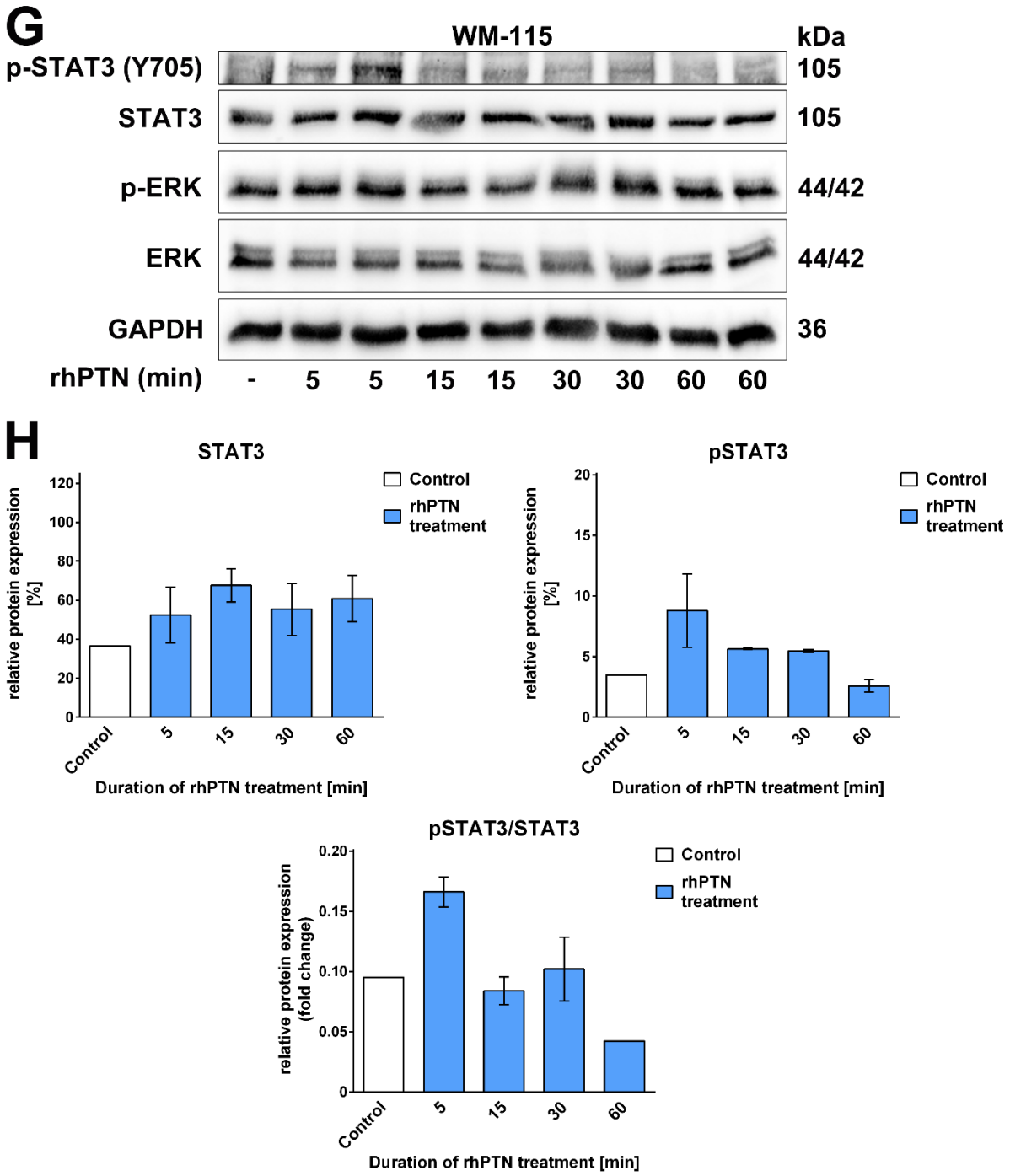

Figure 13. Time series of rhIL-34, rhCSF-1 or rhPTN stimulation in WM-115 cells: G: Shown are representative Western Blots in melanoma cells stimulated with 100 ng/mL rhPTN over a duration of 60 minutes with time measurements of 5, 15 ,30 , 60 minutes. **H:** Protein quantifications of rhPTN stimulation over a time span of 60 minutes.

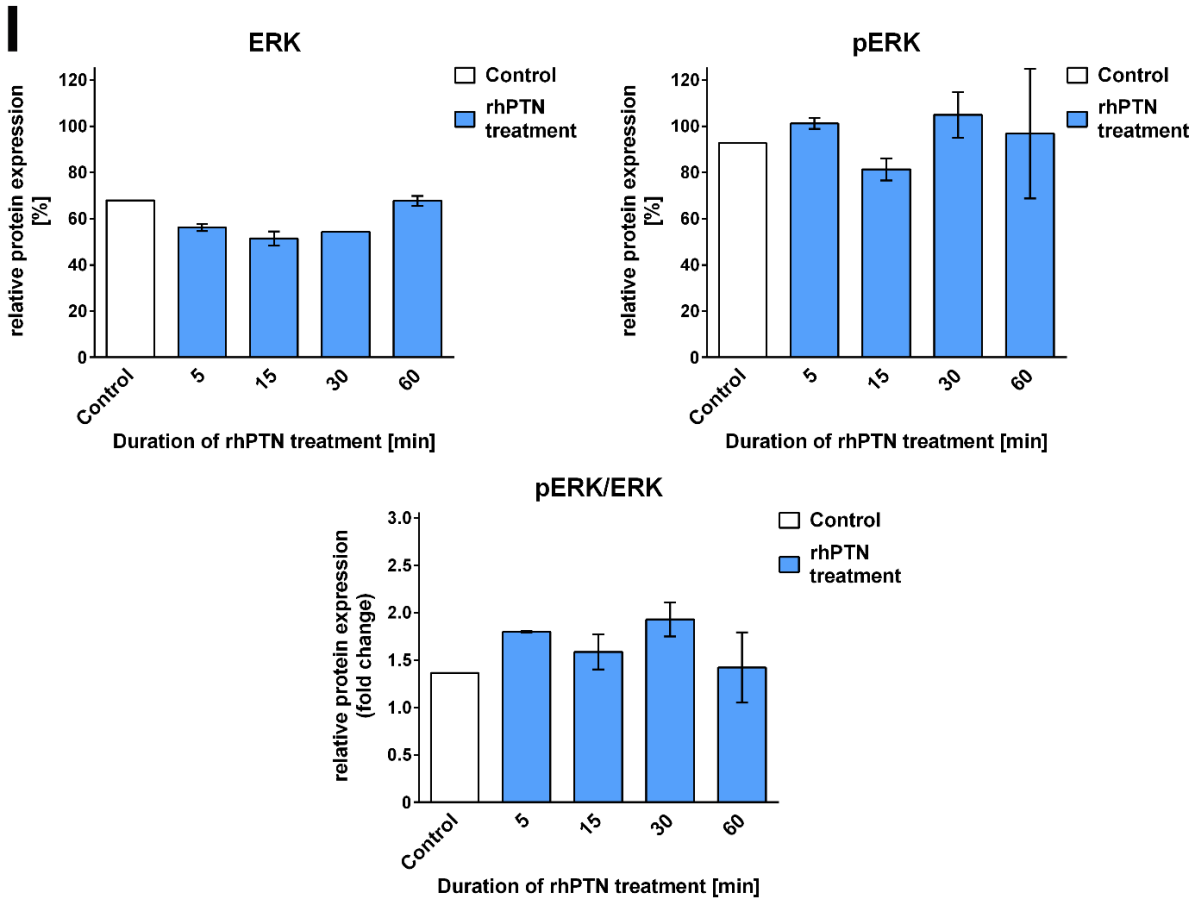

Figure 13. Time series of rhIL-34, rhCSF-1 or rhPTN stimulation in WM-115 cells: I: Protein quantifications of Western Blots shown in G by stimulation of 100 ng/mL rhPTN over a time span of 60 minutes.

4. Novel PTPRζ1 inhibitors – compound 10a & 12b regarding their cytotoxicity and viability in melanoma cell lines

The synthesized small molecule PTPRζ1 inhibitors known as compound 10a (MY10) and compound 12b (MY33-3) were designed to inhibit PTPRζ1 by interacting with its phosphatase activity site in the intracellular domain PD1 resulting in inhibition of the intrinsic phosphatase activity of PTPRζ1. These inhibitors are mimicking the action of PTN which upon binding also inhibits the phosphatase activity of PTPRζ1 and it is known that this receptor inhibition by PTPRζ1 inhibitors are leading to activation of ALK tyrosine kinase receptor followed by increased tyrosine phosphorylation of downstream substrates TrkA and ALK [219, 221]. These inhibitors could be beneficial to study the differences in downstream signaling of PTPRζ1 and CSF-1R upon cytokine stimulations. To determine the adequate dosage usage of these PTPRζ1 inhibitors for further signaling studies in melanoma cell lines, we examined whether compound 10a and 12b effect the viability of melanoma cells by using trypan blue (TB) and Acridine Orange/Propidium Iodide staining (AO/PI) staining methods. A prominent cell viability staining method is the usage of trypan blue which stains nonviable cells blue when viewed by light microscopy whereas viable cells with intact cell membranes remain colorless by excluding the dye. However, trypan blue staining assays can be difficult to interpret due to staining artifacts such as cell debris as well as variable staining or shading of cells [222]. To overcome this issue, we additionally used the AO/PI staining method in combination with the LUNA-FL™ Automated Cell Counter which advanced counting algorithm detecting individual cells in clusters as well as its more precise measurements distinguishes live and dead cells from debris [223]. Additionally, compared to trypan blue, AO and PI simultaneously visualizes viable and nonviable cells [222]. AO is a cell membrane permeable dye and stains nucleic acids of both live and dead cells visualizing the entire cell population by green fluorescence. In comparison, PI is a cell membrane impermeable dye that can only enter dead cells of comprised cell membrane integrity thereby binding to nucleic acids and visualized by red fluorescence. The PI red fluorescence signal absorbs the AO green fluorescence signal in nonviable cells thereby ensuring no double positive results. The combination of the dual staining of AO/PI as well as the automated cell counting system facilitates the precise distinction between live and dead cells as well as accurate cell number determination [223]. Therefore, we incubated WM-115 cells for 24 hours with compound 10a dosages of 20-, 50- and 100 µM (Fig. 14B) and compound 12b dosages of 1-, 2-, 5-, 10-, 20-, 50-, and 100 µM (Fig. 14A). These compound concentrations of 1-, 2-, 5-, 10-, 20-, 50-, and 100 µM were dissolved in 0.005%-, 0.01%-, 0.025%-, 0.05%-, 0.1%-, 0.25% respectively 0.5% DMSO. Moreover, these low concentrations of DMSO can be considered to have no cytotoxic effect to these melanoma cell lines. 4% DMSO was used to simulate cell death. Cell viability analysis of compound 12b treatment (Fig.

14A) at 24 hours showed only differential changes at dosage concentration of 100 µM by a ~29% decrease in WM-115 cell viability measured by trypan blue staining method and by AO/PI staining method a statistical significant decrease of ~41% ($p<0.0001$) WM-115 cell viability. It demonstrates that the viability of WM-115 cells drastically decreases by 100 µM compound 12b treatment after 24 hours as well as the difference staining methods by trypan blue compared to the more accurate AO/PI staining method. In contrast, the compound 10a treatment with 100 µM as well as with 20- and 50 µM (Fig. 14B) showed no differential changes of WM-115 cell viability after 24 hours by using AO/PI staining method. It is demonstrating that concentrations of compound 10a up to 100 µM do not effect WM-115 cell viability and do not mediate cell death.

Collectively, our results demonstrate that compound 10a and 12b up to 50 µM do not effect cell viability and do not mediate cell death in SK-MEL-28- and WM-115 cells.

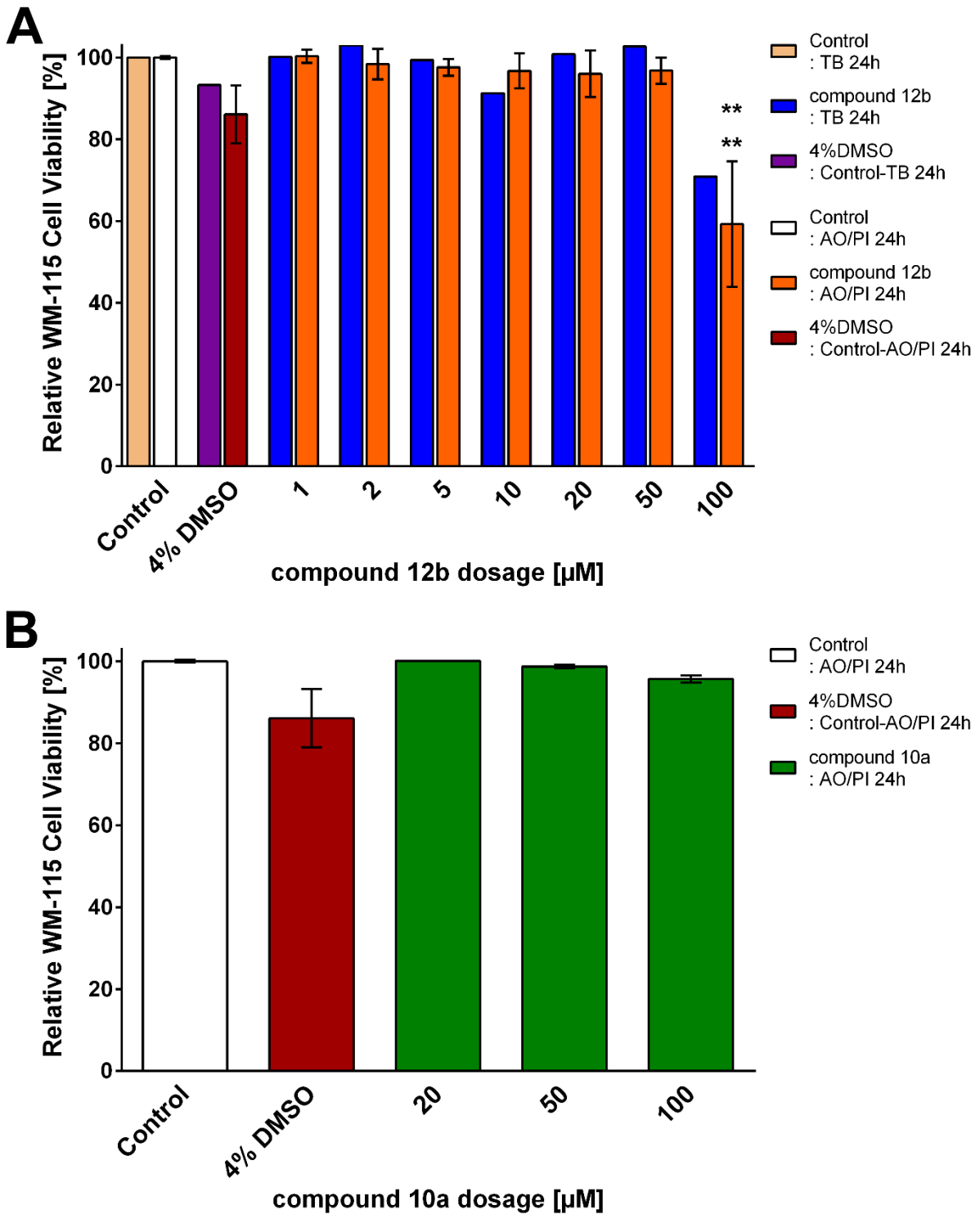

Figure 14. Viability of PTPRζ1 inhibitors compound 10a and 12b in melanoma cell lines: **A-B:** WM-115 cells were treated for 24 hours with various concentration levels of PTPRζ1 inhibitors. Cell viability was measured by LUNA-FL™ Automated Cell Counter using Acridine Orange/Propidium Iodide (AO/PI) double staining method or the trypan blue (TB) staining method. **A:** WM-115 cell viability upon compound 12b treatment with concentration levels of 1-, 2-, 5-, 10-, 20-, 50- and 100 µM. **B:** WM-115 cell viability upon compound 10a treatment with dosages of 20-, 50- and 100 µM.

4.1. Novel PTPRζ1 inhibitors – compound 10a & 12b regarding their proliferation in melanoma cell lines

To further study biological effects of compound 10a and 12b in melanoma cell lines, we investigated whether they influence proliferation. First, in order to determine whether these compounds effect proliferation of melanoma cell lines, we treated SK-MEL-28 cells and WM-115 cells with compound 10a and 12b dosages of 1-, 2-, 5-, 10-, 20-, 50-, and 100 µM for 48 hours and additionally only in SK-MEL-28 cells for 24 hours. After using cell proliferation reagent WST-1, the analyzed proliferation of SK-MEL-28 cells showed in compound 12b treatment (Fig. 15A) as well as in compound 10a treatment (Fig. 15B) for 24 hours the same overall dose-dependent moderate increase of proliferation up to 5 µM followed by an overall slightly decrease up to 100 µM. However, these data did not meet statistical significance demonstrating that compound 10a and 12b do not have an effect on proliferation at a variety of dosages up to 100 µM at 24 hours in SK-MEL-28 cells. Also proliferation of compound 12b treatment for 48 hours in SK-MEL-28 cells (Fig. 15A) showed an overall dose-dependent slightly increase up to 5 µM followed by an overall moderate decrease up to 50 µM and subsequently moderate increase again at 100 µM to a value as high as previously at 5 µM. Again, the data were not significant demonstrating that compound 12b has no proliferatory effect by various dosages of treated SK-MEL-28 cells for 48 hours. In contrast, in WM-115 cells 100 µM compound 12b treatment (Fig. 15C) led to a statistical significant ~30% decrease ($p=0.0163$) whereas no differential changes were in dosages of 1-, 2-, 5-, 10-, 20- and 50 µM. The results demonstrate that 100 µM compound 12b decreases proliferation. In comparison, compound 10a treatment in SK-MEL-28 cells for 48 hours (Fig. 15B) showed an overall moderate dose-dependent increase up to 10 µM and subsequently dose-dependent reduction up to 100 µM. Although, these data did not meet statistical significance demonstrating that compound 10a has no proliferatory effect by various dosages of treated SK-MEL-28 cells for 48 hours. Also compound 10a treatment in SK-MEL-28 cells for 48 hours (Fig. 15D) showed an overall moderate increase in proliferation from 1 µM to 100 µM. Again, the data were not significant demonstrating moderate differential changes in compound 10a for 48 hours at various concentrations.

Collectively, our results demonstrate that compound 10a and 12b do not effect proliferation in both cell lines of SK-MEL-28 cells and WM-115 cells up to 50 µM and only 100 µM compound 12b dosage mediates reduction of cell proliferation in WM-115 cells.

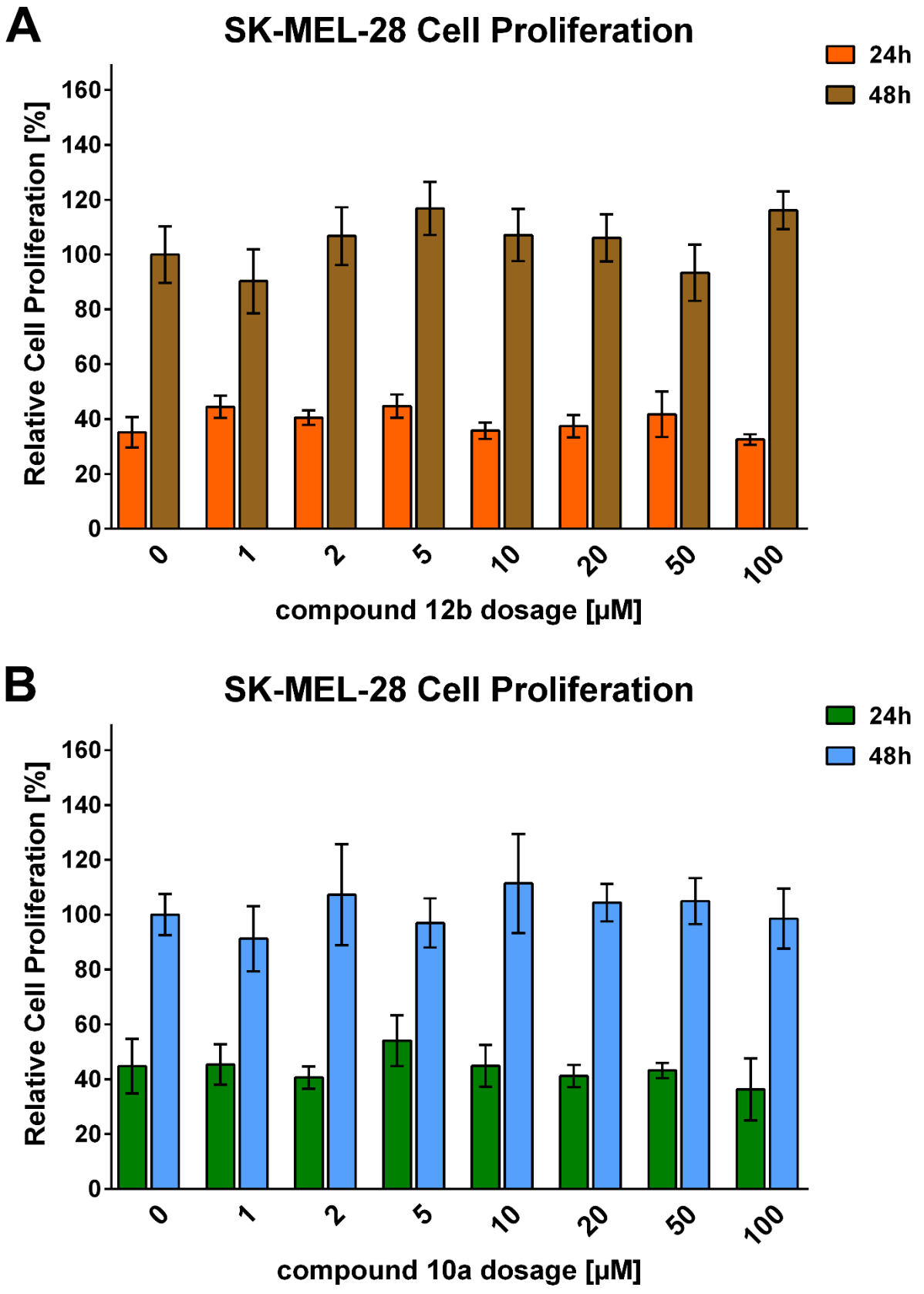

Figure 15. The proliferation of melanoma cell lines upon PTPRζ1 inhibitors: A-D: Proliferation of melanoma cell lines treated with PTPRζ1 inhibitors concentration levels of 1-, 2-, 5-, 10-, 20-, 50-, 100 µM. **A:** Proliferation of SK-MEL-28 cells were treated with compound 12b for 24 and 48 hours. **B:** Proliferation of SK-MEL-28 cells treated with compound 10a for 12 and 48 hours.

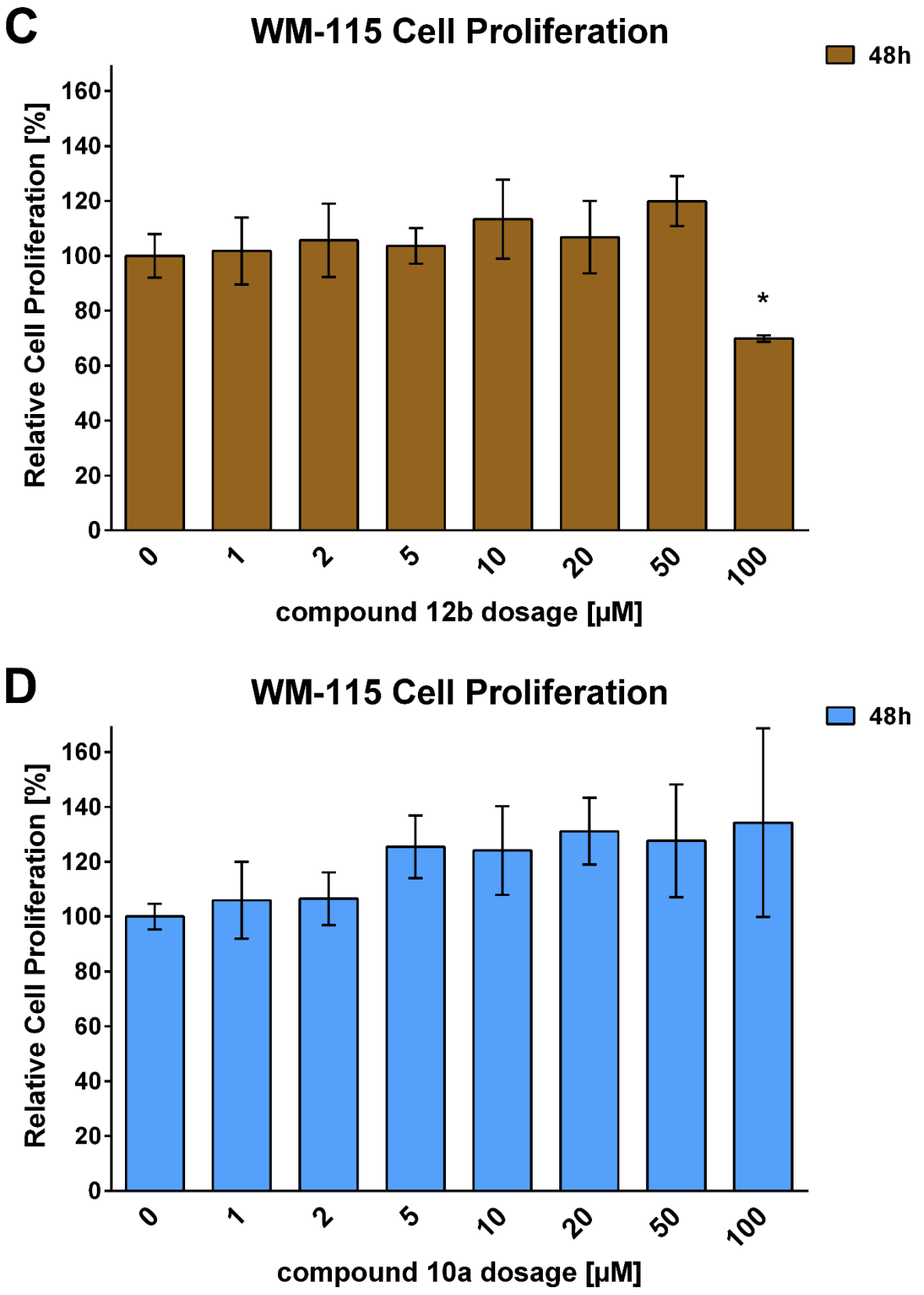

Figure 15. The proliferation of melanoma cell lines upon PTPRζ1 inhibitors: C: Proliferation of WM-115 cells treated with compound 12b for 48 hours. **D:** Proliferation of WM-115 cells treated with compound 10a for 48 hours.

4.2. Novel PTPRζ1 inhibitors – compound 10a & 12b regarding their migration in melanoma cell lines

Next we examined whether compound 10a and 12b influence migration of melanoma cell lines. Therefore, we treated WM-115 cells for 48 hours with compound 12b in dosages of 2-, 5-, 10-, 20-, 50-, 100 µM and with compound 10a concentrations of 20- and 50 µM during transwell migration assay. Treatment with 200 ng/mL rhIL-34 on WM-115 cells was used to simulate cell migration. In WM-115 cells compound 10a treatment led to a decrease at dosages of 20 µM by 23% in cell migration (Fig. 16A) whereas of 50 µM reduced only by 4% demonstrating moderate migration decrease by compound 10a. Furthermore, compound 12b treatment in WM-115 cells increased migration by 41% and 33% upon treatment with 2 µM respectively with 20 µM (Fig. 16A) whereas concentrations of 5, 10, 50 and 100 µM treatment decreased WM-115 cell migration by 37%, 34%, 48% respectively 93%. The results indicate that compound 12b treatment reduces migration the strongest at 50 µM and 100 µM.

Collectively, our results indicate that compound 12b treatment at dosage levels of 50 µM and 100 µM has the strongest effect on reducing migration whereas compound 10a treatment only results in moderate differential changes in migration in WM-115 cells.

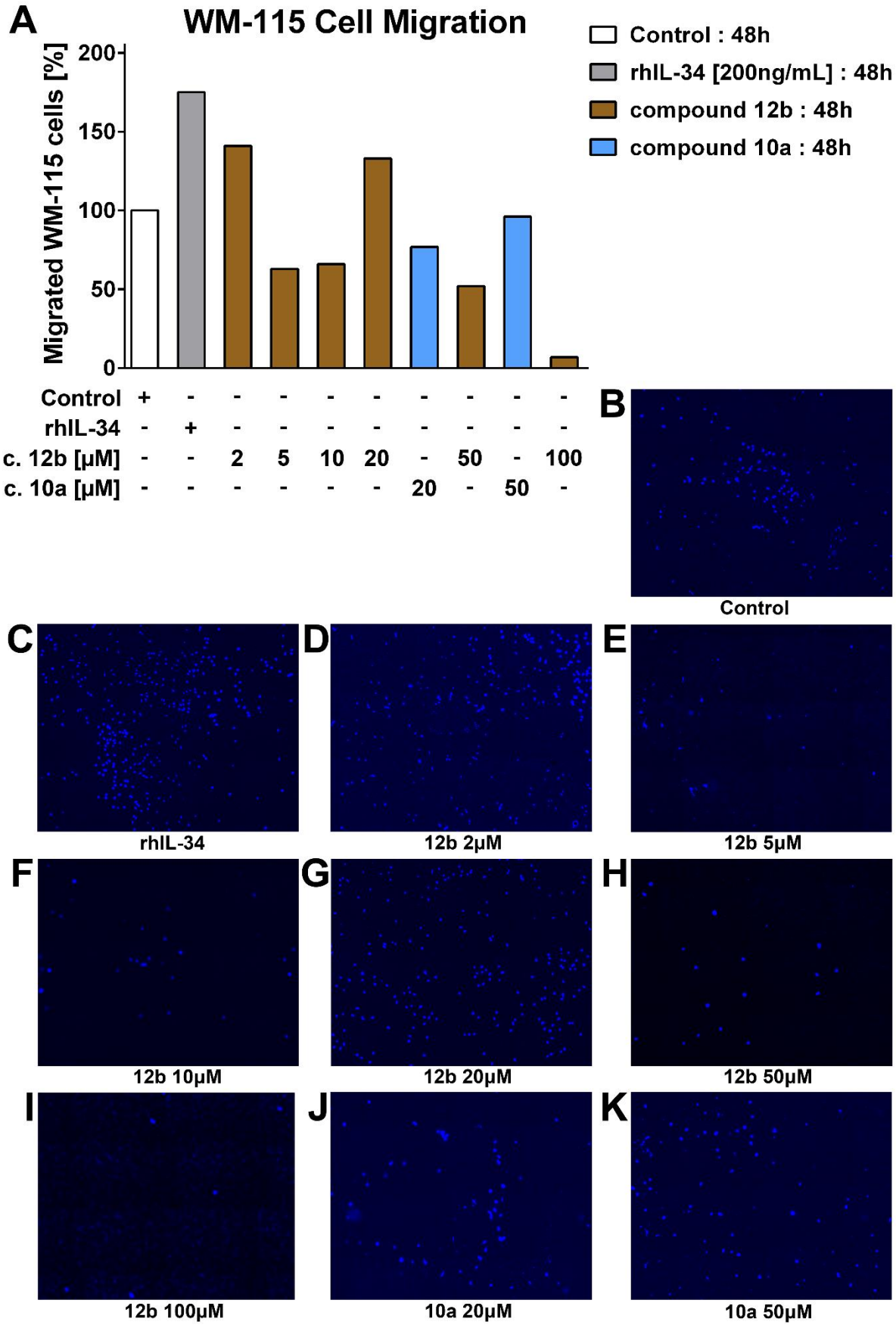

Figure 16. The migration of melanoma cell lines upon PTPRζ1 inhibitors compound 10a and 12b: A-K: The transwell migration of WM-115 cells upon 48 hours treatment with

compound 12b in concentration levels of 2-, 5-, 10-, 20-, 50-, 100 µM and of compound 10a in dosages of 20- and 50 µM. Treatment with 200 ng/mL rhIL-34 was used to simulate cell migration. **A:** The quantification of WM-115 cell migration. **B-I:** Representative images of the transwell membrane migrated WM-115 cells treated with various dosages of compound 12b. **J-K:** Representative images of migrated WM-115 cells upon treatment with compound 10a in a variety of concentrations.

5. Cell signaling in melanoma cell lines upon stimulation with rhIL-34, rhCSF-1 or rhPTN as well as in combination with novel PTPRζ1 inhibitor – compound 12b

It is known that FAK is a substrate of PTPRζ1 and that IL-34 and PTN activate FAK signaling through increased phosphorylation of Tyr397 [136, 166]. Additionally, FAK phosphorylation is also achieved by IL-34/CSF-1R and CSF-1/CSF-1R axes [120]. AKT and ERK phosphorylation can be induced via IL-34/CSF-1R and CSF-1/CSF-1R axes [130]. Also PTN induces the ERK pathway in a PTPRζ1/c-Src/FAK/PI3K/MAPK signaling pathway manner [166, 153]; as well as the AKT pathway in a PTN/PTPRζ1/Fyn/Akt manner [216]. Furthermore, PTPRζ1 inhibitor compound 12b is mimicking the action of PTN which upon binding also inhibits the phosphatase activity of PTPRζ1 [219]. In order to study the molecular mechanisms underlying the effects of compound 12b alone as well as in combination with IL-34, CSF-1 and PTN in influencing downstream phosphorylation of FAK, AKT and ERK, we aimed to test the hypothesis that inhibition of PTPRζ1 by compound 12b modulates cytokine signaling pathways in melanoma cells. To do so, we treated overnight starved SK-MEL-28 cells and WM-115 cells with 10 µM compound 12b for 15 minutes prior stimulating with 125 ng/mL rhIL-34, rhCSF-1 and rhPTN as well as cytokine treatments without compound 12b in 6-wells and were analyzed by Western blotting afterwards (Fig. 17A). The different method approach of utilizing 6-wells instead of 10 cm petri dishes as usually for protein isolation, facilitated cost-effective usage of limited amount of compound 12b, however, led to lower amount of protein sample usage of only 10 µg instead of 20-25 µg for SDS-PAGE. The compound 12b concentration of 10 µM was dissolved in 0.05% DMSO. Treatments with rhIL-34, rhCSF-1 and rhPTN in SK-MEL-28 cells (Fig. 17B, Fig. 17C respectively Fig. 17D) led to no differential significant changes of FAK-, AKT- and ERK phosphorylation. Also in WM-115 cells rhIL-34, rhCSF-1 and rhPTN treatments (Fig. 17E, Fig. 17F respectively Fig. 17G) led to no differential significant changes of FAK-, AKT- and ERK phosphorylation. The results indicate that IL-34, CSF-1 and PTN do not induce signal transduction activation of the FAK, AKT and ERK pathways at lower amount of protein sample usage of only 10 µg for SDS-PAGE. Next we tested the possibility that treatment with PTPRζ1 inhibitor compound 12b alone modulates FAK, AKT and ERK pathways of SK-MEL-28 cells and WM-115 cells. In SK-MEL-28 cells, the inhibition of PTPRζ1 phosphatase activity by compound 12b treatment led to a ~3.7-fold ($p=0.012$) significant increase of AKT phosphorylation (Fig. 17C) compared to untreated cells. In contrast, in WM-115 cells compound 12b treatment only elevated ~1.2-fold (n.s.) AKT phosphorylation (Fig. 17F). Furthermore, the compound 12b treatment alone also showed no significant differential changes in phosphorylations of FAK and ERK in SK-MEL-28 cells (Fig. 17B respectively Fig. 17D) as well as in WM-115 cells (Fig. 17E respectively Fig. 17G). These results demonstrate

that inhibition of PTPRζ1 by compound 12b does not modulate the FAK- and ERK pathway, however, it modulates the AKT pathway by inducing downstream AKT signaling in SK-MEL-28 cells but not in WM-115 cells. Thereby suggesting a role of PTPRζ1 in inducing AKT pathway activation in the SK-MEL-28 cell line. Next we tested whether PTPRζ1 inhibitor compound 12b modulates the effects of IL-34, CSF-1 and PTN in FAK, AKT or ERK phosphorylations. In SK-MEL-28 cells combined treatment with compound 12b and rhIL-34 (Fig. 17C) led to a significant ~4.84-fold ($p=0.0002$) increase of AKT phosphorylations and also significant ~4.1-fold increase ($p=0.0035$) by combined compound 12b with rhCSF-1 treatment when compared to untreated cells whereas combined compound 12b with rhPTN only significantly increased by ~3.6-fold ($p=0.0182$). Furthermore, compound 12b treatment combined with either rhIL-34, rhCSF-1 or rhPTN (Fig. 17C) showed significant increase when compared to each individual cytokine treatment. However, each cytokine concomitant treatment with compound 12b of SK-MEL-28 cells (Fig. 17C) showed moderate-enhanced AKT phosphorylations compared to treatment with compound 12b alone. Nevertheless, the results were not significant. The results above demonstrate the compound 12b modulating potential effects of CSF-1, PTN and especially of IL-34 in the AKT pathway, however, which might be solely a compound 12b effect by PTPRζ1 inhibition thereby suggesting no role of IL-34, CSF-1 and PTN on compound 12b-induced AKT pathway activation. Thus, compound 12b does not modulate the effects of IL-34, CSF-1 and PTN in AKT phosphorylations in SK-MEL-28 cells. In contrast, AKT phosphorylation was not significantly changed in WM-115 cells (Fig. 17F) treated with combined compound 12b and rhIL-34, rhCSF-1 or rhPTN compared to untreated cells, to treatment with compound 12b alone or when compared to each individual cytokine treatment. We observed no differential significant changes of phosphorylations of FAK and ERK in SK-MEL-28 cells (Fig. 17B respectively Fig. 17D) and in WM-115 cells (Fig. 17E respectively Fig. 17G) by combined compound 12b treatment with rhIL-34, rhCSF-1 or rhPTN compared to untreated cells, to compound 12b alone treated cells or when compared to each individual cytokine treatment.

Collectively, our results demonstrate that PTPRζ1 inhibition by compound 12b induces AKT phosphorylation only in SK-MEL-28 cells, suggesting a potential role in downstream signaling of PTPRζ1 in inducing AKT pathway activation merely in the SK-MEL-28 cell line. Furthermore, compound 12b does not modulate the effects of IL-34, CSF-1 and PTN in FAK, AKT and ERK phosphorylations in both melanoma cell lines. The compound 12b potentially modulating effect of CSF-1, PTN and especially of IL-34 in the AKT pathway of SK-MEL-28 cells might be solely a compound 12b effect by PTPRζ1 inhibition thereby suggesting no modulating role of compound 12b on IL-34, CSF-1 and PTN in activating the AKT pathway. Thus, no relevant modulatory potentiating or reducing effects of compound 12b on cytokines in phosphorylations of FAK, AKT and ERK in both cell lines.

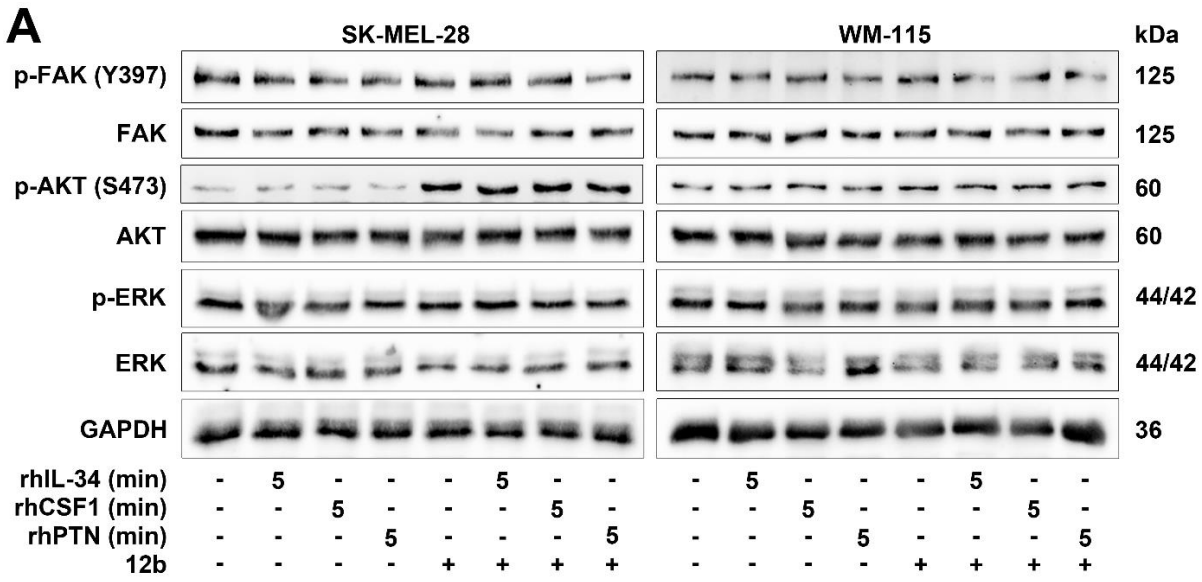

Figure 17. Cell signaling upon stimulation with rhIL-34, rhCSF-1 or rhPTN as well as in combination with PTPRζ1 inhibitor in melanoma cell lines: A: Western blot images of indicated proteins in melanoma cell lines are shown. Overnight starved SK-MEL-28 cells and WM-115 cells were treated 15 minutes with 10 µM compound 12b prior stimulation with 125 ng/mL rhIL-34, rhCSF-1 or rhPTN for 5 minutes as well as cytokine treatments without compound 12b. p- indicates phosphorylated proteins. **B-D:** Quantification of protein expressions in SK-MEL-28 cells. **E-G:** Quantification of protein expressions in WM-115 cells.

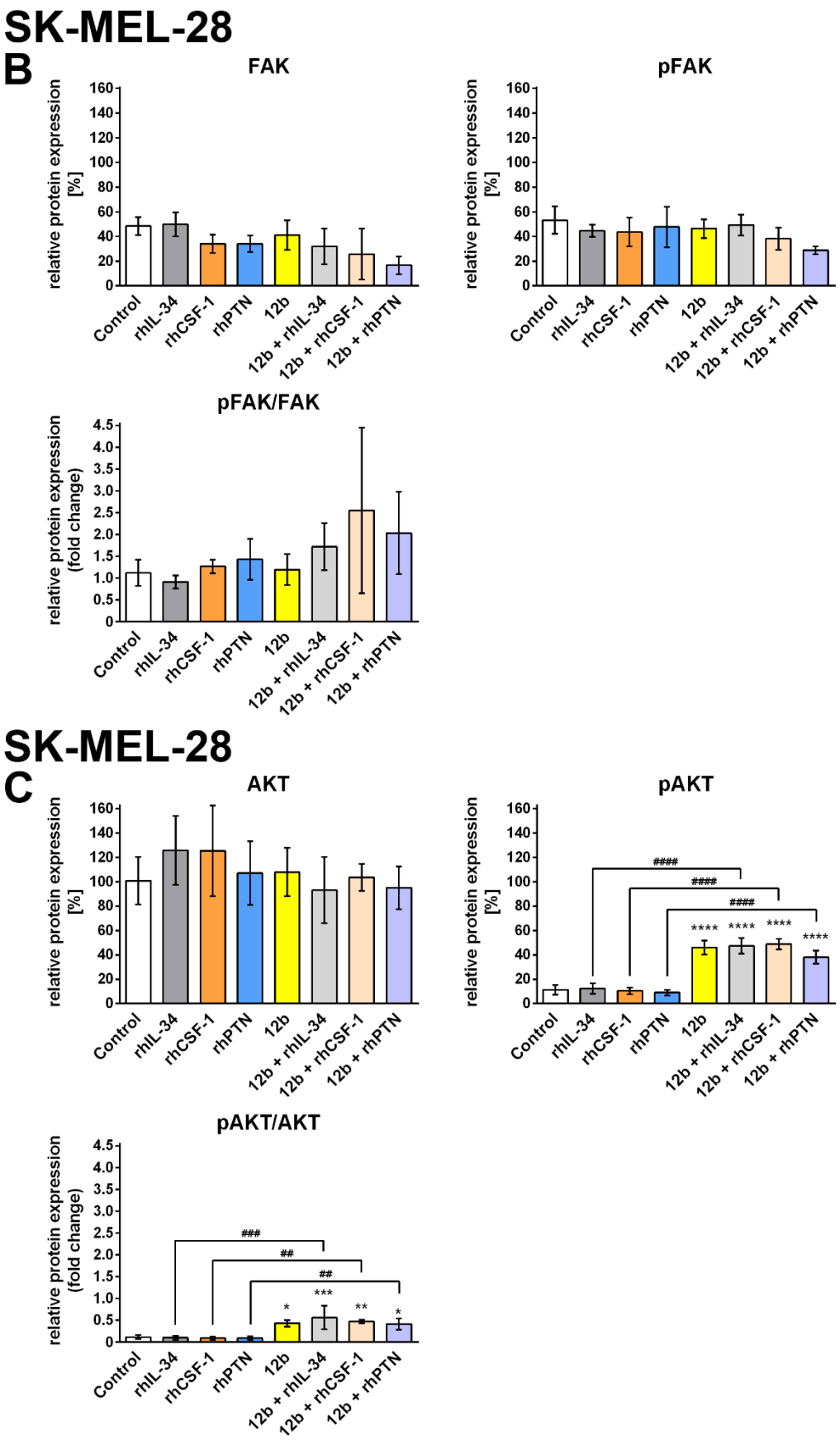

Figure 17. Cell signaling upon stimulation with rhIL-34, rhCSF-1 or rhPTN as well as in combination with PTPRζ1 inhibitor in melanoma cell lines: B-C: Quantification of protein expressions in SK-MEL-28 cells.

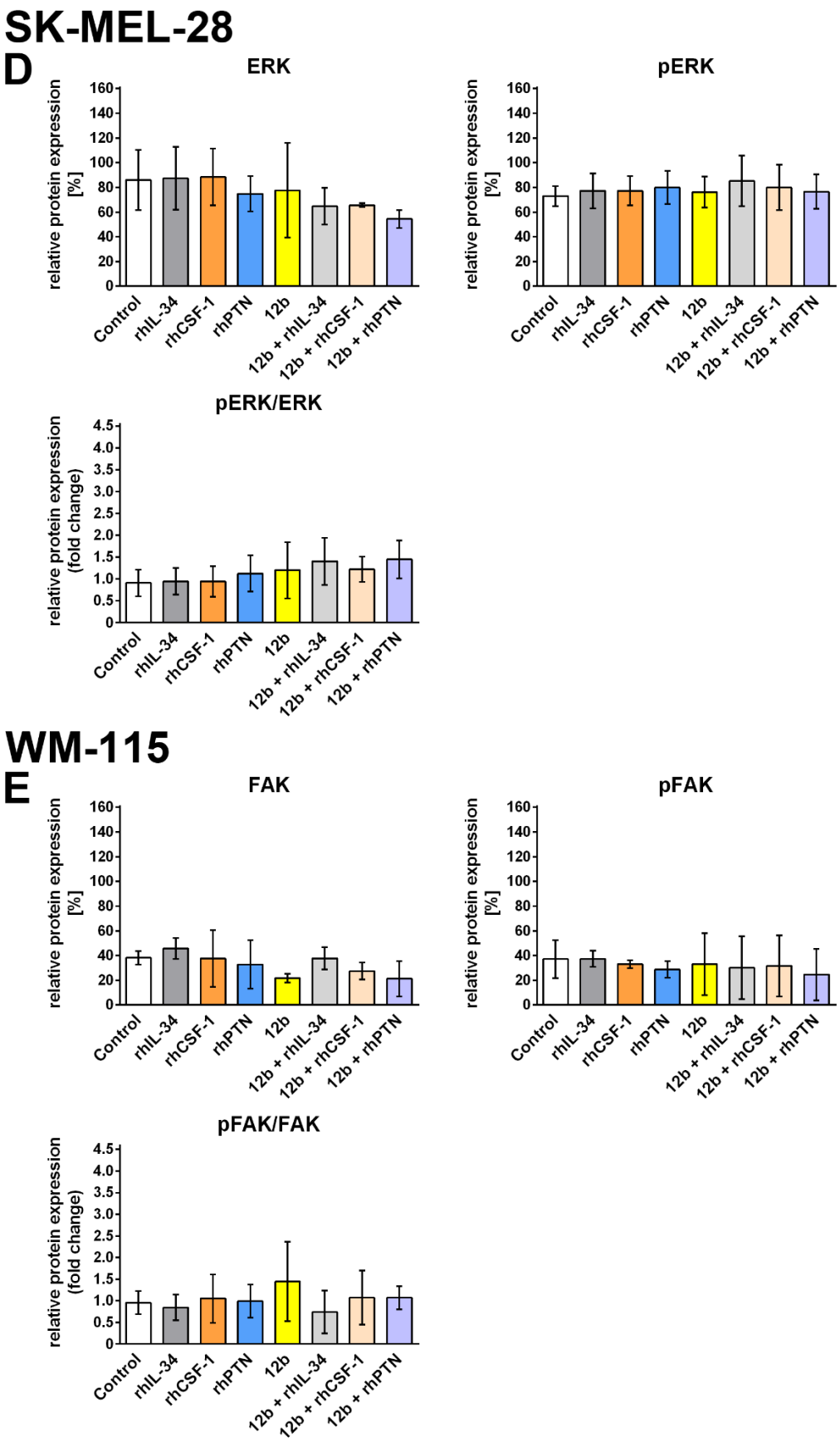

Figure 17. Cell signaling upon stimulation with rhIL-34, rhCSF-1 or rhPTN as well as in combination with PTPRζ1 inhibitor in melanoma cell lines: D: Quantification of protein expressions in SK-MEL-28 cells. **E:** Quantification of protein expressions in WM-115 cells.

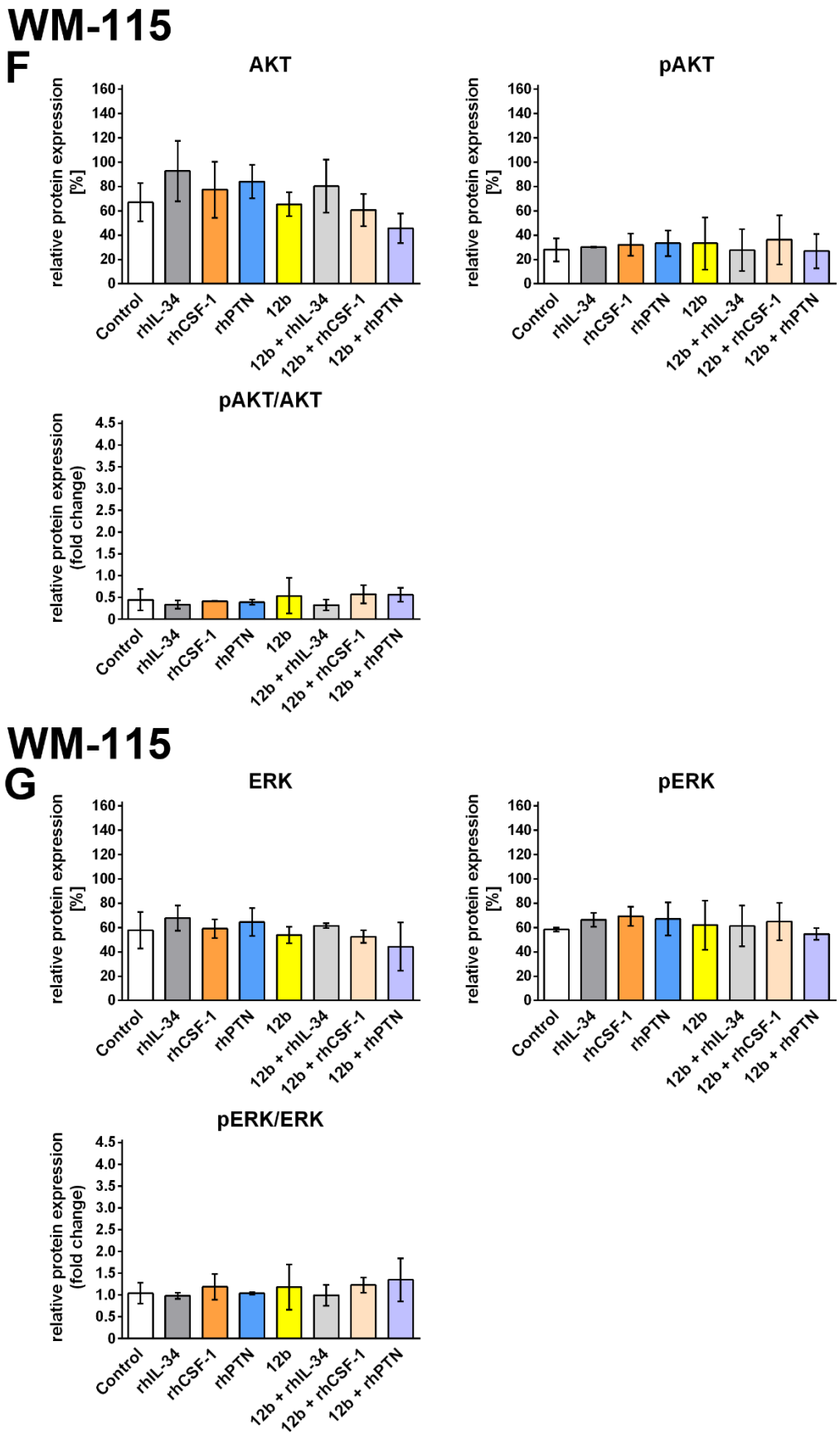

Figure 17. Cell signaling upon stimulation with rhIL-34, rhCSF-1 or rhPTN as well as in combination with PTPRζ1 inhibitor in melanoma cell lines: F-G: Quantification of protein expressions in WM-115 cells.

5.1. Proliferation of melanoma cell lines upon stimulation with rhIL-34, rhCSF-1 or rhPTN as well as in combination with novel PTPRζ1 inhibitor – compound 12b

The proliferation of cells can be influenced by IL-34, CSF-1 and PTN [142, 190, 216]. It is known that the IL-34/ and CSF-1/CSF-1R/ERK axes are involved in proliferation [124], as well as PTN/PTPRζ1 axis [216], whereas IL-34/PTPRζ1 axis is associated with inhibition of proliferation [136]. To examine biological effects of IL-34, CSF-1 and compound 12b alone as well as in combination with these cytokines in melanoma cell lines, we investigated how they influence proliferation by using the WST-1 reagent. To do so, we treated overnight starved SK-MEL-28 cells and WM-115 cells with 10 µM compound 12b for 15 minutes prior stimulating with 200 ng/mL rhIL-34 and rhCSF-1 as well as cytokine treatments without compound 12b for 48 hours. The compound 12b concentration of 10 µM was dissolved in 0.05% DMSO. In SK-MEL-28 cells (Fig. 18A) and WM-115 cells (Fig. 18B) rhIL-34 and rhCSF-1 treatment showed no differential changes in proliferation demonstrating that IL-34 and CSF-1 have no proliferatory effect in both cell lines. Next we tested the possibility that treatment with PTPRζ1 inhibitor compound 12b alone modulates proliferation of SK-MEL-28 cells and WM-115 cells. The treatment with compound 12b alone significantly increased proliferation by 16% ($p<0.0001$) in SK-MEL-28 cells (Fig. 18A) and 18% elevated proliferation ($p<0.0001$) in WM-115 cells (Fig. 18B). These results demonstrate that compound 12b modulates and induces proliferation in both cell lines, suggesting a role of PTPRζ1 in inducing proliferation in SK-MEL-28 cells and WM-115 cells. Next we tested whether the PTPRζ1 inhibitor compound 12b modulates the effects of IL-34 or CSF-1 in proliferation of SK-MEL-28 cells and WM-115 cells. The compound 12b with rhIL-34 treatment (Fig. 18B) led to a 17% ($p<0.0001$) significant increase in WM-115 cells as well as a 13% ($p=0.0009$) proliferatory increase of combined compound 12b with rhCSF-1 treatment. Also in SK-MEL-28 cells combined compound 12b and rhIL-34 treatment (Fig. 18A) led to a significant increase of 9% ($p=0.0008$), and 13% ($p<0.0001$) increase by compound 12b with rhCSF-1 treatment. However, in WM-115 cells cytokines concomitant treatment with compound 12b (Fig. 18B) as well as combined compound 12b with rhCSF-1 treatment in SK-MEL-28 cells (Fig. 18A) showed no significant changes in proliferation compared to treatment with compound 12b alone. It demonstrates that the potentially modulating effects of compound 12b on IL-34 and CSF-1 in inducing proliferation is solely a compound 12b effect by PTPRζ1 inhibition in WM-115 cells, thereby suggesting no role of IL-34 and CSF-1 on compound 12b-induced proliferation. In contrast, combined treatment of compound 12b with rhIL-34 (Fig. 18A) led to a 7% ($p=0.0026$) significant decrease compared to compound 12b treatment alone. The results above demonstrate that in SK-MEL-28 cells compound 12b modulates the effect of IL-34 in reducing proliferation which is not solely a

compound 12b effect. Thereby, suggesting a role of IL-34 on compound 12b in inhibiting proliferation whereas no role of CSF-1 on compound 12b-induced proliferation.

Collectively, our results demonstrate that IL-34 and CSF-1 do not induce proliferation whereas compound 12b induces proliferation in both melanoma cell lines. Furthermore, compound 12b does not modulate the effects of IL-34 and CSF-1 in WM-115 cell proliferation as well as of CSF-1 in SK-MEL-28 cell proliferation. However, compound 12b modulates the effect of IL-34 by inhibiting proliferation in SK-MEL-28 cells. Therefore, IL-34 plays a role on compound 12b in an inhibiting proliferatory effect in only SK-MEL-28 cells.

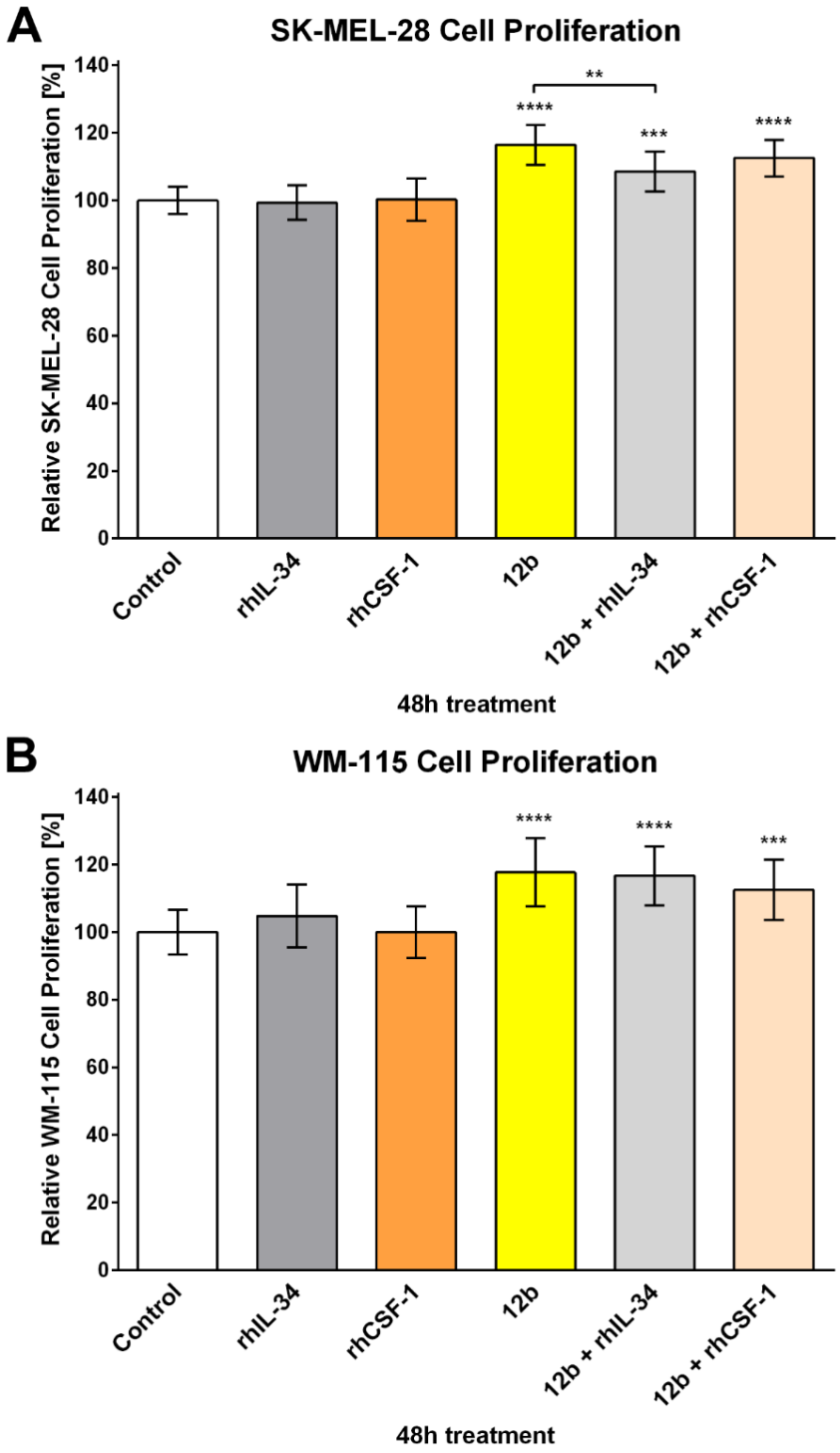

Figure 18. The proliferation of melanoma cell lines upon cytokine stimulation as well as in combination with PTPRζ1 inhibitor compound 12b: A-B: The melanoma cell lines were treated with 10 µM compound 12b for 15 minutes prior stimulating with 200 ng/mL rh-IL-34 or rhCSF-1 as well as cytokine treatments without compound 12b for 48 hours. **A:** The quantification of SK-MEL-28 cell proliferation. **B:** The quantification of WM-115 cell proliferation.

5.2. Migration of melanoma cell lines upon stimulation with rhIL-34, rhCSF-1 or rhPTN as well as in combination with novel PTPRζ1 inhibitor – compound 12b

It is known that cell migration can be influenced by IL-34, CSF-1 and PTN [142, 122, 166]. The PTN/PTPRζ1/FAK axis is involved in migration whereas IL-34/PTPRζ1/FAK axis is known to inhibit migration [166, 136]. Additionally, migration is also achieved in a IL-34/CSF-1R/FAK as well as in a CSF-1/CSF-1R/FAK axes manner [120]. To assess biological effects of IL-34, CSF-1, PTN and compound 12b alone as well as in combination with these cytokines in melanoma cell lines, we investigated how they influence migration by using the transwell migration assay. To do so, we incubated overnight starved SK-MEL-28 cells and WM-115 cells with 10 µM compound 12b for 15 minutes prior stimulating with 200 ng/mL rhIL-34, rhCSF-1 and rhPTN as well as cytokine treatments without compound 12b for 48 hours. The compound 12b concentration of 10 µM was dissolved in 0.05% DMSO. In SK-MEL-28 cells rhIL-34 treatment (Fig.19A) led to an 107% increase in migration and in WM-115 cells (Fig.19B) to a 54% increase. Also rhPTN treatment showed a 48% (n=1) migratory increase in SK-MEL-28 cells (Fig.19A) as well as in WM-115 cells (Fig.19B) of 150% elevated migration. In contrast, in SK-MEL-28 cells rhCSF-1 treatment (Fig.19A) only resulted in 5% increased migration as well as 15% in WM-115 cells (Fig.19B). Although these data did not meet statistical significance, the results indicate that IL-34 and PTN but not CSF-1 increase migration. Next, we tested the possibility that treatment with PTPRζ1 inhibitor compound 12b alone modulates migration of SK-MEL-28 cells and WM-115 cells. We observed that in SK-MEL-28 cells compound 12b treatment alone (Fig.19A) led to an 168% increase in migration as well as an elevated 244% increase in WM-115 cells (Fig. 19B). Again, the data were not significant, however, indicating that compound 12b increases migration. Next we tested whether PTPRζ1 inhibitor compound 12b modulates the effects of IL-34, CSF-1 or PTN in migration of SK-MEL-28 cells and WM-115 cells. In SK-MEL-28 cells compound 12b with rhIL-34 treatment increased migration by 175% (Fig. 19A). In contrast, in WM-115 cells combined compound 12b with rhIL-34 treatment (Fig. 19B) decreased migration by 29%. Also in SK-MEL-28 cells combined treatment of compound 12b with rhCSF-1 or with rhPTN (Fig. 19A) decreased migration by 20% respectively 43%. In contrast, in WM-115 cells combined treatment of compound 12b with rhCSF-1 or with rhPTN (Fig. 19B) increased migration by 42% respectively 40%. Furthermore, in both cell lines combined compound 12b with rhIL-34, rhCSF-1 and with rhPTN decreased migration compared to compound 12b treatment alone except of combined treatment compound 12b with IL-34 showing no differential changes in only SK-MEL-28 cells (Fig. 19A). Although these data did not meet statistical significance, the results indicate modulating effect of compound 12b on IL-34 and PTN in reducing WM-115 cell migration which might not be

solely a compound 12b effect as well as of compound 12b on PTN in SK-MEL-28 cells. Thereby, suggesting a role of IL-34 and PTN on compound 12b in inhibiting migration in WM-115 cells and of PTN on compound 12b in inhibiting migration in SK-MEL-28 cells. Thereby, suggesting a role of IL-34 and PTN on compound 12b in inhibiting migration in WM-115 cells. Collectively, our results indicate the potential of IL-34-,PTN- as well as of compound 12b in inducing migration of SK-MEL-28 cells and WM-115 cells whereas CSF-1 does not induce cell migration of both cell lines. Furthermore, IL-34 might play a role on compound 12b in inhibiting migration of WM-115 cells as well as potentially by PTN of both cell lines. In contrast, CSF-1 might not play a inhibiting migratory role on compound 12b of both melanoma cell lines as well as by IL-34 of SK-MEL-28 cells.

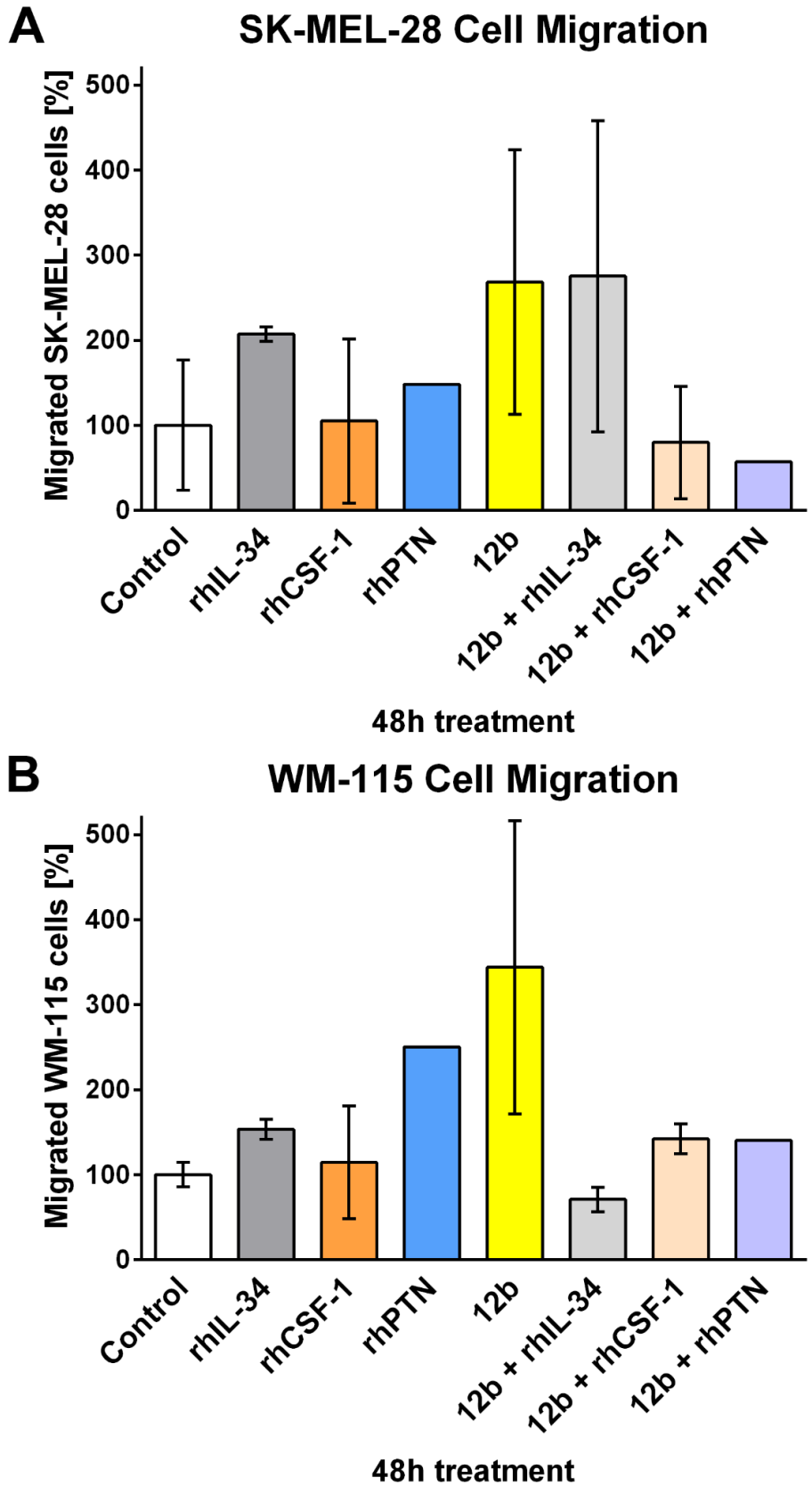

Figure 19. The migration of melanoma cell lines upon cytokine stimulation as well as in combination with PTPRζ1 inhibitor compound 12b: A-R: The melanoma cell lines were treated with 10 µM compound 12b for 15 minutes prior stimulating with 200 ng/mL rh-IL-34, rhCSF-1 or PTN as well as cytokine treatments without compound 12b for 48 hours. **A:** The quantification of SK-MEL-28 cell migration. **B:** The quantification of WM-115 cell migration.

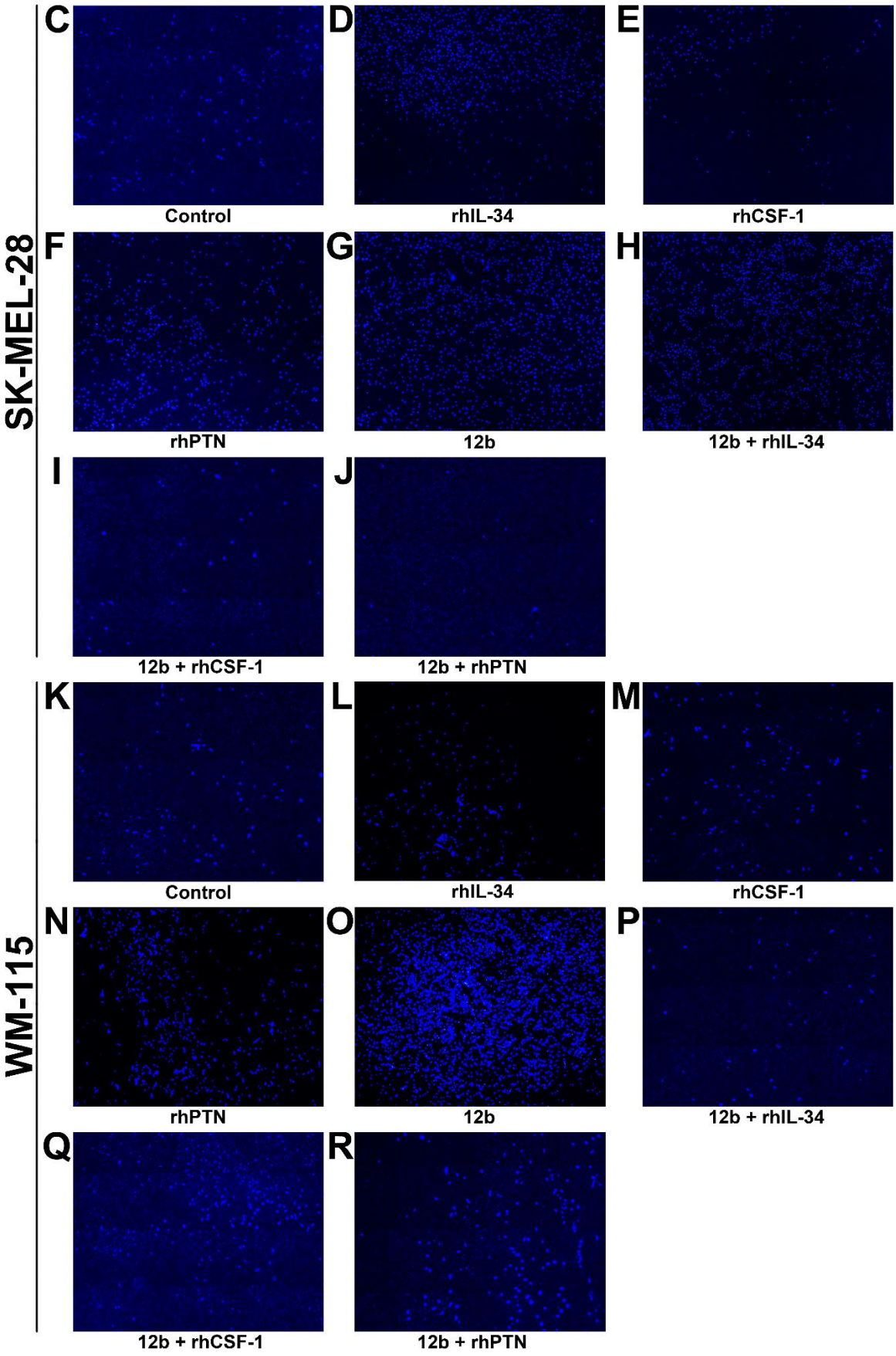

Figure 19. The migration of melanoma cell lines upon cytokine stimulation as well as in combination with PTPRζ1 inhibitor compound 12b: C-J: Representative images of migrated SK-MEL-28 cells. **K-R:** Representative images of migrated WM-115 cells.

5.2.1. F-actin visualization of the cytoskeleton of melanoma cell lines upon stimulation with rhIL-34, rhCSF-1 or rhPTN as well as in combination with novel PTPRζ1 inhibitor – compound 12b

It is known that DAPI is a fluorescent stain binding to DNA whereas phalloidin is also a fluorescent stain binding to polymerized filamentous actin (F-actin) of the cytoskeleton which plays an important role in filopodia and lamellipodia formation in order to drive cell migration [224, 225, 226]. To confirm previously shown migratory effects of IL-34, CSF-1, PTN and compound 12b as well as in their combination with the PTPRζ1 inhibitor in melanoma cell lines, we investigated how they influence the F-actin by fluorescence visualization using phalloidin and comparing their fluorescence cell morphology. To do so, we treated overnight starved SK-MEL-28 cells and WM-115 cells with 10 µM compound 12b for 15 minutes prior stimulating with 200 ng/mL rhIL-34, rhCSF-1 and rhPTN as well as cytokine treatments without compound 12b for 48 hours, on 8 chambered glass slides coated with 0.2% gelatin. Afterwards, melanoma cell lines were stained with phalloidin as well as counterstained with DAPI by incubating for 20 minutes and their fluorescence were analyzed by fluorescence microscopy with 200X and 600X magnification. The compound 12b concentration of 10 µM was dissolved in 0.05% DMSO. When SK-MEL-28 cells were compared by fluorescence microscopy by 600X- (Fig. 20A) and by 200X magnification (Fig. 20C), we observed that SK-MEL-28 cells treated with compound 12b alone as well as combined with cytokines were thinner and more elongated compared to untreated SK-MEL-28 cells as well as in comparison to each cytokine treated melanoma cells. It demonstrates cell motility by cell protrusions such as filopodia at the end of the elongated edges. SK-MEL-28 cells treated with cytokines appeared to have an oval-bulky shaped cell compared to untreated melanoma cells of which rhIL-34 as well as rhPTN treated cells were more elongated than rhCSF-1 treatment demonstrating cell motility by cell protrusions. We also observed in WM-115 cells by fluorescence microscopy by 600X- (Fig. 20B) and by 200X magnification (Fig. 20D) that cell shapes of all three cytokines treated cells as well as compound 12b alone and in combination with cytokine treatments, were larger and more elongated compared to untreated cells. Furthermore, no obvious morphological differences between these treated cells were observed. The results above demonstrate WM-115 cell motility by cell protrusions. Collectively, IL-34, CSF-1, PTN, compound 12b alone as well as in combination with these cytokines do have an altering morphologically effect on WM-115 cell shapes in which they appear to be larger and more elongated. Furthermore, also the morphologically altered cell shapes of SK-MEL-28 cells by compound 12b alone as well as combined with cytokines are thinner and more elongated whereas cytokines alone lead to a more oval-bulky shaped cell. These altering morphologically effects on SK-MEL-28 cells and WM-115 cells might indicate cell motility.

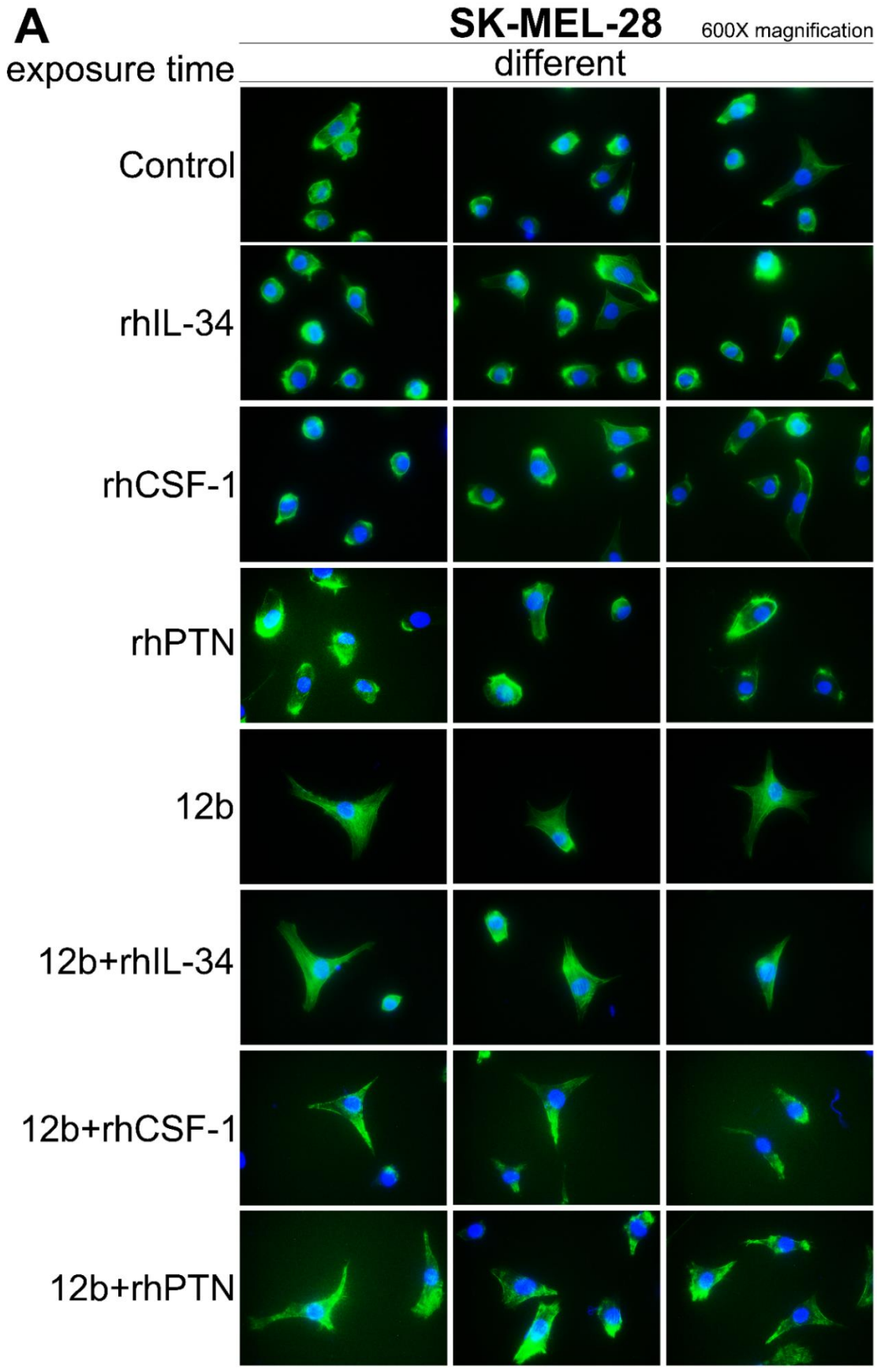

Figure 20. F-actin visualization of the cytoskeleton in melanoma cell lines upon stimulation with rhIL-34, rhCSF-1 and rhPTN as well as in combination with PTPRζ1 inhibitor compound 12b: A: SK-MEL-28 cells with microscope magnification of 600X.

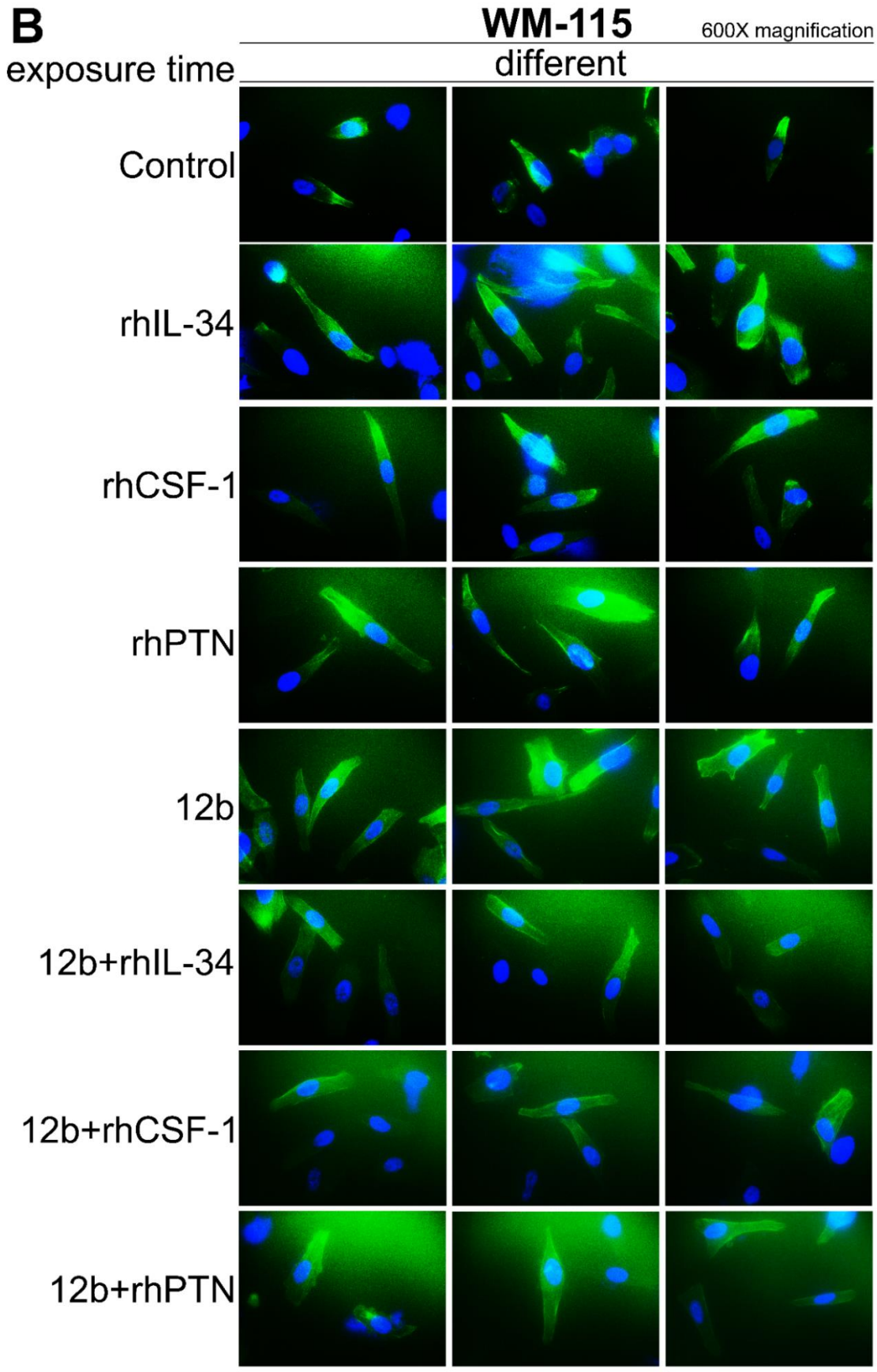

Figure 20. F-actin visualization of the cytoskeleton in melanoma cell lines upon stimulation with rhIL-34, rhCSF-1 and rhPTN as well as in combination with PTPRζ1 inhibitor compound 12b: B: WM-115 cells with microscope magnification of 600X.

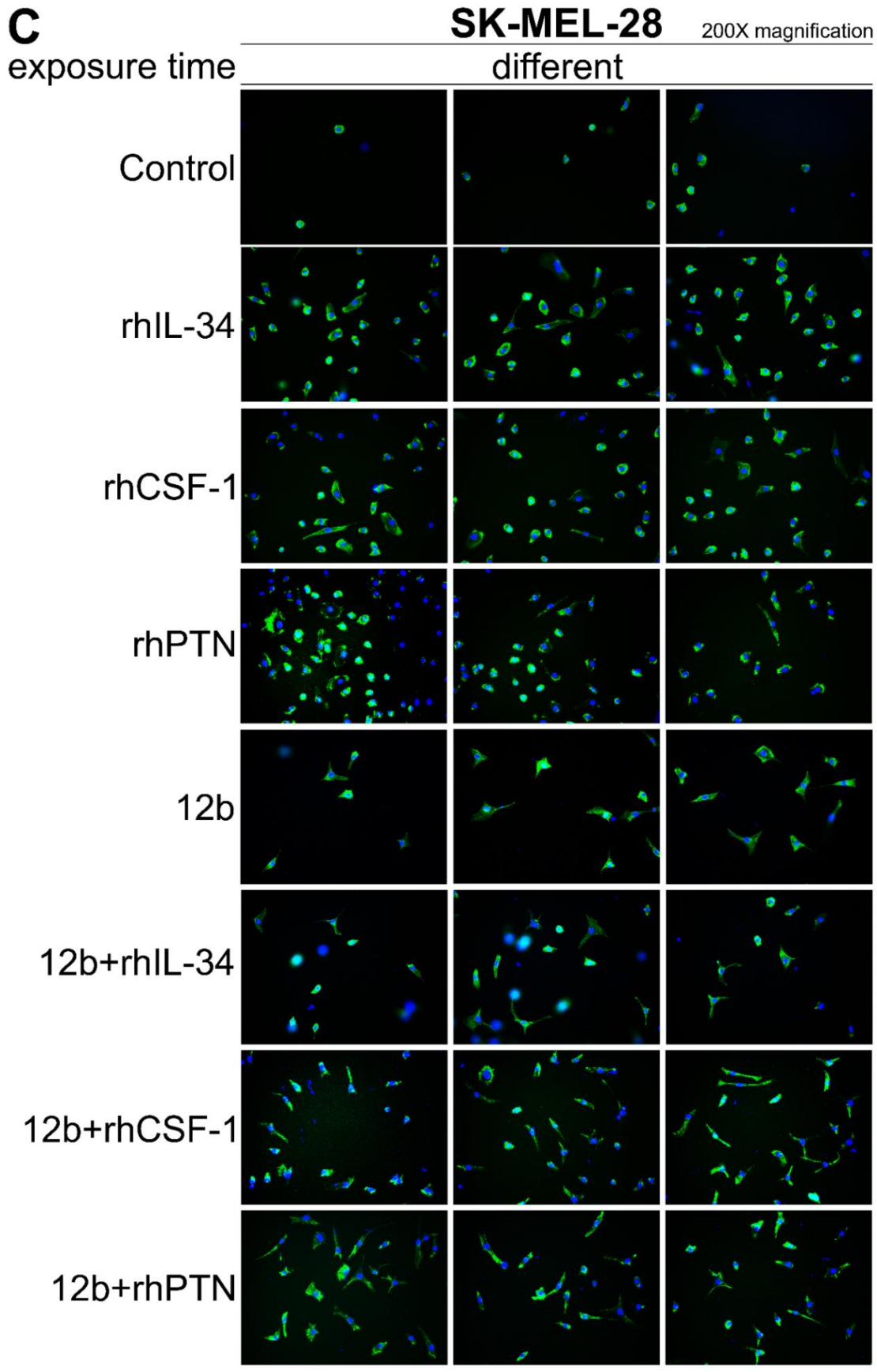

Figure 20. F-actin visualization of the cytoskeleton in melanoma cell lines upon stimulation with rhIL-34, rhCSF-1 and rhPTN as well as in combination with PTPRζ1 inhibitor compound 12b: C: SK-MEL-28 cells with microscope magnification of 200X.

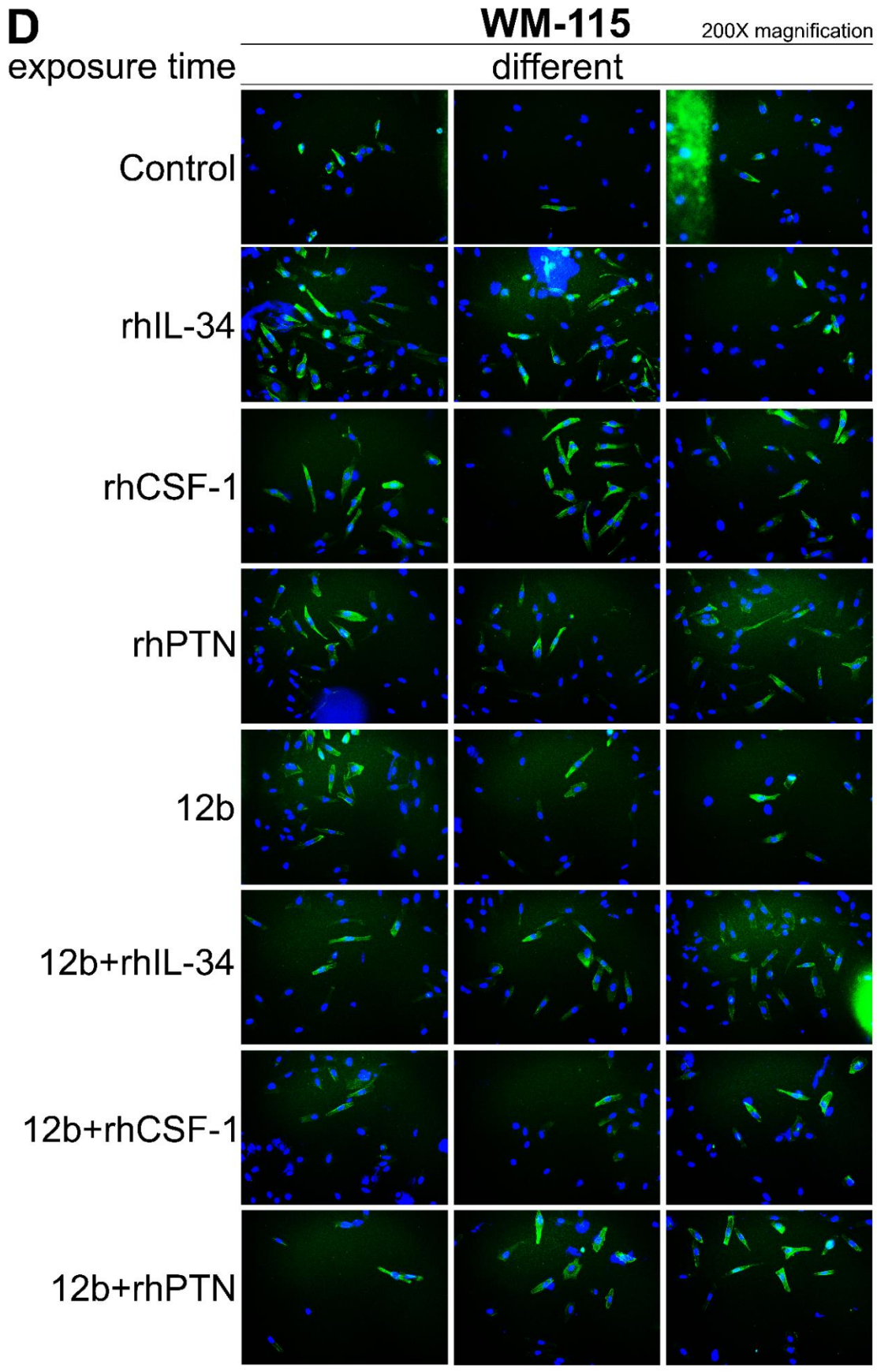

Figure 20. F-actin visualization of the cytoskeleton in melanoma cell lines upon stimulation with rhIL-34, rhCSF-1 and rhPTN as well as in combination with PTPRζ1 inhibitor compound 12b: D: WM-115 cells with microscope magnification of 200X. **A-D:** The

visualization of F-actin in melanoma cell lines by using 20-minute incubation of phalloidin staining as well as DAPI staining for DNA. SK-MEL-28 cells and WM-115 cells were treated with 10 µM compound 12b for 15 minutes prior stimulating with 200 ng/mL rh-IL-34, rhCSF-1 and rhPTN as well as cytokine treatments without compound 12b for 48 hours. Fluorescence images were taken with a fluorescence microscope equipped with DAPI and fluorescein-isothiocyanate (FITC) filters at different magnification as well as different software fluorescence exposure times.

E. Discussion

IL-34 is a newly discovered member of the interleukin family which together with CSF-1 share the same CSF-1R, a receptor tyrosine kinase [117]. In addition, IL-34 was recently identified as a ligand of PTPRζ1, a member of the receptor tyrosine phosphatase family, as well as of syndecan-1 [136, 135]. Moreover, pleiotrophin is an additional ligand of PTPRζ1 and syndecan-1 [170, 159]. However, while the role of IL-34/- and CSF-1/CSF-1R axes have been extensively studied in myeloid cells as well as in several cancers and the cross-talk between cancer cells with immune cells occurs in the tumor microenvironment [122, 118, 151]; the implications of PTN, IL-34 and CSF-1 in signaling transduction via PTPRζ1 respectively CSF-1R and their effects on cellular behavior are still poorly understood in melanoma skin cancer. Here, using a combination of real-time qRT-PCR, immunoblotting, immunofluorescence, proliferation and migration assays, we investigated the signaling potency of the transmembrane receptors PTPRζ1 respectively CSF-1R in cultured melanoma SK-MEL-28 cells and WM-115 cells stimulated with recombinant human IL-34, CSF-1 and PTN as well as by the usage of a novel inhibitor PTPRζ1 compound 12b (MY33-3) [219]. By using qRT-PCR, we demonstrate that gene expressions of *PTPRZ1*, *CSF-1R*, *SDC-1*, *IL-34*, *CSF-1* and *PTN* are not directly regulated by IL-34, CSF-1 and PTN in melanoma SK-MEL-28- and WM-115 cell lines. However, although having a small sample size, our indicated that CSF-1 may induces *CSF-1R* expression in both cell lines. A recent report demonstrated coexpression of *CSF-1R* and *IL-34* leading to constitutively receptor activation in an autocrine loop manner in melanoma cells as a result of BRAF V600E inhibition that led to low-level ERK pathway activity, which induced expression of transcription factor RUNX1 mediating the coexpression of the receptor and IL-34 but not CSF-1, followed by rebound of ERK phosphorylation within 72 hours [215]. However, our results indicate that without inhibition of BRAF, IL-34 does not induce expression of *CSF-1R* or *IL-34* probably due to SK-MEL-28- and WM-115 cell lines containing *BRAF* V600E respectively V600D mutations leading to an activated MAPK pathway [200, 227, 203, 45]. Furthermore, *CSF-1R* is associated with promoter hypomethylation and is overexpressed in melanoma patients [215]. CSF-1R is expressed at higher levels on monocytes and tissue macrophages as well as on tumor associated macrophages (TAMs) [122, 228]. Moreover, expression of CSF-1R and/or CSF-1 (co)-expression was also documented in several cancers promoting tumorigenesis and poor prognosis such as in renal cell carcinoma, coexpression of CSF-1 and CSF-1R in an autocrine manner [229]; in human prostate cancer cell lines expressing CSF-1R [230]; in breast tumor cells expression of CSF-1 and CSF-1R [231]; and in ovarian tumor cells expression of CSF-1 and CSF-1R [232]. Macrophages in skin melanoma are a key element in melanomagenesis and modulate the tumor microenvironment (TME) in an paracrine manner promoting proliferation, tumor growth and invasion [110]. IL-34 can be produced by cancer cells such as melanoma cells

and keratinocytes whereas CSF-1 is expressed by macrophages, TAMs and several cancer cells such as melanoma cells functioning in immunosuppression and tumor-promotion [215, 8, 233, 116]. Furthermore, CSF-1 and IL-34 promote the differentiation and survival of monocytes and macrophages as well as polarization into immunosuppressive pro-tumorigenic M2 macrophages via CSF-1R [130]. In addition, IL-34 and CSF-1 play a role in cancer by recruiting of M2-polarized TAMs whereas IL-34 is also associated with melanoma resistance to BRAF inhibition [133, 214, 215]. Moreover, TAMs are able to secrete PTN to promote PTPRζ1 signaling in glioblastoma stem cells for tumor growth [216]. Our results demonstrate PTPRζ1 expression as well as *PTPRZ1, CSF-1R* and *SDC-1* expressions of both melanoma cell lines in which WM-115 cells have a higher PTPRζ1 protein expression than in SK-MEL-28 cells, supporting earlier reports of identified gene and protein expression of PTPRζ1, CSF-1R and syndecan-1 in melanoma [138, 137, 215, 218, 234]. The PTPRζ1, a cell surface chondroitin sulfate (CS) proteoglycan, is believed to exist as a monomer and has a constantly active phosphatase. Binding of ligands such as IL-34 and PTN leads to oligomerization of the ectodomain triggering auto-inhibition of the phosphatase domain leading to downstream tyrosine phosphorylation and induces several signaling transductions [136, 157, 170]. Furthermore, the binding of IL-34 as well as of PTN to PTPRζ1 depends on the presence of the CS glycosaminoglycan (GAG) chain(s) moiety on PTPRζ1, however, IL-34 binding might involve different once which are not recognized by PTN [136]. The CS moieties also appear to be prerequisite for IL-34 binding to syndecan-1 which regulates the IL-34 activation levels of the CSF-1R [135]. Furthermore, IL-34 shares together with CSF-1 the same CSF-1R of which ligand binding induces the dimerization and activation of the tyrosine kinase activity of the receptor leading to autophosphorylation of define tyrosine residues in the CSF-1R cytoplasmic domain. Moreover, these subsequently phosphorylated tyrosine residues interact with other signaling proteins resulting in specific signaling pathways [120, 122]. The proliferation of cells can be influenced by IL-34, CSF-1 and PTN [142, 190, 216]. The IL-34/ and CSF-1/CSF-1R/ERK axes are involved in proliferation [124], as well as PTN/PTPRζ1 axis [216], whereas IL-34/PTPRζ1 axis is associated with inhibition of proliferation [136]. Also PTN induces the ERK pathway in a PTPRζ1/c-Src/FAK/PI3K/MAPK signaling pathway manner [166, 153]; as well as the AKT pathway in a PTN/PTPRζ1/Fyn/Akt manner [216]. However, our results demonstrate that IL-34, CSF-1 and PTN do not induce activation of the ERK and AKT pathways above baseline activation levels as well as no increase of proliferation by IL-34 or CSF-1 in melanoma SK-MEL-28- and WM-115 cell lines. Other reports, demonstrate that AKT and ERK phosphorylation by IL-34 and CSF-1 via CSF-1R in human primary monocytes and in lung cancer cell lines [130, 235] as well as in macrophages leads to proliferation in a IL-34/ and CSF-1/CSF-1R/ERK manner [124]; AKT phosphorylation by PTN via PTPRζ1 in human glioblastoma cells [216]; ERK phosphorylation by PTN via PTPRζ1 in lung cancer A549 cell line [236]; and also in human melanoma A375 cell line [167]; as well as in HUVECs [166]. However, our

results are in agreement with previously published evidence of PTN not inducing AKT phosphorylation in human melanocytes [140]. Furthermore, in our study, we used melanoma SK-MEL-28 and WM-115 cell lines which are containing *BRAF* V600E respectively V600D mutations leading to an activated MAPK pathway [200, 227, 203, 45]. Moreover, loss of functional PTEN results in constitutively active phospho-Akt status leading to activated PI3K/Akt pathway in SK-MEL-28 cells as well as in WM-115 cells [76, 206, 204]. Therefore, we suggest that IL-34, CSF-1 and PTN do not further induce already activated AKT- and ERK pathways of SK-MEL-28 cells and WM-115 cells. Recently, newly synthesized small molecule inhibitors known as compound 12b (MY33-3) and compound 10a (MY10) were designed to inhibit PTPRζ1 by interacting with its active site of the intracellular domain PD1 thereby inhibiting the intrinsic phosphatase activity of PTPRζ1 [219]. It is known that PTPRζ1 inhibition by compound 12b leads to activation of ALK tyrosine kinase receptor followed by increased tyrosine phosphorylation of its downstream substrates such as TrkA and ALK. These inhibitors are mimicking the action of PTN which also inhibits the PTPRζ1 phosphatase activity [219, 221]. Our results of PTPRζ1 inhibitor compound 12b modulation experiments show that the AKT pathway of SK-MEL-28 cells is activated during inhibition of PTPRζ1 phosphatase activity by the exogenous PTPRζ1 inhibitor compound 12b, whereas no AKT pathway activation of WM-115 cells occurred suggesting a cell line-specific effect. The ALK receptor could play a role which is known to be overexpressed in melanoma [237]. Furthermore, PTPRζ1 inhibition by compound 12b leads to activation of ALK tyrosine kinase receptor [219, 221] which might activate the AKT pathway in a potentiating ALK/PI3K/Akt manner [237]. The potentiating of AKT phosphorylation could be more significant in SK-MEL-28 cells because our results show very low AKT pathway activity at baseline of SK-MEL-28 cells compared to WM-115 cells. However, PTN should have a similar effect as compound 12b on AKT phosphorylation of SK-MEL-28 cells, which it did not have, since compound 12b should be mimicking the action of PTN and inhibit PTPRζ1 phosphatase activity [219, 221]. Furthermore, compound 12b induces increased proliferation of SK-MEL-28 cells and WM-115 cells. The AKT pathway has an important role in several cellular processes such as survival and cell proliferation [2, 105, 220]. Therefore, proliferation of SK-MEL-28 cells induced by compound 12b might be associated with the compound 12b-induced AKT pathway activation of SK-MEL-28 cells only suggesting an AKT-pathway-independent mechanism for proliferation. It suggests that the AKT pathway might play an important role in PTPRζ1 downstream signaling in SK-MEL-28 cells for proliferation but not in WM-115 cells, which might involve a different PTPRζ1 downstream proliferating pathway. In contrast, our results showed no PTN-induced signaling transduction activation of the AKT pathway of both melanoma cell lines. Another puzzling observation was that SK-MEL-28 cells pretreated with the PTPRζ1 inhibitor compound 12b prior to IL-34 stimulation lead to decreased proliferation levels, compared to compound 12b treatment alone. Therefore, compound 12b modulates the effect

of IL-34 on SK-MEL-28 cell proliferation. Fittingly, IL-34/PTPRζ1 axis is associated with inhibition of proliferation [136], thus it might suggest that IL-34 binds to PTPRζ1 during PTPRζ1 inhibition by compound 12b resulting in proliferation inhibition of SK-MEL-28 cells, indicating a IL-34/PTPRζ1 inhibiting proliferatory effect. In contrast, compound 12b does not modulate the effects of IL-34 and CSF-1 in proliferation of WM-115 cells as well as of CSF-1 in proliferation of SK-MEL-28 cells. Thus, the compound 12b modulating the effect of IL-34 by inhibiting SK-MEL-28 cell proliferation might be cell line specific. Our results of compound 12b modulations also suggest that the ERK pathway might not play an important role in PTPRζ1 downstream signaling of SK-MEL-28 cells and of WM-115 cells. Furthermore, the ERK pathway might not be associated with compound 12b-induced proliferation. which is in agreement with our other results of PTN not inducing the ERK pathway of both melanoma cell lines. The migration of cells can be influenced by IL-34, CSF-1 and PTN [142, 122, 166]. The PTN/PTPRζ1/FAK axis is involved in migration whereas IL-34/PTPRζ1/FAK axis is known to inhibit migration [166, 136]. Additionally, migration is also achieved in a IL-34/CSF-1R/FAK and CSF-1/CSF-1R/FAK axes manner [120]. However, our results demonstrate that CSF-1 neither induces activation of the FAK pathway nor cell migration of SK-MEL-28- and WM-115 cells. In contrast, other reports demonstrate FAK phosphorylation as well as migration in a CSF-1/CSF-1R dependent manner in MCF7 breast cancer cells [121]. Furthermore, PTN induced FAK phosphorylation of both melanoma cell lines and increased migration. This is in line with previous reports of PTN inducing FAK phosphorylation via PTPRζ1 in human umbilical vein endothelial cells (HUVECs) [166]. Our results also show that IL-34 induces FAK phosphorylation of WM-115 cells. Moreover, IL-34 might potentially increase migration of both melanoma cell lines. Likewise, earlier reports show the IL-34/CSF-1R axis inducing FAK phosphorylation as well as increasing TF-1 cell migration [120]. We show that compound 12b potentially increases migration of SK-MEL-28 cells and WM-115 cells indicating that PTPRζ1 phosphatase activity inhibition by compound 12b leads to cell migration and thus PTPRζ1 signaling might play a role in cell migration. However, pretreatment of WM-115 cells with the PTPRζ1 inhibitor compound 12b prior to IL-34, CSF-1, or PTN stimulation reduced cell migration. Thus, these factors might play a role in modulating the compound 12b migratory effect in both cell lines. It might suggest signaling of WM-115 cells in a IL-34/PTPRζ1/FAK manner and in a PTN/PTPRζ1/FAK manner in both cell lines affecting the cell migration regulation effect of compound 12b inhibited PTPRζ1 phosphatase activity. Other reports of CSF-1R-deficient U251 human glioblastoma cells demonstrated that IL-34/PTPRζ1 increased FAK phosphorylation and led to suppression of cell motility [136]. The biology of IL-34 is complex. IL-34 shares together with CSF-1 the same CSF-1R although IL-34 shares very little homology with CSF-1, and has a higher affinity to the CSF-1R [117, 126]. Furthermore, other reports suggest that IL-34 has biological activity and signal activation not necessarily identical to CSF-1/CSF-1R signaling [126, 120].

Taken together, we give new insights of the implications of PTN, IL-34 and CSF-1 as well as of the novel inhibitor PTPRζ1 compound 12b (MY33-3) in signaling transduction via PTPRζ1 respectively CSF-1R and their effects on cellular behavior in melanoma skin cancer cell lines. However, further investigations of IL-34/- PTN/PTPRζ1 signaling in melanoma cells as well as other cancers cells expressing the PTPRζ1 receptor will be necessary to understand its biological complexity.

F. Literature

1. Liu, Y. & Sheikh, M. S. Melanoma: Molecular pathogenesis and therapeutic management. *Mol. Cell. Pharmacol.* **6**, 31–44 (2014).
2. Chamcheu, J. C. *et al.* Role and Therapeutic Targeting of the PI3K / Akt / mTOR Signaling Pathway in Skin Cancer : Natural and Synthetic Agents Therapy. *Cells* **8**, 1–33 (2019).
3. Paluncic, J. *et al.* Roads to melanoma: Key pathways and emerging players in melanoma progression and oncogenic signaling. *Biochim. Biophys. Acta - Mol. Cell Res.* **1863**, 770–784 (2016).
4. Thompson, J. F., Scolyer, R. A. & Kefford, R. F. Cutaneous melanoma. *Lancet* **365**, 687–701 (2005).
5. Hirt, P. A. & Paus, R. *Healthy Hair (Anatomy, Biology, Morphogenesis, Cycling, and Function)*. *Alopecia* vol. 20 (Elsevier Inc., 2019).
6. Ito, S. & Wakamatsu, K. Quantitative analysis of eumelanin and pheomelanin in humans, mice, and other animals: A comparative review. *Pigment Cell Res.* **16**, 523–531 (2003).
7. Chamcheu, J. C. *et al.* Keratin gene mutations in disorders of human skin and its appendages. *Arch. Biochem. Biophys.* **508**, 123–137 (2011).
8. Yan, B. *et al.* The role of Langerhans cells in epidermal homeostasis and pathogenesis of psoriasis. *J. Cell. Mol. Med.* **24**, 11646–11655 (2020).
9. Abraham, J. & Mathew, S. Merkel Cells: A Collective Review of Current Concepts. *Int. J. Appl. basic Med. Res.* **9**, 9–13 (2017).
10. Chamcheu, J., Adhami, V., Siddiqui, I. & Mukhtar, H. Cutaneous Cell- and Gene-Based Therapies for Inherited and Acquired Skin Disorders. *Gene Cell Ther.* 1091–1122 (2015) doi:10.1201/b18002-52.
11. Ciążyńska, M. *et al.* The incidence and clinical analysis of non-melanoma skin cancer. *Sci. Rep.* **11**, 1–10 (2021).
12. Cai, W. Anatomical and molecular imaging of skin cancer. *Clin. Cosmet. Investig. Dermatol.* 1 (2008) doi:10.2147/ccid.s4249.
13. Rudolph, C., Schnoor, M., Eisemann, N. & Katalinic, A. Incidence trends of nonmelanoma skin cancer in Germany from 1998 to 2010. *JDDG J. der Dtsch. Dermatologischen Gesellschaft* **13**, 788–797 (2015).
14. Maio, M. Melanoma as a model tumour for immuno-oncology. *Ann. Oncol.* **23**, viii10–viii14 (2012).
15. Abildgaard, C. & Guldberg, P. Molecular drivers of cellular metabolic reprogramming in melanoma. *Trends Mol. Med.* **21**, 164–171 (2015).

16. Gilchrest, B. A., Eller, M. S., Geller, A. C. & Yaar, M. The Pathogenesis of Melanoma Induced by Ultraviolet Radiation. *N. Engl. J. Med.* **340**, 1341–1348 (1999).
17. Watson, M., Holman, D. M. & Maguire-Eisen, M. Ultraviolet Radiation Exposure and Its Impact on Skin Cancer Risk. *Semin. Oncol. Nurs.* **32**, 241–254 (2016).
18. Böhm, M. *et al.* α-melanocyte-stimulating hormone protects from ultraviolet radiation-induced apoptosis and DNA damage. *J. Biol. Chem.* **280**, 5795–5802 (2005).
19. Brand, R. M. *et al.* Targeting mitochondrial oxidative stress to mitigate UV-induced skin damage. *Front. Pharmacol.* **9**, 1–10 (2018).
20. Mouret, S. *et al.* UVA-induced cyclobutane pyrimidine dimers in DNA: A direct photochemical mechanism? *Org. Biomol. Chem.* **8**, 1706–1711 (2010).
21. Chang, Y. M. *et al.* Sun exposure and melanoma risk at different latitudes: A pooled analysis of 5700 cases and 7216 controls. *Int. J. Epidemiol.* **38**, 814–830 (2009).
22. Manuscript, A. *Cutaneous Melanoma: Etiology and Therapy*. vol. 6 (Codon Publications, 2017).
23. Razmjooy, N. *et al.* Computer-aided Diagnosis of Skin Cancer: A Review. *Curr. Med. Imaging Former. Curr. Med. Imaging Rev.* **16**, 781–793 (2020).
24. Lancet, T. ICD-10: There's a code for that. *Lancet* **386**, 1420 (2015).
25. Leiter, U. *et al.* Incidence, Mortality, and Trends of Nonmelanoma Skin Cancer in Germany. *J. Invest. Dermatol.* **137**, 1860–1867 (2017).
26. Eisemann, N. *et al.* Non-melanoma skin cancer incidence and impact of skin cancer screening on incidence. *J. Invest. Dermatol.* **134**, 43–50 (2014).
27. Sung, H. *et al.* Global Cancer Statistics 2020: GLOBOCAN Estimates of Incidence and Mortality Worldwide for 36 Cancers in 185 Countries. *CA. Cancer J. Clin.* **71**, 209–249 (2021).
28. Bray, F. *et al.* Global cancer statistics 2018: GLOBOCAN estimates of incidence and mortality worldwide for 36 cancers in 185 countries. *CA. Cancer J. Clin.* **68**, 394–424 (2018).
29. Siegel, R. L., Miller, K. D. & Jemal, A. Cancer statistics, 2020. *CA. Cancer J. Clin.* **70**, 7–30 (2020).
30. Gershenwald, J. E. *et al.* Melanoma staging: Evidence-based changes in the American Joint Committee on Cancer eighth edition cancer staging manual. *CA. Cancer J. Clin.* **67**, 472–492 (2017).
31. Hargadon, K. M., Johnson, C. E. & Williams, C. J. Immune checkpoint blockade therapy for cancer: An overview of FDA-approved immune checkpoint inhibitors. *Int. Immunopharmacol.* **62**, 29–39 (2018).
32. Dobry, A. S. *et al.* Management of metastatic melanoma: improved survival in a national cohort following the approvals of checkpoint blockade immunotherapies and

targeted therapies. *Cancer Immunol. Immunother.* **67**, 1833–1844 (2018).

33. Singh, P., Kim, H. J. & Schwartz, R. A. Superficial spreading melanoma: An analysis of 97 702 cases using the SEER database. *Melanoma Res.* **26**, 395–400 (2016).
34. Shaikh, W. R., Xiong, M. & Weinstock, M. A. The contribution of nodular subtype to melanoma mortality in the United States, 1978 to 2007. *Arch. Dermatol.* **148**, 30–36 (2012).
35. Elder DE, Massi D, Scolyer RA, W. R. *WHO Classification of Skin Tumours*. (International Agency for Research on Cancer, 2018).
36. Elder, D. E., Bastian, B. C., Cree, I. A., Massi, D. & Scolyer, R. A. The 2018 World Health Organization classification of cutaneous, mucosal, and uveal melanoma detailed analysis of 9 distinct subtypes defined by their evolutionary pathway. *Arch. Pathol. Lab. Med.* **144**, 500–522 (2020).
37. Clark, W. H., From, L., Bernardino, E. A. & Mihm, M. C. The Histogenesis and Biologic Behavior of Primary Human Malignant Melanomas of the Skin. *Cancer Res.* **29**, 705–727 (1969).
38. Elder, D. E. *et al.* Invasive malignant melanomas lacking competence for metastasis. *Am. J. Dermatopathol.* **6 Suppl**, 55–61 (1984).
39. Dupont Guerry, I., Synnestvedt, M., Elder, D. E. & Schultz, D. Lessons from tumor progression: The invasive radial growth phase of melanoma is common, incapable of metastasis, and indolent. *J. Invest. Dermatol.* **100**, S342–S345 (1993).
40. Puglisi, R. *et al.* Biomarkers for Diagnosis, Prognosis and Response to Immunotherapy in Melanoma. *Cancers (Basel).* **13**, 2875 (2021).
41. Scolyer, R. A., Long, G. V. & Thompson, J. F. Evolving concepts in melanoma classification and their relevance to multidisciplinary melanoma patient care. *Mol. Oncol.* **5**, 124–136 (2011).
42. Ingraffea, A. Melanoma. *Facial Plast. Surg. Clin. North Am.* **21**, 33–42 (2013).
43. Maldonado, J. L. *et al.* Determinants of BRAF mutations in primary melanomas. *J. Natl. Cancer Inst.* **95**, 1878–1880 (2003).
44. Viros, A. *et al.* Improving melanoma classification by integrating genetic and morphologic features. *PLoS Med.* **5**, 0941–0952 (2008).
45. Richtig, G. *et al.* Beyond the BRAF V 600E hotspot: biology and clinical implications of rare BRAF gene mutations in melanoma patients. *Br. J. Dermatol.* **177**, 936–944 (2017).
46. Shain, A. H. *et al.* Genomic and Transcriptomic Analysis Reveals Incremental Disruption of Key Signaling Pathways during Melanoma Evolution. *Cancer Cell* **34**, 45-55.e4 (2018).
47. Zeng, H. *et al.* Bi-allelic Loss of CDKN2A Initiates Melanoma Invasion via BRN2

Activation. *Cancer Cell* **34**, 56-68.e9 (2018).

48. Dessinioti, C. *et al.* Distinct Clinicopathological and Prognostic Features of Thin Nodular Primary Melanomas: An International Study from 17 Centers. *J. Natl. Cancer Inst.* **111**, 1314–1322 (2019).
49. Gutiérrez-Castañeda, L. D., Nova, J. A. & Tovar-Parra, J. D. Frequency of mutations in BRAF, NRAS, and KIT in different populations and histological subtypes of melanoma: A systemic review. *Melanoma Res.* 62–70 (2020) doi:10.1097/CMR.0000000000000628.
50. Akslen, L. A. *et al.* BRAF and NRAS mutations are frequent in nodular melanoma but are not associated with tumor cell proliferation or patient survival. *J. Invest. Dermatol.* **125**, 312–317 (2005).
51. McGovern, V. J. The classification of melanoma and its relationship with prognosis. *Pathology* **2**, 85–98 (1970).
52. Lee, E. Y. *et al.* Sun exposure and host phenotype as predictors of cutaneous melanoma associated with neval remnants or dermal elastosis. *Int. J. Cancer* **119**, 636–642 (2006).
53. Kasprzak, J. M. & Xu, Y. G. Diagnosis and management of lentigo maligna: A review. *Drugs Context* **4**, 1–16 (2015).
54. Bastian, B. C. The Molecular Pathology of Melanoma: An Integrated Taxonomy of Melanocytic Neoplasia. *Annu. Rev. Pathol. Mech. Dis.* **9**, 239–271 (2014).
55. Uzdensky, A., Demyanenko, S. & Bibov, M. Signal Transduction in Human Cutaneous Melanoma and Target Drugs. *Curr. Cancer Drug Targets* **13**, 843–866 (2013).
56. I. Evan, G. & H. Vousden, K. Proliferation, cell cycle and apoptosis in cancer. *Nature* **411**, 342–348 (2001).
57. Carnero, A. Targeting the cell cycle for cancer therapy. *Br. J. Cancer* **87**, 129–133 (2002).
58. Coqueret, O. Linking cyclins to transcriptional control. *Gene* **299**, 35–55 (2002).
59. Sulaimon, S. S. & Kitchell, B. E. The Basic Biology of Malignant Melanoma: Molecular Mechanisms of Disease Progression and Comparative Aspects. *J. Vet. Intern. Med.* **17**, 760–772 (2003).
60. Bennett, D. C. How to make a melanoma: What do we know of the primary clonal events? *Pigment Cell Melanoma Res.* **21**, 27–38 (2008).
61. Ibrahim, N. & Haluska, F. G. Molecular pathogenesis of cutaneous melanocytic neoplasms. *Annu. Rev. Pathol. Mech. Dis.* **4**, 551–579 (2009).
62. Yang, K., Oak, A. S. W., Slominski, R. M., Brożyna, A. A. & Slominski, A. T. Current molecular markers of melanoma and treatment targets. *Int. J. Mol. Sci.* **21**, (2020).
63. Mihić, L. L., Bulat, V., Šitum, M., Krolo, I. & Šešerko, A. The role of apoptosis in the

pathogenesis of malignant melanoma. *Coll. Antropol.* **34**, 303–306 (2010).

64. Soufir, N. *et al.* Prevalence of p16 and CDK4 germline mutations in 48 melanoma-prone families in France. *Hum. Mol. Genet.* **7**, 209–216 (1998).
65. Zuo, L. *et al.* Germline mutations in the p16(INK4a) binding domain of CDK4 in familial melanoma. *Nat. Genet.* **12**, 97–99 (1996).
66. Sekulic, A. *et al.* Malignant Melanoma in the 21st Century: The Emerging Molecular Landscape. *Mayo Clin. Proc.* **83**, 825–846 (2008).
67. Krauthammer, M. *et al.* Exome sequencing identifies recurrent mutations in NF1 and RASopathy genes in sun-exposed melanomas. *Nat. Genet.* **47**, 996–1002 (2015).
68. Wan, P. T. C. *et al.* Mechanism of activation of the RAF-ERK signaling pathway by oncogenic mutations of B-RAF. *Cell* **116**, 855–867 (2004).
69. Fofaria, N. M., Kim, S. H. & Srivastava, S. K. Piperine causes G1 phase cell cycle arrest and apoptosis in melanoma cells through checkpoint kinase-1 activation. *PLoS One* **9**, 1–10 (2014).
70. Rodriguez-Viciana, P. *et al.* Phosphatidylinositol-3-OH kinase direct target of Ras. *Nature* vol. 370 527–532 (1994).
71. Shepherd, P. R., Withers, D. J. & Siddle, K. Phosphoinositide 3-kinase: The key switch mechanism in insulin signalling. *Biochem. J.* **333**, 471–490 (1998).
72. Datta, S. R. *et al.* Akt phosphorylation of BAD couples survival signals to the cell-intrinsic death machinery. *Cell* **91**, 231–241 (1997).
73. Mayo, L. D. & Donner, D. B. A phosphatidylinositol 3-kinase/Akt pathway promotes translocation of Mdm2 from the cytoplasm to the nucleus. *Proc. Natl. Acad. Sci. U. S. A.* **98**, 11598–11603 (2001).
74. Inoki, K., Li, Y., Zhu, T., Wu, J. & Guan, K. L. TSC2 is phosphorylated and inhibited by Akt and suppresses mTOR signalling. *Nat. Cell Biol.* **4**, 648–657 (2002).
75. Maehama, T. & Dixon, J. E. The Tumor Suppressor, PTEN/MMAC1, Dephosphorylates the Lipid Second Messenger, Phosphatidylinositol 3,4,5-Trisphosphate. *J. Biol. Chem.* **273**, 13375–13378 (1998).
76. Wu, H., Goel, V. & Haluska, F. G. PTEN signaling pathways in melanoma. *Oncogene* **22**, 3113–3122 (2003).
77. Ma, X. *et al.* The clinical significance of c-Kit mutations in metastatic oral mucosal melanoma in China. *Oncotarget* **8**, 82661–82673 (2017).
78. Ponti, G. *et al.* BRAF, NRAS and c-KIT advanced melanoma: Clinico-pathological features, targeted-therapy strategies and survival. *Anticancer Res.* **37**, 7043–7048 (2017).
79. Price, E. R. *et al.* α-melanocyte-stimulating hormone signaling regulates expression of Microphthalmia, a gene deficient in Waardenburg syndrome. *J. Biol. Chem.* **273**,

33042–33047 (1998).

80. Bertolotto, C. *et al.* Microphthalmia gene product as a signal transducer in cAMP-induced differentiation of melanocytes. *J. Cell Biol.* **142**, 827–835 (1998).
81. Hsiao, J. J. & Fisher, D. E. The roles of microphthalmia-associated transcription factor and pigmentation in melanoma. *Arch. Biochem. Biophys.* **563**, 28–34 (2014).
82. Carreira, S. *et al.* Mitf regulation of Dia1 controls melanoma proliferation and invasiveness. *Genes Dev.* **20**, 3426–3439 (2006).
83. Madonna, G., Ullman, C. D., Gentilcore, G., Palmieri, G. & Ascierto, P. A. NF-κB as potential target in the treatment of melanoma. *J. Transl. Med.* **10**, 53 (2012).
84. Ueda, Y. & Richmond, A. NF-kappaB activation in melanoma. *Pigment Cell Res.* **19**, 112–124 (2006).
85. Kashani-Sabet, M. *et al.* NF-κB in the vascular progression of melanoma. *Journal of Clinical Oncology* vol. 22 617–623 (2004).
86. Kashani-Sabet, M. *et al.* Identification of gene function and functional pathways by systemic plasmid-based ribozyme targeting in adult mice. *Proc. Natl. Acad. Sci. U. S. A.* **99**, 3878–3883 (2002).
87. LEE, K. R., LEE, J. S., KIM, Y. R., SONG, I. G. & HONG, E. K. Polysaccharide from Inonotus obliquus inhibits migration and invasion in B16-F10 cells by suppressing MMP-2 and MMP-9 via downregulation of NF-κB signaling pathway. *Oncol. Rep.* **31**, 2447–2453 (2014).
88. Guarneri, C. *et al.* NF-κB inhibition is associated with OPN/MMP-9 downregulation in cutaneous melanoma. *Oncology Reports* vol. 37 737–746 (2017).
89. Breslow, A. Thickness, cross-sectional areas and depth of invasion in the prognosis of cutaneous melanoma. *Ann. Surg.* **172**, 902–908 (1970).
90. Keung, E. Z. & Gershenwald, J. E. The eighth edition American Joint Committee on Cancer (AJCC) melanoma staging system: implications for melanoma treatment and care. *Expert Rev. Anticancer Ther.* **18**, 775–784 (2018).
91. Barth, A., Wanek, L. A. & Morton, D. L. Prognostic factors in 1,521 melanoma patients with distant metastases. *J. Am. Coll. Surg.* **181**, 193–201 (1995).
92. Manola, J., Atkins, M., Ibrahim, J. & Kirkwood, J. Prognostic factors in metastatic melanoma: A pooled analysis of Eastern Cooperative Oncology Group trials. *J. Clin. Oncol.* **18**, 3782–3793 (2000).
93. Balch, C. M. *et al.* Multivariate analysis of prognostic factors among 2,313 patients with stage III melanoma: Comparison of nodal micrometastases versus macrometastases. *J. Clin. Oncol.* **28**, 2452–2459 (2010).
94. Leonardi, G. C. *et al.* Cutaneous melanoma: From pathogenesis to therapy (Review). *Int. J. Oncol.* **52**, 1071–1080 (2018).

95. Ju, R. J., Stehbens, S. J. & Haass, N. K. The role of melanoma cell-stroma interaction in cell motility, invasion, and metastasis. *Front. Med.* **5**, 1–9 (2018).
96. Pietras, K. & Östman, A. Hallmarks of cancer: Interactions with the tumor stroma. *Exp. Cell Res.* **316**, 1324–1331 (2010).
97. Mueller, M. M. & Fusenig, N. E. Friends or foes - Bipolar effects of the tumour stroma in cancer. *Nat. Rev. Cancer* **4**, 839–849 (2004).
98. Brandner, J. M. & Haass, N. K. Melanoma's connections to the tumour microenvironment. *Pathology* **45**, 443–52 (2013).
99. Mao, X. *et al.* Crosstalk between cancer-associated fibroblasts and immune cells in the tumor microenvironment: new findings and future perspectives. *Mol. Cancer* **20**, 1–30 (2021).
100. Karta, J., Bossicard, Y., Kotzamanis, K., Dolznig, H. & Letellier, E. Mapping the metabolic networks of tumor cells and cancer-associated fibroblasts. *Cells* **10**, 1–25 (2021).
101. Ganguly, D. *et al.* Cancer-associated fibroblasts: Versatile players in the tumor microenvironment. *Cancers (Basel).* **12**, 1–35 (2020).
102. Han, C., Liu, T. & Yin, R. Biomarkers for cancer-associated fibroblasts. *Biomark. Res.* **8**, 64 (2020).
103. Papaccio, F. *et al.* Profiling cancer-associated fibroblasts in melanoma. *Int. J. Mol. Sci.* **22**, (2021).
104. Jobe, N. P. *et al.* Simultaneous blocking of IL-6 and IL-8 is sufficient to fully inhibit CAF-induced human melanoma cell invasiveness. *Histochemistry and Cell Biology* vol. 146 205–217 (2016).
105. Hess, A. R. *et al.* Focal adhesion kinase promotes the aggressive melanoma phenotype. *Cancer Res.* **65**, 9851–9860 (2005).
106. Giraldo, N. A. *et al.* The clinical role of the TME in solid cancer. *Br. J. Cancer* **120**, 45–53 (2019).
107. Gauci, C. L. & Alexander, P. The macrophage content of some human tumours. *Cancer Lett.* **1**, 29–32 (1975).
108. Bingle, L., Brown, N. J. & Lewis, C. E. The role of tumour-associated macrophages in tumour progression: Implications for new anticancer therapies. *J. Pathol.* **196**, 254–265 (2002).
109. Mrad, M. *et al.* Downregulation of sphingosine kinase-1 induces protective tumor immunity by promoting M1 macrophage response in melanoma. *Oncotarget* **7**, 71873–71886 (2016).
110. Pieniazek, M., Matkowski, R. & Donizy, P. Macrophages in skin melanoma-the key element in melanomagenesis (Review). *Oncol. Lett.* **15**, 5399–5404 (2018).

111. Hussein, M. R. Tumour-associated macrophages and melanoma tumourigenesis: Integrating the complexity. *Int. J. Exp. Pathol.* **87**, 163–176 (2006).
112. Lewis, C. E., Harney, A. S. & Pollard, J. W. The Multifaceted Role of Perivascular Macrophages in Tumors. *Cancer Cell* **30**, 18–25 (2016).
113. Mantovani, A. & Sica, A. Macrophages, innate immunity and cancer: balance, tolerance, and diversity. *Curr. Opin. Immunol.* **22**, 231–237 (2010).
114. Ilkovitch, D. & Lopez, D. M. Immune modulation by melanoma-derived factors. *Exp. Dermatol.* **17**, 977–985 (2008).
115. Nesbit, M., Schaider, H., Miller, T. H. & Herlyn, M. Low-Level Monocyte Chemoattractant Protein-1 Stimulation of Monocytes Leads to Tumor Formation in Nontumorigenic Melanoma Cells. *J. Immunol.* **166**, 6483–6490 (2001).
116. Varney, M. L., Olsen, K. J., Mosley, R. L. & Singh, R. K. Paracrine regulation of vascular endothelial growth factor-A expression during macrophage-melanoma cell interaction: Role of monocyte chemotactic protein-1 and macrophage colony-stimulating factor. *J. Interf. Cytokine Res.* **25**, 674–683 (2005).
117. Lin, H. *et al.* Discovery of a Cytokine and Its Receptor by Functional Screening of the Extracellular Proteome. *Science (80-.).* **320**, 807–811 (2008).
118. Franzè, E., Stolfi, C., Troncone, E., Scarozza, P. & Monteleone, G. Role of Interleukin-34 in Cancer. *Cancers (Basel).* **12**, 252 (2020).
119. Ma, X. *et al.* Structural basis for the dual recognition of helical cytokines IL-34 and CSF-1 by CSF-1R. *Structure* **20**, 676–687 (2012).
120. Chihara, T. *et al.* IL-34 and M-CSF share the receptor Fms but are not identical in biological activity and signal activation. *Cell Death Differ.* **17**, 1917–1927 (2010).
121. Zins, K., Heller, G., Mayerhofer, M. & Schreiber, M. Differential prognostic impact of interleukin-34 mRNA expression and infiltrating immune cell composition in intrinsic breast cancer subtypes. *Oncotarget* **9**, 23126–23148 (2018).
122. Stanley, E. R. & Chitu, V. CSF-1 Receptor Signaling in Myeloid Cells. *Cold Spring Harb. Perspect. Biol.* **6**, a021857–a021857 (2014).
123. Droin, N. & Solary, E. Editorial: CSF1R, CSF-1, and IL-34, a “ménage à trois” conserved across vertebrates. *J. Leukoc. Biol.* **87**, 745–747 (2010).
124. Wei, S. *et al.* Functional overlap but differential expression of CSF-1 and IL-34 in their CSF-1 receptor-mediated regulation of myeloid cells. *J. Leukoc. Biol.* **88**, 495–505 (2010).
125. Chen, X., Liu, H., Focia, P. J., Shim, A. H. R. & He, X. Structure of macrophage colony stimulating factor bound to FMS: Diverse signaling assemblies of class III receptor tyrosine kinases. *Proc. Natl. Acad. Sci. U. S. A.* **105**, 18267–18272 (2008).
126. Liu, H. *et al.* The mechanism of shared but distinct CSF-1R signaling by the non-

homologous cytokines IL-34 and CSF-1. *Biochim. Biophys. Acta - Proteins Proteomics* **1824**, 938–945 (2012).

127. Ségaliny, A. I. *et al.* IL-34 and M-CSF form a novel heteromeric cytokine and regulate the M-CSF receptor activation and localization. *Cytokine* **76**, 170–181 (2015).
128. Lelios, I. *et al.* Emerging roles of IL-34 in health and disease. *J. Exp. Med.* **217**, 1–11 (2020).
129. Foucher, E. D. *et al.* IL-34 Induces the Differentiation of Human Monocytes into Immunosuppressive Macrophages. Antagonistic Effects of GM-CSF and IFNγ. *PLoS ONE* vol. 8 (2013).
130. Boulakirba, S. *et al.* IL-34 and CSF-1 display an equivalent macrophage differentiation ability but a different polarization potential. *Sci. Rep.* **8**, 1–11 (2018).
131. Zhou, R. P. *et al.* Functions of interleukin-34 and its emerging association with rheumatoid arthritis. *Immunology* vol. 149 362–373 (2016).
132. Baghdadi, M. *et al.* Chemotherapy-induced IL34 enhances immunosuppression by tumor-associated macrophages and mediates survival of chemoresistant lung cancer cells. *Cancer Res.* **76**, 6030–6042 (2016).
133. Baghdadi, M., Endo, H., Tanaka, Y., Wada, H. & Seino, K. ichiro. Interleukin 34, from pathogenesis to clinical applications. *Cytokine* **99**, 139–147 (2017).
134. Mantovani, A., Marchesi, F., Malesci, A., Laghi, L. & Allavena, P. Tumour-associated macrophages as treatment targets in oncology. *Nat. Rev. Clin. Oncol.* **14**, 399–416 (2017).
135. Segaliny, A. I. *et al.* Syndecan-1 regulates the biological activities of interleukin-34. *Biochim. Biophys. Acta - Mol. Cell Res.* **1853**, 1010–1021 (2015).
136. Nandi, S. *et al.* Receptor-type Protein-tyrosine Phosphatase ζ Is a Functional Receptor for Interleukin-34. *J. Biol. Chem.* **288**, 21972–21986 (2013).
137. Goldmann, T., Otto, F. & Vollmer, E. A receptor-type protein tyrosine phosphatase PTP zeta is expressed in human cutaneous melanomas. *Folia Histochem. Cytobiol.* **38**, 19–20 (2000).
138. Alonso, S. R. *et al.* A high-throughput study in melanoma identifies epithelial-mesenchymal transition as a major determinant of metastasis. *Cancer Res.* **67**, 3450–3460 (2007).
139. Xia, Z. *et al.* The expression, functions, interactions and prognostic values of PTPRZ1: A review and bioinformatic analysis. *J. Cancer* **10**, 1663–1674 (2019).
140. Choi, W. J., Kim, M., Park, J. Y., Park, T. J. & Kang, H. Y. Pleiotrophin inhibits melanogenesis via Erk1/2-MITF signaling in normal human melanocytes. *Pigment Cell Melanoma Res.* **28**, 51–60 (2015).
141. Fukada, M. *et al.* Protein tyrosine phosphatase receptor type Z is inactivated by

ligand-induced oligomerization. *FEBS Lett.* **580**, 4051–4056 (2006).

142. Baghdadi, M. *et al.* Interleukin-34, a comprehensive review. *J. Leukoc. Biol.* **104**, 931–951 (2018).
143. Greter, M. *et al.* Stroma-Derived Interleukin-34 Controls the Development and Maintenance of Langerhans Cells and the Maintenance of Microglia. *Immunity* **37**, 1050–1060 (2012).
144. Boström, E. A. & Lundberg, P. The newly discovered cytokine IL-34 is expressed in gingival fibroblasts, shows enhanced expression by pro-inflammatory cytokines, and stimulates osteoclast differentiation. *PLoS One* **8**, 1–7 (2013).
145. Yu, Y. *et al.* Tumor necrosis factor-α induces interleukin-34 expression through nuclear factor-κB activation in MC3T3-E1 osteoblastic cells. *Molecular Medicine Reports* vol. 10 1371–1376 (2014).
146. Franzé, E. *et al.* Interleukin-34 sustains inflammatory pathways in the gut. *Clin. Sci.* **129**, 271–280 (2015).
147. Guillonneau, C., Bézie, S. & Anegon, I. Immunoregulatory properties of the cytokine IL-34. *Cell. Mol. Life Sci.* **74**, 2569–2586 (2017).
148. Wang, B. *et al.* Integrative genomic analyses of a novel cytokine, interleukin-34 and its potential role in cancer prediction. *Int. J. Mol. Med.* **35**, 92–102 (2015).
149. Kobayashi, T. *et al.* Prognostic value of IL-34 in colorectal cancer patients. *Immunol. Med.* **42**, 169–175 (2019).
150. Ries, C. H. *et al.* Targeting tumor-associated macrophages with anti-CSF-1R antibody reveals a strategy for cancer therapy. *Cancer Cell* **25**, 846–859 (2014).
151. Achkova, D. & Maher, J. Role of the colony-stimulating factor (CSF)/CSF-1 receptor axis in cancer. *Biochem. Soc. Trans.* **44**, 333–341 (2016).
152. Papadimitriou, E. *et al.* Pleiotrophin and its receptor protein tyrosine phosphatase beta/zeta as regulators of angiogenesis and cancer. *Biochim. Biophys. Acta - Rev. Cancer* **1866**, 252–265 (2016).
153. Constantinos Mikelis, Marina Koutsioumpa & Evangelia Papadimitriou. Pleiotrophin as a Possible New Target for Angiogenesis-Related Diseases and Cancer. *Recent Pat. Anticancer. Drug Discov.* **2**, 175–186 (2008).
154. Papadimitriou, E. *et al.* Roles of pleiotrophin in tumor growth and angiogenesis. *Eur. Cytokine Netw.* **20**, 180–190 (2009).
155. Rauvala, H. An 18-kd heparin-binding protein of developing brain that is distinct from fibroblast growth factors. *EMBO J.* **8**, 2933–2941 (1989).
156. González-Castillo, C., Ortuño-Sahagún, D., Guzmán-Brambila, C., Pallàs, M. & Rojas-Mayorquín, A. E. Pleiotrophin as a central nervous system neuromodulator, evidences from the hippocampus. *Front. Cell. Neurosci.* **8**, 1–7 (2015).

157. Wang, X. Pleiotrophin: Activity and mechanism. *Adv. Clin. Chem.* (2020) doi:10.1016/bs.acc.2020.02.003.
158. Ryan, E., Shen, D. & Wang, X. Structural studies reveal an important role for the pleiotrophin C-terminus in mediating interactions with chondroitin sulfate. *FEBS J.* **283**, 1488–1503 (2016).
159. Deepa, S. S., Yamada, S., Zako, M., Goldberger, O. & Sugahara, K. Chondroitin sulfate chains on syndecan-1 and syndecan-4 from normal murine mammary gland epithelial cells are structurally and functionally distinct and cooperate with heparan sulfate chains to bind growth factors: A novel function to control binding of m. *J. Biol. Chem.* **279**, 37368–37376 (2004).
160. Koyama-Nasu, R. *et al.* The pleiotrophin-ALK axis is required for tumorigenicity of glioblastoma stem cells. *Oncogene* **33**, 2236–2244 (2014).
161. Mikelis, C., Sfaelou, E., Koutsioumpa, M., Kieffer, N. & Papadimitriou, E. Integrin α v β 3 is a pleiotrophin receptor required for pleiotrophin-induced endothelial cell migration through receptor protein tyrosine phosphatase β/ζ . *FASEB J.* **23**, 1459–1469 (2009).
162. Koutsioumpa, M. *et al.* Pleiotrophin expression and role in physiological angiogenesis in vivo: potential involvement of nucleolin. *Vasc. Cell* **4**, 4 (2012).
163. Elahouel, R. *et al.* Pleiotrophin Exerts Its Migration and Invasion Effect through the Neuropilin-1 Pathway. *Neoplasia* **17**, 613–624 (2015).
164. Meng, K. *et al.* Pleiotrophin signals increased tyrosine phosphorylation of beta -catenin through inactivation of the intrinsic catalytic activity of the receptor-type protein tyrosine phosphatase beta /zeta. *Proc. Natl. Acad. Sci.* **97**, 2603–2608 (2000).
165. Deuel, T. F. Anaplastic lymphoma kinase: 'Ligand Independent Activation' mediated by the PTN/RPTPβ/ζ signaling pathway. *Biochim. Biophys. Acta - Proteins Proteomics* **1834**, 2219–2223 (2013).
166. Polykratis, A., Katsoris, P., Courty, J. & Papadimitriou, E. Characterization of heparin affin regulatory peptide signaling in human endothelial cells. *J. Biol. Chem.* **280**, 22454–22461 (2005).
167. Gao, S. Bin *et al.* Menin represses malignant phenotypes of melanoma through regulating multiple pathways. *J. Cell. Mol. Med.* **15**, 2353–2363 (2011).
168. Pariser, H., Ezquerra, L., Herradon, G., Perez-Pinera, P. & Deuel, T. F. Fyn is a downstream target of the pleiotrophin/receptor protein tyrosine phosphatase β/ζ-signaling pathway: Regulation of tyrosine phosphorylation of Fyn by pleiotrophin. *Biochem. Biophys. Res. Commun.* **332**, 664–669 (2005).
169. Pariser, H., Herradon, G., Ezquerra, L., Peres-Pinera, P. & Deuel, T. F. Pleiotrophin regulates serine phosphorylation and the cellular distribution of β-adducin through

activation of protein kinase C. *Proc. Natl. Acad. Sci. U. S. A.* **102**, 12407–12412 (2005).

170. Maeda, N., Nishiwaki, T., Shintani, T., Hamanaka, H. & Noda, M. 6B4 proteoglycan/phosphacan, an extracellular variant of receptor-like protein-tyrosine phosphatase ζ/RPTPβ, binds pleiotrophin/heparin-binding growth-associated molecule (HB-GAM). *J. Biol. Chem.* **271**, 21446–21452 (1996).
171. Pantazaka, E. & Papadimitriou, E. Chondroitin sulfate-cell membrane effectors as regulators of growth factor-mediated vascular and cancer cell migration. *Biochim. Biophys. Acta - Gen. Subj.* **1840**, 2643–2650 (2014).
172. Tate Riegel, A. & Wellstein, A. The potential role of the heparin-binding growth factor pleiotrophin in breast cancer. *Breast Cancer Res. Treat.* **31**, 309–314 (1994).
173. Aigner, A. *et al.* Marked increase of the growth factors pleiotrophin and fibroblast growth factor-2 in serum of testicular cancer patients. *Ann. Oncol.* **14**, 1525–1529 (2003).
174. Zhang, L. *et al.* Overexpression of heparin-binding growth-associated molecule in malignant glioma cells. *Neurol. Med. Chir. (Tokyo).* **44**, 637–643 (2004).
175. Nakagawara, A. *et al.* Differential Expression of Pleiotrophin and Midkine in Advanced Neuroblastomas. *Cancer Res.* **55**, 1792–1797 (1995).
176. Jäger, R. *et al.* Differential expression and biological activity of the heparin-binding growth-associated molecule (HB-GAM) in lung cancer cell lines. *Int. J. Cancer* **73**, 537–543 (1997).
177. Czubayko, F., Schulte, A. M., Berchem, G. J. & Wellstein, A. Melanoma angiogenesis and metastasis modulated by ribozyme targeting of the secreted growth factor pleiotrophin. *Proc. Natl. Acad. Sci. U. S. A.* **93**, 14753–14758 (1996).
178. Seykora, J. T., Jih, D., Elenitsas, R., Horng, W. H. & Elder, D. E. Gene expression profiling of melanocytic lesions. *Am. J. Dermatopathol.* **25**, 6–11 (2003).
179. Wu, H. *et al.* Pleiotrophin expression correlates with melanocytic tumor progression and metastatic potential. *J. Cutan. Pathol.* **32**, 125–130 (2005).
180. Satyamoorthy, K., Oka, M. & Herlyn, M. An antisense strategy for inhibition of human melanoma growth targets the growth factor pleiotrophin. *Pigment Cell Res.* **13**, 87–93 (2000).
181. Sherr, C. J. *et al.* The c-fms proto-oncogene product is related to the receptor for the mononuclear phagocyte growth factor, CSF 1. *Cell* **41**, 665–676 (1985).
182. Walter, M. *et al.* The 2.7 Å Crystal Structure of the Autoinhibited Human c-Fms Kinase Domain. *J. Mol. Biol.* **367**, 839–847 (2007).
183. Flick, M. B. *et al.* Recognition of activated CSF-1 receptor in breast carcinomas by a tyrosine 723 phosphospecific antibody. *Oncogene* **14**, 2553–2561 (1997).

184. Knowlton, M. L. *et al.* Profiling Y561-dependent and -independent substrates of CSF-1R in epithelial cells. *PLoS One* **5**, (2010).
185. Reedijk, M. *et al.* Tyr721 regulates specific binding of the CSF-1 receptor kinase insert to PI 3'-kinase SH2 domains: A model for SH2-mediated receptor-target interactions. *EMBO J.* **11**, 1365–1372 (1992).
186. Bourette, R. P., Myles, G. M., Choi, J. L. & Rohrschneider, L. R. Sequential activation of phoshatidylinositol 3-kinase and phospholipase C-γ2 by the M-CSF receptor is necessary for differentiation signaling. *EMBO J.* **16**, 5880–5893 (1997).
187. Bourette, R. P. *et al.* Suppressor of Cytokine Signaling 1 Interacts with the Macrophage Colony-stimulating Factor Receptor and Negatively Regulates Its Proliferation Signal. *J. Biol. Chem.* **276**, 22133–22139 (2001).
188. Husson, H., Mograbi, B., Schmid-Antomarchi, H., Fischer, S. & Rossi, B. CSF-1 stimulation induces the formation of a multiprotein complex including CSF-1 receptor, c-Cbl, PI 3-kinase, Crk-II and Grb2. *Oncogene* **14**, 2331–2338 (1997).
189. Wilhelmsen, K., Burkhalter, S. & Van der Geer, P. C-Cbl binds the CSF-1 receptor at tyrosine 973, a novel phosphorylation site in the receptor's carboxy-terminus. *Oncogene* **21**, 1079–1089 (2002).
190. Pixley, F. J. & Stanley, E. R. CSF-1 regulation of the wandering macrophage: Complexity in action. *Trends Cell Biol.* **14**, 628–638 (2004).
191. Mun, S. H., Park, P. S. U. & Park-Min, K. H. The M-CSF receptor in osteoclasts and beyond. *Exp. Mol. Med.* **52**, 1239–1254 (2020).
192. Fixe, P. & Praloran, V. M-CSF: Haematopoietic growth factor or inflammatory cytokine? *Cytokine* **10**, 32–37 (1998).
193. Tamimi, R. M. *et al.* Circulating Colony Stimulating Factor-1 and Breast Cancer Risk. *Cancer Res.* **68**, 18–21 (2008).
194. Chambers, S. K. Role of CSF-1 in progression of epithelial ovarian cancer. *Futur. Oncol.* **5**, 1429–1440 (2009).
195. Mroczko, B. *et al.* Serum macrophage-colony stimulating factor levels in colorectal cancer patients correlate with lymph node metastasis and poor prognosis. *Clin. Chim. Acta* **380**, 208–212 (2007).
196. Groblewska, M. *et al.* Serum levels of granulocyte colony-stimulating factor (G-CSF) and macrophage colony-stimulating factor (M-CSF) in pancreatic cancer patients. *Clin. Chem. Lab. Med.* **45**, 30–34 (2007).
197. Kowalska, M. *et al.* Serum macrophage colony-stimulating factor (M-CSF) in patients with Hodgkin lymphoma. *Med. Oncol.* **29**, 2143–2147 (2012).
198. Neubert, N. J. *et al.* T cell–induced CSF1 promotes melanoma resistance to PD1 blockade. *Sci. Transl. Med.* **10**, 1–30 (2018).

199. Vincent, K. M. & Postovit, L. M. Investigating the utility of human melanoma cell lines as tumour models. *Oncotarget* **8**, 10498–10509 (2017).
200. Davies, H. *et al.* Mutations of the BRAF gene in human cancer. *Nature* **417**, 949–954 (2002).
201. Ikediobi, O. N. *et al.* Mutation analysis of 24 known cancer genes in the NCI-60 cell line set. *Mol. Cancer Ther.* **5**, 2606–2612 (2006).
202. Tsao, H., Zhang, X., Fowlkes, K. & Haluska, F. G. Relative reciprocity of NRAS and PTEN/MMAC1 alterations in cutaneous melanoma cell lines. *Cancer Res.* **60**, 1800–1804 (2000).
203. Tanami, H. *et al.* Involvement of overexpressed wild-type BRAF in the growth of malignant melanoma cell lines. *Oncogene* **23**, 8796–8804 (2004).
204. Milella, M. *et al.* PTEN status is a crucial determinant of the functional outcome of combined MEK and mTOR inhibition in cancer. *Sci. Rep.* **7**, 1–15 (2017).
205. Abel, E. V. *et al.* Melanoma adapts to RAF/MEK inhibitors through FOXD3-mediated upregulation of ERBB3. *J. Clin. Invest.* **123**, 2155–2168 (2013).
206. Gomez-Gutierrez, J. G. *et al.* Adenovirus-mediated gene transfer of FKHRL1 triple mutant efficiently induces apoptosis in melanoma cells. *Cancer Biol. Ther.* **5**, 875–883 (2006).
207. Rossi, S. *et al.* TNF-alpha and metalloproteases as key players in melanoma cells aggressiveness. *J. Exp. Clin. Cancer Res.* **37**, 1–17 (2018).
208. Castellano, M. *et al.* CDKN2A/p16 is inactivated in most melanoma cell lines. *Cancer Res.* **57**, 4868–4875 (1997).
209. Mahgoub, T. *et al.* Kinase inhibitor screening identifies CDK4 as a potential therapeutic target for melanoma. *Int. J. Oncol.* **47**, 900–908 (2015).
210. Stark, M. & Hayward, N. Genome-wide loss of heterozygosity and copy number analysis in melanoma using high-density single-nucleotide polymorphism arrays. *Cancer Res.* **67**, 2632–2642 (2007).
211. Vallarelli, A. F. *et al.* TERT promoter mutations in melanoma render TERT expression dependent on MAPK pathway activation. *Oncotarget* **7**, 53127–53136 (2016).
212. Young, R. J. *et al.* Loss of CDKN2A expression is a frequent event in primary invasive melanoma and correlates with sensitivity to the CDK4/6 inhibitor PD0332991 in melanoma cell lines. *Pigment Cell Melanoma Res.* **27**, 590–600 (2014).
213. Spofford, L. S., Abel, E. V., Boisvert-Adamo, K. & Aplin, A. E. Cyclin D3 expression in melanoma cells is regulated by adhesion-dependent phosphatidylinositol 3-kinase signaling and contributes to G1-S progression. *J. Biol. Chem.* **281**, 25644–25651 (2006).
214. Ségaliny, A. I. *et al.* Interleukin-34 promotes tumor progression and metastatic process

in osteosarcoma through induction of angiogenesis and macrophage recruitment. *Int. J. Cancer* **137**, 73–85 (2015).

215. Giricz, O. *et al.* The RUNX1/IL-34/CSF-1R axis is an autocrinally regulated modulator of resistance to BRAF-V600E inhibition in melanoma. *JCI insight* **3**, (2018).
216. Shi, Y. *et al.* Tumour-associated macrophages secrete pleiotrophin to promote PTPRZ1 signalling in glioblastoma stem cells for tumour growth. *Nat. Commun.* **8**, 1–17 (2017).
217. Wang, Y. *et al.* IL-34 is a tissue-restricted ligand of CSF1R required for the development of Langerhans cells and microglia. *Nat. Immunol.* **13**, 753–760 (2012).
218. Orecchia, P. *et al.* A novel human anti-syndecan-1 antibody inhibits vascular maturation and tumour growth in melanoma. *Eur. J. Cancer* **49**, 2022–2033 (2013).
219. Pastor, M. *et al.* Development of inhibitors of receptor protein tyrosine phosphatase β/ζ (PTPRZ1) as candidates for CNS disorders. *Eur. J. Med. Chem.* **144**, 318–329 (2018).
220. Libra. Melanoma: Molecular pathogenesis and emerging target therapies (Review). *Int. J. Oncol.* **34**, 547–557 (2009).
221. Fernández-Calle, R. *et al.* Pharmacological inhibition of Receptor Protein Tyrosine Phosphatase β/ζ (PTPRZ1) modulates behavioral responses to ethanol. *Neuropharmacology* **137**, 86–95 (2018).
222. Mascotti, K., McCullough, J. & Burger, S. R. HPC viability measurement: trypan blue versus acridine orange and propidium iodide. *Transfusion* **40**, 693–696 (2000).
223. Hong, D., Lee, G., Jung, N. C. & Jeon, M. Fast automated yeast cell counting algorithm using bright-field and fluorescence microscopic images. *Biol. Proced. Online* **15**, 1 (2013).
224. Kapuscinski, J. DNA-Specific Fluorescent Probe. *Biotech. Histochem.* **70**, 220–233 (1979).
225. Cooper, J. A. Effects of cytochalasin and phalloidin on actin. *J. Cell Biol.* **105**, 1473–1478 (1987).
226. Ridley, A. J. Life at the leading edge. *Cell* **145**, 1012–1022 (2011).
227. Sandri, S. *et al.* Vemurafenib resistance increases melanoma invasiveness and modulates the tumor microenvironment by MMP-2 upregulation. *Pharmacol. Res.* **111**, 523–533 (2016).
228. Ao, J. Y. *et al.* Colony-stimulating factor 1 receptor blockade inhibits tumor growth by altering the polarization of tumor-associated macrophages in hepatocellular carcinoma. *Mol. Cancer Ther.* **16**, 1544–1554 (2017).
229. Menke, J. *et al.* Autocrine CSF-1 and CSF-1 Receptor Coexpression Promotes Renal Cell Carcinoma Growth. *Cancer Res.* **72**, 187–200 (2012).
230. Ide, H. *et al.* Expression of colony-stimulating factor 1 receptor during prostate

development and prostate cancer progression. *Proc. Natl. Acad. Sci. U. S. A.* **99**, 14404–14409 (2002).

231. Tang, R. *et al.* M-CSF (monocyte colony stimulating factor) and M-CSF receptor expression by breast tumour cells: M-CSF mediated recruitment of tumour infiltrating monocytes? *J. Cell. Biochem.* **50**, 350–356 (1992).
232. Baiocchi, G. *et al.* Expression of the macrophage colony-stimulating factor and its receptor in gynecologic malignancies. *Cancer* **67**, 990–996 (1991).
233. Freuchet, A., Salama, A., Remy, S., Guillonneau, C. & Anegon, I. IL-34 and CSF-1, deciphering similarities and differences at steady state and in diseases. *J. Leukoc. Biol.* **110**, 771–796 (2021).
234. Rambow, F. *et al.* New Functional Signatures for Understanding Melanoma Biology from Tumor Cell Lineage-Specific Analysis. *Cell Rep.* **13**, 840–853 (2015).
235. Uemura, Y. *et al.* Effects of GM-CSF and M-CSF on tumor progression of lung cancer: Roles of MEK1/ERK and AKT/PKB pathways. *Int. J. Mol. Med.* **18**, 365–373 (2006).
236. Feng, Z. J. *et al.* Lung cancer cell migration is regulated via repressing growth factor PTN/RPTP B/ζ signaling by menin. *Oncogene* vol. 29 5416–5426 (2010).
237. Palmer, R. H., Vernersson, E., Grabbe, C. & Hallberg, B. Anaplastic lymphoma kinase: Signalling in development and disease. *Biochem. J.* **420**, 345–361 (2009).